Multi–objective Optimization of Nonconventional Laminated Composite Panels

by

Gökhan Serhat

A Dissertation Submitted to the
Graduate School of Sciences and Engineering
in Partial Fulfillment of the Requirements for
the Degree of

Doctor of Philosophy

in

Mechanical Engineering

October 26, 2018

Multi–objective Optimization of Nonconventional Laminated Composite Panels

Koç University

Graduate School of Sciences and Engineering

This is to certify that I have examined this copy of a doctoral dissertation by

Gökhan Serhat

and have found that it is complete and satisfactory in all respects,
and that any and all revisions required by the final
examining committee have been made.

Committee Members:

_____

Assoc. Prof. Ipek Basdogan (Advisor)

_____

Prof. Dr. Fabian Duddeck

_____

Assoc. Prof. Murat Sözer

_____

Assoc. Prof. Cetin Yilmaz

_____

Asst. Prof. Bekir Bediz

Date: _____

To my beloved family and my love

ABSTRACT

Laminated composite panels are extensively used in various industries due to their high stiffness–to–weight ratio and directional properties that allow optimization of stiffness characteristics for specific applications. With the recent improvements in the manufacturing techniques, the technology trend has been shifting towards the development of nonconventional composites. This work aims to develop new methods for the design and optimization of nonconventional laminated composites. Lamination parameters method is used to characterize laminate stiffness matrices in a compact form. An optimization framework based on finite element analysis was developed to calculate the solutions for different panel geometries, boundary conditions and load cases. The first part of the work addresses the multi–objective optimization of composite laminates to maximize dynamic and load–carrying performances simultaneously. Conforming and conflicting behaviors of multiple objective functions are investigated by determining Pareto–optimal solutions, which provide a valuable insight for multi–objective optimization problems. In the second part, design of curved laminated panels for optimal dynamic response is studied in detail. Firstly, the designs yielding maximum fundamental frequency values are computed. Next, optimal designs minimizing equivalent radiated power are obtained for the panels under harmonic pressure excitation, and their effective frequency bands are shown. The relationship between these two design sets is investigated to study the effectiveness of the frequency maximization technique. In the last part, a new method based on lamination parameters is proposed for the design of variable–stiffness composite panels. The results demonstrate that the proposed method provides manufacturable designs with smooth fiber paths that outperform the constant–stiffness laminates, while utilizing the advantages of lamination parameters formulation.

ÖZETÇE

Lamine kompozit paneller yüksek sertlik/ağırlık oranlarından ve sertlik özelliklerinin belirli uygulamalara özgü optimizasyonuna izin veren yönsel niteliklerinden dolayı çeşitli endüstrilerde yaygın olarak kullanılmaktadır. Üretim tekniklerindeki son gelişmelerle birlikte teknolojideki eğilim yenilikçi kompozitlerin geliştirilmesine doğru kaymaktadır. Bu çalışma yenilikçi kompozitlerin dizaynı ve optimizasyonu için yeni yöntemler geliştirmeyi amaçlamaktadır. Lamine sertlik matrislerinin kompakt bir şekilde tanımlanması için laminasyon parametreleri yöntemi kullanılmaktadır. Çözümleri farklı panel geometrileri, sınır koşulları ve yük durumlarına göre hesaplayabilmek için sonlu elemanlar analizine dayalı bir optimizasyon sistemi geliştirilmiştir. Çalışmanın ilk kısmı dinamik ve yük taşıma performanslarının beraberce maksimize edilmesi için kompozit panellerin çok amaçlı optimizasyonunu konu almaktadır. Birden çok amaç fonksiyonunun uyumlu ve çelişen davranışları, çok amaçlı optimizasyon problemleri için değerli bir kavrayış sağlayan Pareto–optimal çözümlerin bulunmasıyla araştırılmıştır. İkinci kısımda, kavisli lamine panellerin en iyi dinamik performans için dizaynı detaylı olarak çalışılmaktadır. Öncelikle, en yüksek birinci doğal frekansı sağlayacak dizaynlar belirlenmiştir. Daha sonra, harmonik basınç altındaki panellerin eşdeğer güç yayımını minimize edecek en iyi dizaynlar belirlenmiş ve etkin frekans aralıkları gösterilmiştir. Bu iki dizayn grubu arasındaki ilişki, frekans maksimizasyonu tekniğinin etkinliğini araştırmak için incelenmiştir. Son kısımda, değişken–sertlikli kompozit panellerin dizaynı için laminasyon parametrelerine dayalı yeni bir metot önerilmiştir. Sonuçlar önerilen metodun sabit–sertlikli laminelerden üstün gelen, düzgün fiber yörüngeli üretilebilir dizaynlar sağlarken; laminasyon parametreleri formulasyonunun yararlarından da faydalandığını göstermektedir.

ACKNOWLEDGMENTS

I would like to thank, first and foremost, to my advisor Dr. Ipek Basdogan and for her guidance and support throughout my Ph.D. study. She provided me a research environment that motivated me to be an independent, curious, analytical, and creative researcher. I am glad that I found the opportunity to benefit from her experiences that helped me to develop myself as a scientist.

I thank Prof. Dr. Fabian Duddeck for always supporting me in my postgraduate education and informing me about the research position in Koc University. I also want to thank him and Dr. Murat Sözer for agreeing to join my thesis monitoring committee.

I want to thank Dr. Cetin Yilmaz and Dr. Bekir Bediz along with my thesis committee members for agreeing to join my thesis defense jury. They spent their precious time to listen to my presentation and read my thesis.

I would like to thank to my beloved family for their everlasting love and support. They raised me with lots of love, care and patience. They understood my lack of time during my Ph.D. study and bear with me as I moved on. In particular, I thank my mother as she did her best to understand my struggle, and she has intimately tracked my progression throughout the entire period. I thank my father for inspiring me with the love of science and always believing in me. I thank my sister for always being a great mentor to me as I climbed the stairs in my career. I thank my aunt and my cousins for their warm welcome and their efforts in helping me to relocate in Istanbul.

I would like to thank Yasemin Vardar for her endless love and support. We walked this road hand to hand. We shared happiness and frustration together. My Ph.D. years have meant much more with her and I have been very lucky to have her by my side. I also want to thank her family for their care and support.

I would like to thank the former members of VAL; Mehmet Murat Gözüm, Buğra Bayık, Amirreza Aghakhani, Utku Boz, Hakan Yenerer, and Stan Andrei Cristian. We were like brothers during this journey and we endured all difficulties side by side.

I thank the director of RML, Prof. Dr. Cagatay Basdogan, for his support and all social activities we enjoyed together. I also thank my colleagues in RML, particularly, Ömer Şirin, Ozan Çaldıran and Yusuf Aydın. As the members of fellow labs we always supported each other and we had so many great moments to remember.

I would like to thank the members of the Marie Curie Initial Training Network "Aerospace Multidisciplinarity Enabling DEsign Optimization (AMEDEO)". It was such a great opportunity for me to get to know such extra–ordinary people and learn from them.

I would like to thank all my teachers who educated me since my primary school years and helped me to become the person I am today. Particularly, I would like to thank my primary school teacher Selim Küçükkaraca and high school teacher Kurtuluş Bingöl. They have become my friends and thought me things that would guide me for the rest of my life.

Finally, I would like to thank Onur Özkan, İnanç Örge, Sena Uzunpınar, Anıl Korkmaz, Simge Gülhan, Deniz Atasoy, Mine Kaya, Vlad Somesan, Cristina Somesan, Emre Şendağ, Tiago Faria, Laszlo Kudela, Fatima Fakharian, Emin Oğuz İnci, Eyüp Can Kökan, Çağrı Tanyıldız, Dima Sarafova, Stefanie Nedjalkova, Joshua Russo, Yen Nguyen, Yunkyung Cho, Lucas Chilelli Silva, Sofie Wenzhen Chen, Lena Fesiuk, Walker Mattingly, Anastasia Wilkening, Tomek Suarez, Can Pehlivantürk, Seçil Üstünkol, Tağra Bayık, Sinemis Temel, Ece Özkul, İpek Karakuş, Yavuzer Karakuş, Niloofar Akhavan, Ümmü Çakmak, Mahmut Biçer, Hasan Çağlar, Oğuzalp Bakır, Buket Baylan, Utku Erdem, Serena Muratçıoğlu, Itır Bakış Doğru, Gökay Yüksel, Bilgesu Erdoğan, Efe Elbeyli, Rustamjon Melikov, Erdem Kayserilioğlu, Jonathan Ollar, Andrea Viti, Anna Arsenyeva, Christopher Chahine, Kristofer Jovanov, Sam Duckitt, Marco Tito Bordogna and Paul Lancelot for their great friendship.

European Union Seventh Framework Programme “FP7–PEOPLE–2012–ITN” supported this work under grant agreement 316394.

TABLE OF CONTENTS

LIST OF TABLES

LIST OF FIGURES

NOMENCLATURE

A	in–plane stiffness matrix
A_e	elemental areas
A_p	panel area
a	panel length
a_p	planform panel length $(= 2r \sin(a/2r))$
B	in–plane/bending coupling tensor
b	panel width
c_f	speed of sound
D	bending stiffness matrix
D_{ij}	bending stiffness matrix entities
D_λ, D_Ω	reference flexural rigidities $(= (E_{11}, E_{22})h^3/12(1 - \nu_{12}\nu_{21}))$
d_i	distances between the element centers and the master nodes
E	generic stiffness material stiffness which may refer to E_x, $\bar{E}$ or G_{xy}
E_1	elastic modulus of uni–directional layers along the fibers
E_2	elastic modulus of uni–directional layers perpendicular to the fibers
E_x, E_x^0	normalized and true elastic moduli in x–direction
E_y, E_y^0	normalized and true elastic moduli in y–direction
$\bar{E}$	normalized mean of elastic moduli in x and y–directions
ERP	equivalent radiated power of the panels
$\overline{ERP}$	ERP normalized by the maximum amplitude
$\widetilde{ERP}$	ERP normalized by the minimum amplitude at the maximum ω_1
f, f^*	real and complex global force vectors
G_{12}	in–plane shear modulus of uni–directional layers
G_{13}, G_{23}	transverse shear moduli of uni–directional layers

G_{xy}	normalized in–plane shear modulus
G^0_{xy}	true in–plane shear modulus
h	panel thickness
K, K^*	real and complex global stiffness matrices
K_g	geometric stiffness matrix
M	global mass matrix
M_x, M_y, M_{xy}	bending moment resultants per unit length
m	number of half–waves in x–direction
m_{cr}	number of half–waves in x–direction for the critical buckling mode
N_e	number of elements
N_l	number of laminate layers
N_x, N_y, N_{xy}	in–plane load resultants per unit length
n	number of half–waves in y–direction
n_{cr}	number of half–waves in y–direction for the critical buckling mode
P_e	elemental center points
P_i	master node points
Q_{ij}	reduced stiffness matrix terms
R_l, R_r	volumetric ratios of $90° - 45°$ and $45° - 0°$ layers
r	radius of panel curvature
t_k	layer thicknesses
U_i	material invariants
u, u^*	real and complex nodal displacement vectors
u_n	mode shape vector
$\ddot{u}$	nodal acceleration vector
V_1, V_3	lamination parameters
v, v^*	real and complex nodal velocity vectors
v_f	particle velocity of the fluid
v_s	normal velocity at the structure surface

v_{se}	elemental normal velocity at the structure surface
x_e, x_i	x–coordinates of the elements and master nodes
y_e, y_i	y–coordinates of the elements and master nodes
ϵ_x^0, ϵ_y^0, ϵ_y^0	mid–plane strains
η	structural damping coefficient
κ_x, κ_y, κ_{xy}	panel curvatures
λ_b	buckling parameter
λ_{cr}	critical buckling parameter
λ_n	normalized frequency parameter $(= \omega_n a_p b\sqrt{\rho h/D_\lambda})$
ν_{12}, ν_{21}	major and minor Poisson ratios of uni–directional layers
Ω_n	normalized frequency parameter $(= \omega_n a^2\sqrt{\rho h/D_\Omega})$
ω	excitation frequency
ω_n	natural frequency
ω_1, ω_2	1^{st} (fundamental) and 2^{nd} natural frequencies
ω_{21}	difference between the 1^{st} and 2^{nd} natural frequencies $(= \omega_2 - \omega_1)$
ω^*	normalized fundamental frequency $(= \omega_1 b^2\sqrt{12\rho/Q_{22}}/(\pi^2 h)$
$\overline{\omega}$	frequency ratio $(= \omega/\max(\omega_1))$
$\overline{\omega}_n$	normalized natural frequency $(= \omega_n(b^2/h)\sqrt{\rho/E_2})$
$\overline{\omega}_1$, $\overline{\omega}_2$	normalized 1^{st} and 2^{nd} natural frequencies
$\overline{\omega}_{21}$	normalized difference between the 1^{st} and 2^{nd} natural frequencies
Ψ	stream functions defining the fiber paths
ρ	laminate density
ρ_f	fluid density
θ_k	fiber orientation angle of the layers
θ_l	variable stiffness laminate layer angles for $90^\circ - 45^\circ$ layers
θ_r	variable stiffness laminate layer angles for $45^\circ - 0^\circ$ layers

Chapter 1

INTRODUCTION

1.1 Motivation

Laminated composites become increasingly widespread due to their high stiffness and strength, low density and directional properties which offer additional potential for design tailoring. These materials are particularly suitable for the construction of shell structures, such as the panels of land, sea and air vehicles [Marsh, 2014].

With the recent improvements in the manufacturing techniques, the technology trend has been shifting towards the development of nonconventional laminated composites. These materials exhibit superior structural characteristics compared to conventional laminates. Nonconventional laminates can be produced by using unrestricted fiber orientation angles rather than prescribed sets of available layers. Moreover, such laminates can have nonuniform fiber orientation angles across the laminate domain and provide variable–stiffness properties.

One of the shortcomings of the laminate optimization approaches using number of layers, layer thicknesses and angles is that, the solution depends on the initial assumptions on the laminate configuration. As a remedy, lamination parameters formulation has been utilized in various studies to describe the stiffness properties in a compact form [Tsai and Hahn, 1980]. Even though there are many available studies relying on the lamination parameters, several important points still need to be addressed. These gaps in the literature are outlined in the following.

In multi-objective optimization problems, the optimal designs for different performance metrics may be conflicting [Abouhamze and Shakeri, 2007], [Nik et al., 2012].

Therefore, it is essential to develop methodologies for multi-objective optimization of composite laminated plates to determine the optimal parameters in the given design space. Although Pareto-optimal solutions for multi-objective optimization of fiber-reinforced composites have been studied in the literature, lamination parameters have not been used as the parametrization technique in the existing studies.

In certain applications, laminated composite panels can be exposed to dynamic excitation which may cause resonances leading to excessive vibrations or even failure [Niu et al., 2010]. Attaining optimum dynamic response requires an elaborate design process since dynamic properties of the panels directly depend on the structural parameters [Farshi and Rabiei, 2007]. Existing design studies, which use lamination parameters formulation to optimize stiffness properties of the composite panels to improve dynamic response, are restricted to modifying natural frequencies. Performance of such panels under dynamic excitations has not been investigated in frequency domain using lamination parameters.

The potential of constant–stiffness laminates reach its limits for the enhancement of operational performance. The existing values of the optimal responses can be further improved by using variable–stiffness laminates [Gürdal and Olmedo, 1993]. For variable–stiffness laminates, there are a few available design studies relying on lamination parameters. The studies show that, in the absence of manufacturing constraints, resulting lamination parameter distribution can be very irregular complicating the retrieval of an actual laminate configuration [Abdalla et al., 2007]. Utilization of lamination parameters in an optimization framework which properly considers manufacturing constraints is an active research topic, and the development of the new methods addressing the problem is beneficial.

1.2 Contribution

The contribution of this study is threefold. Initially, a multi-objective design optimization framework for dynamic and load-carrying requirements of laminated composite plates is introduced. Laminate stiffness properties are represented and optimized

using lamination parameters as design variables. Maximization of the fundamental frequency, buckling load, and effective stiffness are chosen as the design objectives. Pareto-optimal solutions are determined for the first time in the literature for different combinations of design objectives using lamination parameters. Different panel aspect ratios and load cases are considered. The results are visualized on Miki's lamination diagram to provide an insight into potential solutions for multi-objective optimization problems. Significant changes in the trends of the optimal solutions in the lamination parameters domain are demonstrated for different problem types.

Secondly, lamination parameters technique was utilized to examine the dynamic response of flat and curved composite panels. Finite element analyses are performed to investigate the individual and combined effects of varying panel aspect ratios, curvatures and boundary conditions on the dynamic responses. Fundamental frequency contours in lamination parameters domain are obtained for different sets of model parameters. In addition, equivalent radiated power (ERP) contours for the panels excited by harmonic pressure are shown. Optimal laminate configurations providing the best dynamic performance are determined by initially maximizing the fundamental frequencies, then minimizing ERP at different frequencies. The relationship between the designs optimized for maximum fundamental frequency and minimum ERP responses is investigated to study the effectiveness of the frequency maximization technique. The results demonstrated the potential of using lamination parameters technique in the design of flat/curved composite panels for the optimal dynamic response, and provided valuable insight into the effect of various design parameters.

Lastly, a novel variable–stiffness laminate optimization technique that considers the manufacturability of the composite panels is proposed. It constrains the design space which controls the direction of change for the lamination parameters and subsequently leads a smooth change in the layer angles. The method differs from the existing methods by its simplicity and provides an efficient mean to estimate the required stiffness distributions within variable–stiffness composite panels. Finite element analyses are used to calculate solutions for various panel geometries and

boundary conditions. After finding optimal lamination parameter distributions, corresponding fiber orientations of the layers are also calculated. In addition to the novelty of the proposed method, the eigenfrequency separation problem for curved variable–stiffness panels is studied for the first time in the literature using lamination parameters. The developed method is utilized to maximize the fundamental frequencies of panels having different aspect ratios, curvatures and boundary conditions as example cases. The results demonstrated that variable–stiffness designs with smooth manufacturable fiber paths can be obtained and better performances can be achieved compared to the constant–stiffness designs by utilizing the proposed method.

1.3 Outline

In the following chapter, the details of the panel models, lamination parameters formulation and finite element analysis framework are provided. Chapter 3 addresses multi–objective optimization of composite laminates to maximize the dynamic and load–carrying performances simultaneously. Chapter 4 covers design of curved laminated panels for optimal dynamic response including forced vibration. In Chapter 5, a novel methodology for the design of variable–stiffness laminates is presented. The conclusions and possible directions for future work are outlined in Chapter 6.

Chapter 2

PROBLEM DESCRIPTION

2.1 Panel Models

In Chapter 3 the calculations are done for flat laminated composite plates whose schematics are depicted in Fig. 2.1. In Chapters 4 and 5 curved laminated panels illustrated in Fig. 2.2 are considered.

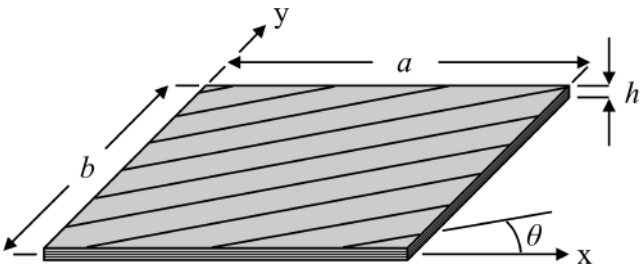

Figure 2.1: Flat laminated composite plate.

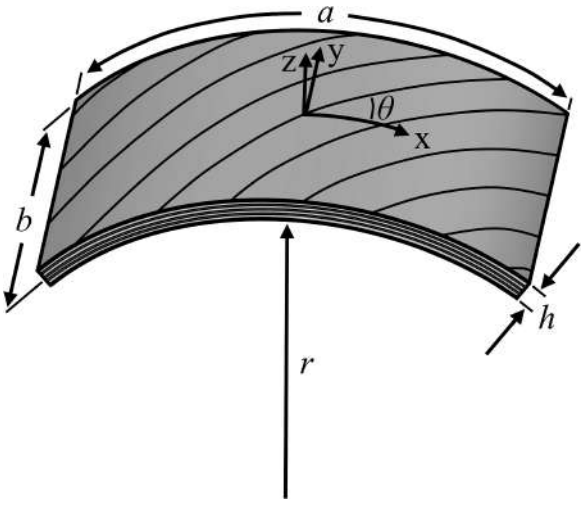

Figure 2.2: Curved laminated composite panel.

2.2 Lamination Parameters

2.2.1 Formulation

Lamination parameters were initially proposed by [Tsai and Hahn, 1980]. They allow compact representation of the laminate configuration by approximating the overall stiffness properties in terms of material invariants and lamination parameters. Instead of the number of plies, their relative thicknesses, and orientation angles; the lamination parameters can be used as the design variables. Another attractive feature of lamination parameters is their convex solution space shown by [Grenestedt and Gudmundson, 1993], which eliminates local optimality problems except for a few cases such as forced vibration analysis [Serhat and Basdogan, 2016a].

Using the classical laminated plate theory, the constitutive equations for a laminated composite plate are defined as [Gürdal et al., 1999]:

$$\begin{Bmatrix} N_x \\ N_y \\ N_{xy} \\ M_x \\ M_y \\ M_{xy} \end{Bmatrix} = \begin{bmatrix} A & B \\ B & D \end{bmatrix} \begin{Bmatrix} {\epsilon_x}^0 \\ {\epsilon_y}^0 \\ {\epsilon_{xy}}^0 \\ \kappa_x \\ \kappa_y \\ \kappa_{xy} \end{Bmatrix} \tag{2.1}$$

where N_x, N_y and N_{xy} are the force resultants per unit depth; M_x, M_y and M_{xy} are the moment resultants per unit depth; ϵ_x^0, ϵ_y^0 and ϵ_{xy}^0 are the mid-plane strains; κ_x, κ_y and κ_{xy} are the plate curvatures. A, B and D are in-plane stiffness, in-plane/bending coupling and bending stiffness tensors, respectively, which can be formulated in terms of the lamination parameters and material invariants. For balanced and symmetric laminated plates, it is possible to model normalized in-plane stiffness tensor using only two lamination parameter variables as follows [Gürdal et al., 1999]:

$$\frac{A}{h} = \begin{bmatrix} U_1 & U_4 & 0 \\ U_4 & U_1 & 0 \\ 0 & 0 & U_5 \end{bmatrix} + \begin{bmatrix} U_2 & 0 & 0 \\ 0 & -U_2 & 0 \\ 0 & 0 & 0 \end{bmatrix} V_1 + \begin{bmatrix} U_3 & -U_3 & 0 \\ -U_3 & U_3 & 0 \\ 0 & 0 & -U_3 \end{bmatrix} V_3 \tag{2.2}$$

where V_i are the normalized lamination parameters:

$$V_1 = \frac{1}{h}\sum_{k=1}^{N_l} t_k 2\theta_k \tag{2.3a}$$

$$V_3 = \frac{1}{h}\sum_{k=1}^{N_l} t_k 4\theta_k \tag{2.3b}$$

N_l, t_k and θ_k are number of layers, layer thicknesses and layer angles, respectively. U_i are the material invariants calculated using the following equation [Diaconu et al., 2002]:

$$\begin{Bmatrix} U_1 \\ U_2 \\ U_3 \\ U_4 \\ U_5 \end{Bmatrix} = \begin{bmatrix} 3/8 & 3/8 & 1/4 & 1/2 \\ 1/2 & -1/2 & 0 & 0 \\ 1/8 & 1/8 & -1/4 & -1/2 \\ 1/8 & 1/8 & 3/4 & -1/2 \\ 1/8 & 1/8 & -1/4 & 1/2 \end{bmatrix} \begin{Bmatrix} Q_{11} \\ Q_{22} \\ Q_{12} \\ Q_{66} \end{Bmatrix} \tag{2.4}$$

Q_{ij} are the reduced stiffness matrix entities given by

$$\begin{Bmatrix} Q_{11} \\ Q_{22} \\ Q_{12} \\ Q_{66} \end{Bmatrix} = \begin{Bmatrix} E_1/\gamma \\ E_2/\gamma \\ \nu_{12}E_2/\gamma \\ G_{12} \end{Bmatrix} \tag{2.5}$$

Here, E_1, E_2, G_{12} and ν_{12} are elastic modulus in the fiber direction, elastic modulus perpendicular to the fiber direction, in-plane shear modulus and major Poisson's ratio of a uni-directional composite layer, respectively. $\gamma = (1-\nu_{12}\nu_{21})$ where reciprocity relations for orthotropic layers require minor Poisson's ratio to be: $\nu_{21} = \nu_{12}E_2/E_1$. For symmetric laminates in-plane/ bending coupling tensor is zero. Additionally, when the laminate consists of a large number of balanced layers distributed homogenously through the thickness, bending stiffness matrix satisfies the relation: $D = Ah^2/12$. Therefore, similar to A, D also becomes a function of V_1 and V_3 [Fukunaga and Vanderplaats, 1991]. This is the assumption adopted in this study which results in a reduced design space for D.

2.2.2 Miki's Lamination Diagram

Miki's Lamination Diagram is a graphical tool to visualize the feasible domain of the balanced and symmetric laminates [Miki, 1984]. In Fig. 2.3, the diagram is illustrated with exemplary points for [0°], [±45°], and [90°] and [0° ±45° 90°] (quasi-isotropic) laminates. The horizontal axis (V_1) and the vertical axis (V_3) are the normalized lamination parameters. All the feasible design points need to be within the diagram. The lower part of the feasible domain is bounded by the curve: $V_3 = 2V_1^2 - 1$. Every point on this curve is only achievable by a balanced symmetric laminate with one distinct angle defined by

$$\theta = \frac{\cos^{-1}(V_1)}{2} \tag{2.6}$$

The upper part is bounded by $V_3 = 1$ line. The points on this line can be obtained by different combinations of 0° and 90° layers.

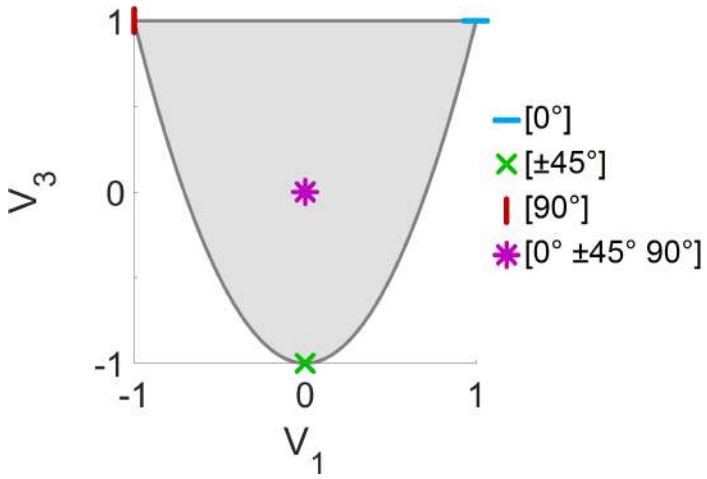

Figure 2.3: Miki's lamination diagram.

2.3 Responses

In this paper, fundamental natural frequencies, buckling loads and forced dynamic responses are computed by using the developed in-house finite element analysis (FEA)

software. This FEA framework allows establishing the connection between lamination parameters and nodal stiffness matrices and performing the analyses repeatedly for various cases. In the laminate modeling, 2D shell elements which can carry both in-plane and bending loads are used. The analyses are performed to obtain solutions for different plate aspect ratios, stiffness properties and boundary conditions.

2.3.1 Fundamental Frequency

Following element formulation, discretization and assembly processes; Newton's second law provides the following system of equations:

$$Ku + M\ddot{u} = f \tag{2.7}$$

where K is the global stiffness matrix, M is the global mass matrix; u, $\ddot{u}$ and f are the nodal displacement, acceleration and force vectors, respectively. Then, the natural frequencies of the plate (ω_n) and corresponding mode shape vectors (u_n) can be obtained by solving Eq. 2.8 and Eq. 2.9, respectively (Liu and Quek 2003):

$$\det(K - \omega_n^2 M) = 0 \tag{2.8}$$

$$(K - \omega_n^2 M)u_n = 0 \tag{2.9}$$

2.3.2 Buckling Load

In buckling analyses, initially the geometric stiffness matrix K_g is computed using the stress field obtained for the selected loading type. After that, the buckling parameter λ_b can be obtained by solving the following eigenvalue equation [Anderson et al., 1968]:

$$\det(K - \lambda_b K_g) = 0 \tag{2.10}$$

The minimum eigenvalue is the critical buckling coefficient λ_{cr} which depends on plate aspect ratio, loading case and material properties. The true buckling load can be obtained by multiplying the critical buckling coefficient and the loading magnitude. Therefore, for unit loading, the buckling load is equal to the λ_{cr} value.

2.3.3 Equivalent Radiated Power (ERP)

In the analyses, the forced dynamic response of the composite panels with respect to various parameters is studied. Equivalent radiated power (ERP) is chosen as the response of interest. ERP is a widely used performance metric for vibrating panels which provides information about maximum possible acoustic radiation at the specific excitation frequencies. It is the defined as the power of a vibrating panel radiated into the surrounding media which can be calculated using the following equation [Fritze et al., 2009]:

$$ERP = \frac{1}{2}\rho_f c_f \int_{A_p} v_f \mathrm{d}A_p \tag{2.11}$$

where ρ_f, c_f, v_f and A_p are the fluid density, the speed of sound, particle velocity at the structural surface and the panel area, respectively. Assuming the particle velocity of the fluid v_f to be equal to the normal velocity of the structure at its surface v_s and discretizing the integral into a summation formula for finite element analysis, Eq. 2.11 can be rewritten as follows [Fritze et al., 2009]:

$$ERP = \frac{1}{2}\rho_f c_f \sum_{e=1}^{N_e} A_e v_{se}^2 \tag{2.12}$$

where N_e, A_e and v_{se} are the number of elements, elemental areas and the structural velocity magnitudes at the center of each element, respectively.

In forced vibration analyses, structural damping method is used to account for material damping. Using a structural damping coefficient η, the stiffness matrix is modified as $K^* = K(i\eta + 1)$, where K^* is the complex stiffness matrix providing damping in addition to stiffness properties. When a complex harmonic loading f^* with the circular frequency ω is applied to the system, corresponding complex displacement vector u^* can be obtained by solving:

$$(K^* - \omega^2 M)u^* = f^* \tag{2.13}$$

By differentiating u^*, the complex nodal velocity vector required for ERP calculations can be obtained as $v^* = i\omega u^*$.

2.3.4 Effective Stiffness

In lamination parameters domain, effective laminate stiffnesses in the x and y-directions (E_x^0 and E_y^0) can be obtained using (-) and (+) signs for ($\pm$)'s in Eq. 2.14, respectively, which is given as follows (Gürdal et al. 1999):

$$\frac{E_x^0 + E_y^0}{2} \pm \frac{E_y^0 - E_x^0}{2} = \frac{{U_1}^2 - {U_5}^2 - {U_2}^2{V_1}^2 + 2(U_1U_5)U_3V_3}{U_1 \pm U_2V_1 + U_3V_3} \tag{2.14}$$

Similarly, effective shear stiffness can be written as (Gürdal et al. 1999)

$$G_{xy}^0 = U_5 - V_3U_3 \tag{2.15}$$

For the calculations, the stiffness metrics are normalized as $E_x = E_x^0/E_1$, $E_y = E_y^0/E_2$ and $G_{xy} = G_{xy}^0/G_{12}$. For uni-axial loading in x-direction, the minimization of strains essentially implies maximization of E_x, which is the stiffness in the loading direction. Similarly, bi-axial loading with $N_x/N_y = 1$ requires maximizing the normalized mean stiffness: $\bar{E} = (E_x + E_y)/\max(E_x + E_y)$. To attain minimum shear strain under uniform shear stress, G_{xy} is maximized.

Chapter 3

MULTI–OBJECTIVE OPTIMIZATION OF LAMINATED PLATES

Many composite stacking-sequence optimization studies are concerned with increasing fundamental frequency, buckling load and effective stiffness. Maximization of the fundamental frequency is used to reduce the dynamic response amplitudes of the structures excited with the frequencies up to the fundamental frequency. Increasing buckling load is an important criterion used in the design of plate structures carrying compressive loads. Maximizing the overall stiffness is essentially equivalent to reducing the maximum strain which is a common design objective used to enhance the integrity of load-carrying structures. In particular cases, simultaneous consideration of a multiple of aforementioned metrics is required to improve both dynamic and load-carrying performances. For instance, in the design of aircraft panels, maximization of fundamental frequency, buckling load and effective stiffness can be all important.

There are many available optimization studies which take maximization of the fundamental frequency as the design objective. For instance, [Bert, 1977] developed a closed-form formula for simply-supported thin rectangular laminated plates based on the classical lamination theory. He used it to maximize the fundamental frequency of symmetric and balanced laminates by choosing fiber orientation angles as design variables. [Narita and Robinson, 2006] conducted a layerwise optimization to obtain the maximum fundamental frequency for laminated composite panels using Ritz method to calculate the natural frequencies. [Apalak et al., 2008] calculated the fundamental frequencies of laminated composite plates using an artificial neural network model which is trained by finite element analyses. They utilized a genetic algorithm

to find optimal laminate configurations providing maximum frequencies for various edge conditions.

Optimization of composite panels to increase buckling load is also extensively covered in the literature. [Hirano, 1979] analyzed laminated plates with orthotropic, equally thick layers subjected to uni-axial and bi-axial compression. He computed optimal layer angles maximizing critical buckling load using an analytical relation for different panel aspect ratios, number of layers and load ratios. [Hu and Lin, 1995] investigated the effects of panel aspect ratio and boundary conditions on buckling optimization of symmetrically laminated plates. They used finite element analyses and sequential linear programming method to calculate the optimal responses. [Erdal and Sonmez, 2005] determined optimum laminate stacking-sequences for maximum laminate buckling load capacity using analytical expressions together with simulated annealing algorithm. They were able to obtain a number of coequal optimal designs using the search algorithm which circumvents termination at the local minima.

Overall stiffness maximization of laminated composites is similarly investigated by many researchers. For example, [Kam and Lai, 1995] maximized the stiffness of laminated composite plates by determining the optimal fiber angles and layer thicknesses. In their work, they used shear deformable finite elements and augmented Lagrangian method for optimization. [Gürdal et al., 2008] introduced the concept of using curvilinear fibers within the laminates which allows variable-stiffness properties. They employed a uni-directional variation based on a linear function to define the fiber orientation angles of the individual layers. For flat rectangular composite laminates, they calculated overall panel stiffness and buckling load for different design parameters to demonstrate the trade-off between these responses.

In several studies, lamination parameters are used as design variables instead of number of layers, layer angles, and thicknesses to formulate the problem in a more compact way and avoid local optima. For maximization of the fundamental frequency, [Fukunaga et al., 1994] performed layup optimization of symmetrically laminated plates based on classical laminated plate theory (CLPT) by formulating

the responses in terms of lamination parameters. [Diaconu et al., 2002] conducted a similar study for thick panels by using First-order Shear Deformation Theory (FSDT) and compared the results with the ones obtained via CLPT. [Abdalla et al., 2007] also used lamination parameters in their optimization study to maximize the fundamental frequency of variable-stiffness laminated plates. [Serhat and Basdogan, 2018] calculated the fundamental frequency contours of curved panels in lamination parameter plane using finite element analyses. They investigated the combined effects of panel aspect ratio, curvature and boundary conditions on the maximum frequency points. Considering buckling, [Fukunaga et al., 1995] obtained the contours of uni-axial and shear buckling loads for square plates, on the feasible region of lamination parameter plane. [Grenestedt, 1991] found optimal lamination parameters providing maximum buckling load for shear panels of various aspect ratios. [Ijsselmuiden et al., 2010] also used lamination parameters to maximize buckling load but they extended the approach for variable-stiffness panels. Regarding the maximum effective stiffness requirements, [Fukunaga and Sekine, 1992] demonstrated the contours of in-plane and coupling stiffness components for symmetric laminates as a function of lamination parameters. They also proposed a method for determining laminate configurations corresponding to the lamination parameters. [Miki and Sugiyama, 1993] used lamination parameters for optimal stiffness design of orthotropic laminates. They showed contour plots of strain energy within the feasible design space for plates undergoing bending due to centrally applied concentrated load. They also calculated optimal laminate configurations providing maximum bending stiffness as a function of plate aspect ratio. [Setoodeh et al., 2006] investigated the optimal design of fiber reinforced rectangular composite plates for minimum compliance design problem for variable-stiffness laminates in lamination parameters space. They showed that significant improvements in stiffness can be obtained compared to constant-stiffness designs by using variable-stiffness laminates.

In multi-objective optimization studies, different metrics frequently require different optimal designs. On this matter, several multi-objective laminate optimiza-

tion studies have been conducted to improve both dynamic and load-carrying performance. For instance, [Kam and Chang, 1993] performed a layerwise optimization study to find maximum buckling load and maximum vibration frequency for thick laminated composite plates using FEM together with weighted-sum optimization method. They investigated effects of side-to-thickness ratio, aspect ratio and numbers of layers for simply-supported symmetrically and antisymmetrically laminated plates exposed to uni-axial compression. [Abouhamze and Shakeri, 2007] also used weighted-sum method for the maximization of first natural frequency and critical buckling load of cylindrical panels. One shortcoming of weighted-sum optimization is obtaining only a single solution instead of a set of nondominated solutions. As a more general approach, [Nik et al., 2012] carried out optimization studies to find Pareto-optimal solutions for maximizing overall stiffness and buckling load of a composite laminate plate with curvilinear fiber paths by varying the fiber orientations. They demonstrated the conflicting behavior of overall stiffness and buckling load when they are used together as the performance metrics. [Serhat et al., 2016] conducted a multi-objective lamination parameter optimization study to maximize fundamental frequency and effective stiffness using weighted-sum optimization approach. They investigated the effects of the weight coefficients on the optimal design points.

Although Pareto-optimal solutions for multi-objective optimization of fiber-reinforced composites have been studied in the literature, lamination parameters have not been used as the parametrization technique in the existing studies. In this chapter, a multi-objective design optimization framework for dynamic and load-carrying requirements of laminated composite plates is introduced. Laminate stiffness properties are represented and optimized using lamination parameters as design variables. Maximization of the fundamental frequency, buckling load, and effective stiffness are chosen as the design objectives. Pareto-optimal solutions are determined for the first time for different combinations of design objectives using lamination parameters. Two different panel aspect ratios and three different load cases are considered. The results are visualized on Miki's lamination diagram to provide an insight into potential solutions

for multi-objective optimization problems. Significant changes in the trends of the optimal solutions in the lamination parameters domain are demonstrated for different problem types.

3.1 Single–objective Optimization Results

In general, gradient-based optimization algorithms work very well with the lamination parameter formulation due to convex nature of the design space. However, in addition to determining the optimal design points, obtaining the response contours is also aimed in this study to provide a broader insight. For this reason, a full-factorial search with a resolution of 0.05 in the lamination parameter variables is applied ensuring the complete exploration of the design space.

In this section, the results regarding single-objective optimization of composite panels are presented. Each performance metric is investigated for the simply-supported and clamped panels with two different panel aspect ratios. In addition, different load cases are considered for maximum critical buckling coefficient and maximum effective stiffness metrics. The panel thickness-to-length ratio (h/a) is held constant at 0.01 complying with the thin plate assumption. The plate material is chosen as carbon fiber-reinforced epoxy with the properties given in Table 3.1 [Fukunaga et al., 1994]. The response data obtained for individual metrics is also used as the input for the multi-objective optimization studies performed in the next section.

Table 3.1: Material properties of unidirectional carbon-epoxy composite laminate

E_1(GPa)	142.0
E_2(GPa)	10.8
G_{12}(GPa)	5.49
ν_{12}	0.3
ρ(kg/m^3)	1.6

3.1.1 Fundamental Frequency Maximization

In the following, the maximum value of fundamental frequency is searched. The calculated frequency values are normalized using the frequency parameter ω^* defined as [Fukunaga et al., 1994]

$$\omega^* = \frac{\omega_n b^2}{\pi^2 h}\sqrt{\frac{12\rho}{Q_{22}}} \tag{3.1}$$

where ρ is the laminate density. Figure 3.1 shows the non-dimensional fundamental natural frequency contours for a balanced and symmetric plates as a function of lamination parameters V_1 and V_3 for different aspect ratios and boundary conditions. The contour plots agree with the ones presented in [Fukunaga et al., 1994]. One should

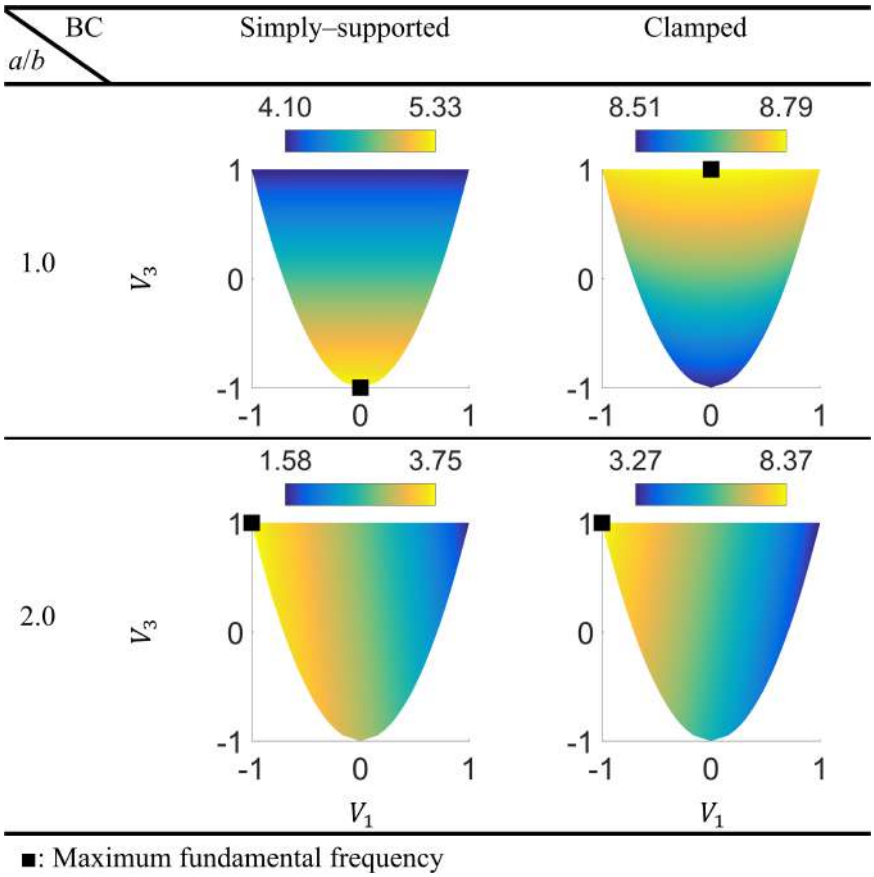

Figure 3.1: Fundamental frequency parameter $\omega^* = \omega_n b^2\sqrt{12\rho/Q_{22}}/(\pi^2 h)$ contours on lamination parameter plane for simply-supported and clamped panels with different aspect ratios.

note the convex nature of the response surfaces resulting from modeling in lamination parameters domain. The maximum fundamental frequency points are indicated by black squares. The variables at the optimum points are denoted by "opt" superscript. Table 3.2 shows the calculated optimal values and the ones from [Fukunaga et al., 1994] presented for validation purposes. The results are in almost perfect agreement. When the optimal solutions lie on the lower boundary of Miki's lamination diagram, they can only be obtained by specific layer angles which can be calculated using Eq. 2.6. In such instances, the optimal laminate angles (θ^{opt}'s) are also presented in the results together with optimal lamination parameters. In the current case, the optimum angle for $a/b = 1.0$ is 45° for simply-supported panels. However, for clamped panels, the optimum point lies on the upper boundary which cannot be obtained by single-angle laminates. For $a/b = 2.0$, 90° laminates are required for both boundary conditions which is a common result for high aspect ratio panels [Serhat et al., 2016]. The fundamental mode shapes for the maximum fundamental frequency designs are shown in Fig. 3.2.

Table 3.2: Optimal design points yielding maximum fundamental frequency values and corresponding layer angles for simply-supported and clamped panels with different aspect ratios

a/b		Simply-supported				Clamped			
		V_1^{opt}	V_3^{opt}	θ^{opt}	ω^{*opt}	V_1^{opt}	V_3^{opt}	θ^{opt}	ω^{*opt}
1.0	Present FE	0.0	-1.0	45°	5.33	0.0	1.0	N.A.	8.79
	Fukunaga and Sekine (1994)	0.0	-1.0	45°	5.32	0.0	1.0	N.A.	8.77
2.0	Present FE	-1.0	1.0	90°	3.75	-1.0	1.0	90°	8.37
	Fukunaga and Sekine (1994)	-1.0	1.0	90°	3.73	-1.0	1.0	90°	8.31

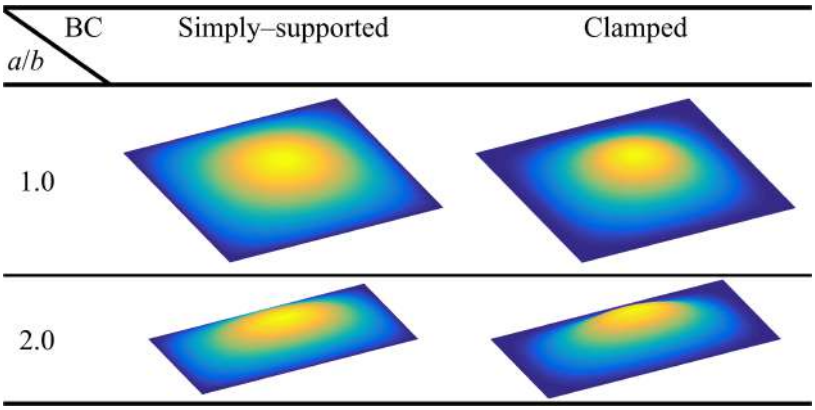

Figure 3.2: Fundamental mode shapes of simply-supported and clamped panels with different aspect ratios for the maximum fundamental frequency designs.

3.1.2 Buckling Load Maximization

For the buckling analyses, 3 different unit load cases are considered: uni-axial loading, bi-axial loading with $N_x/N_y = 1$ and shear loading which are illustrated in Fig. 3.3. The critical buckling coefficient contours for simply-supported panels are presented in Fig. 3.4. The sharp bends occurring on the responses originate from the change of buckling modes characterized by the number of half-waves in x and y-directions denoted by m and n, respectively. For example, for $a/b = 1.0$ and uni-axial loading, buckling occurs with ($m = 2$, $n = 1$) in the vicinity of ($V_1 = -1.0$, $V_3 = 1.0$) corner, where for the remaining region it occurs with ($m = 1$, $n = 1$). The optimum points resulting in maximum buckling load are denoted by red diamonds. The values of the design parameters and responses at the optimum points are tabulated in Table 3.3, together with the results from [Fukunaga et al., 1995]. As the results show, all load cases require ($V_1^{opt} = 0.0$, $V_3^{opt} = -1.0$) as optimal solution which is the same point yielding the maximum fundamental frequency for the simply-supported square panel. However, for $a/b = 2.0$, the optimum point changes for bi-axial and shear loading cases conforming to results of [Fukunaga et al., 1995]. Figure 3.5 shows the critical buckling modes for the simply-supported panels with the maximum buckling load designs.

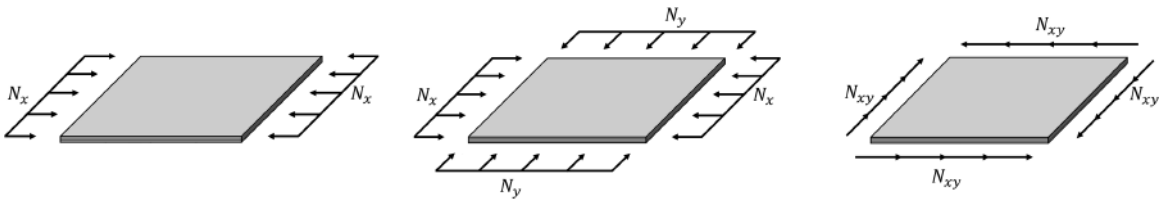

(a) Uni–axial loading (b) Bi–axial loading (c) Shear loading

Figure 3.3: Load cases used for the buckling analyses.

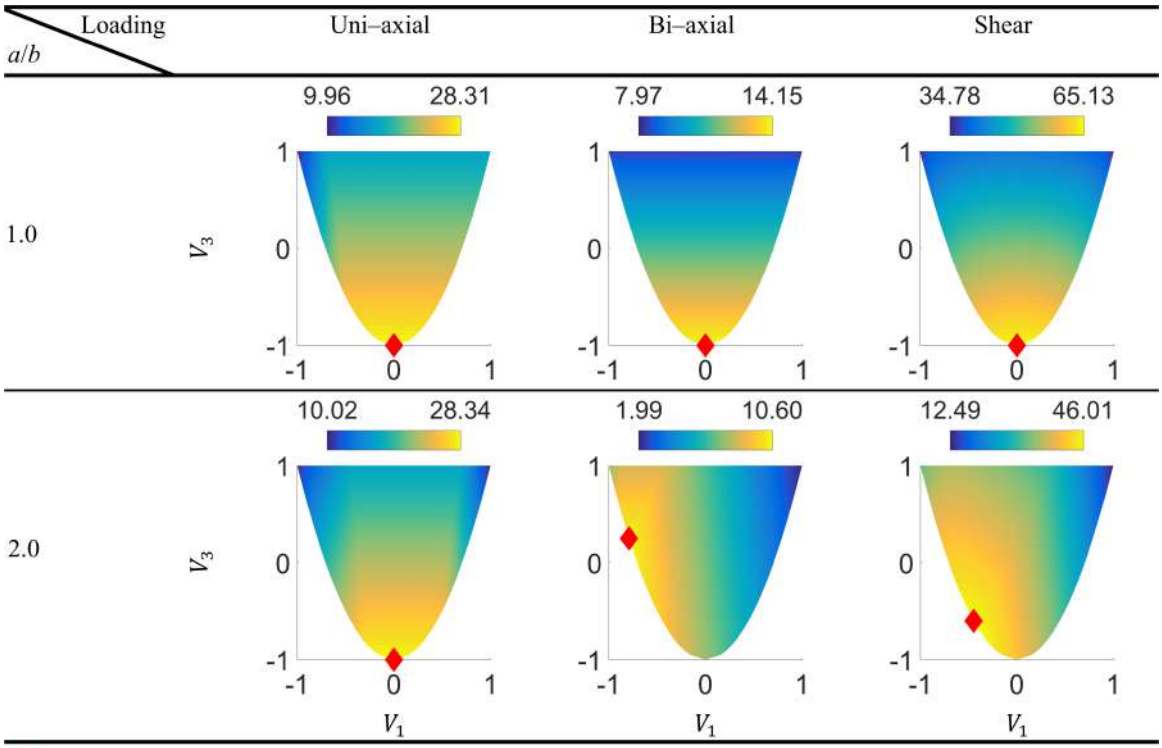

Figure 3.4: Critical buckling coefficient contours in lamination parameter plane for simply-supported panels subjected to different loadings.

Figure 3.6 and Table 3.4 show the critical buckling coefficient contours and tabulated optimal results for clamped panels, respectively. The results demonstrate the significant changes in the critical buckling coefficient contours and the optimal designs occurring with the alteration of the boundary conditions. Figure 3.7 shows the critical buckling modes for the clamped panels with the maximum buckling load designs.

Table 3.3: Optimal design points yielding maximum critical buckling coefficient values and corresponding layer angles for simply-supported panels of different aspect ratios

a/b		Uni-axial				Bi-axial				Shear			
		V_1^{opt}	V_3^{opt}	$\pm\theta^{opt}$	λ_{cr}^{opt}	V_1^{opt}	V_3^{opt}	$\pm\theta^{opt}$	λ_{cr}^{opt}	V_1^{opt}	V_3^{opt}	$\pm\theta^{opt}$	λ_{cr}^{opt}
1.0	Present FE	0.0	-1.0	45°	28.31	0.0	-1.0	45°	14.15	0.0	-1.0	45°	65.13
	Fukunaga and Sekine (1995)	0.0	-1.0	45°	28.30	N.A.	N.A.	N.A.	N.A.	0.0	-1.0	45°	63.88
2.0	Present FE	0.0	-1.0	45°	28.34	-0.791	0.250	71.12°	10.60	-0.447	-0.600	58.28°	46.01
	Fukunaga and Sekine (1995)	0.0	-1.0	45°	28.30	N.A.	N.A.	N.A.	N.A.	-0.391	-0.695	56.50°	44.61

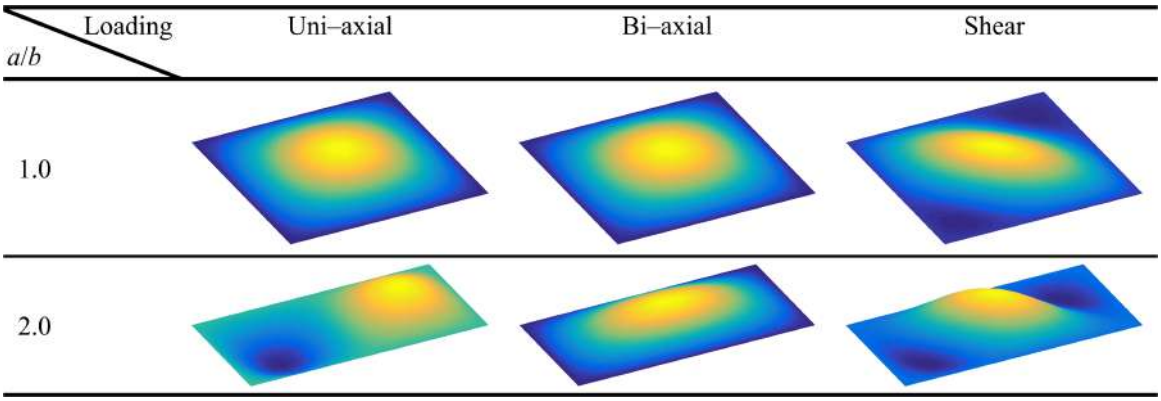

Figure 3.5: Critical buckling modes for the simply-supported panels with the maximum buckling load designs.

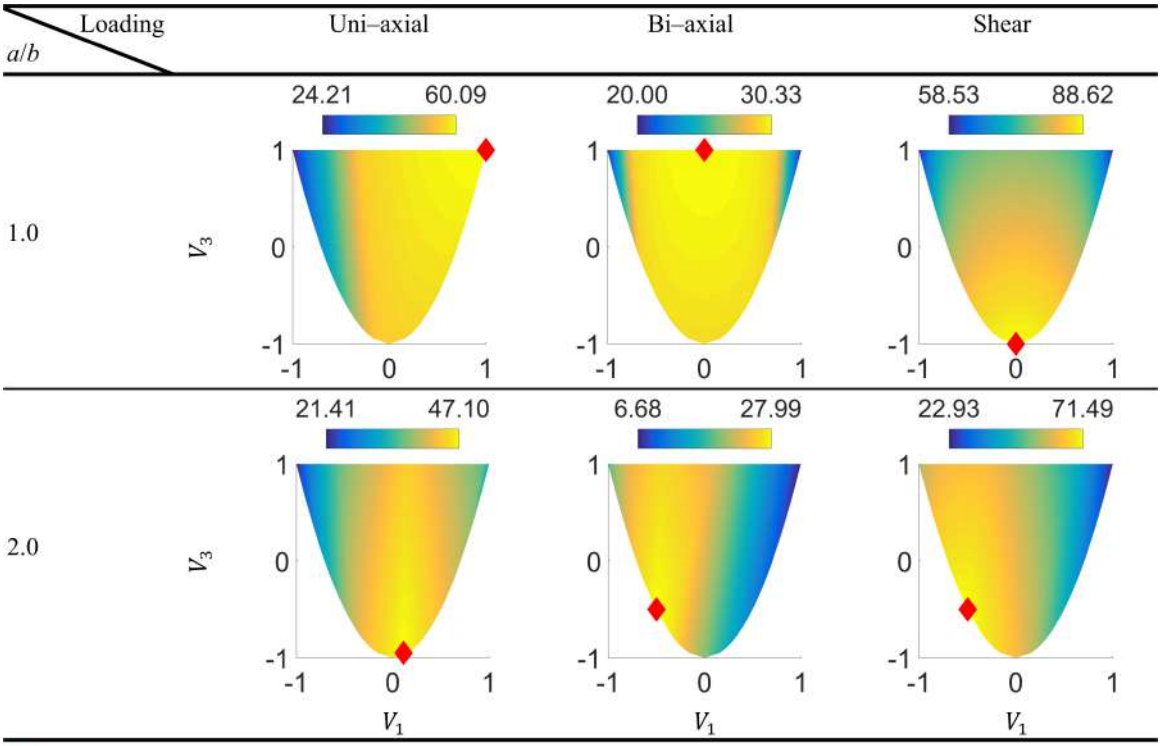

Figure 3.6: Critical buckling coefficient contours in lamination parameter plane for clamped panels subjected to different loadings.

Table 3.4: Optimal design points yielding maximum critical buckling coefficient values and corresponding layer angles for clamped panels of different aspect ratios

a/b		Uni-axial				Bi-axial				Shear			
		V_1^{opt}	V_3^{opt}	$\pm\theta^{opt}$	λ_{cr}^{opt}	V_1^{opt}	V_3^{opt}	$\pm\theta^{opt}$	λ_{cr}^{opt}	V_1^{opt}	V_3^{opt}	$\pm\theta^{opt}$	λ_{cr}^{opt}
1.0	Present FE	1.0	1.0	0°	60.09	0.0	1.0	N.A.	30.33	0.0	-1.0	45°	88.62
	Fukunaga and Sekine (1995)	1.0	1.0	0°	59.66	N.A.	N.A.	N.A.	N.A.	0.0	-1.0	45°	89.08
2.0	Present FE	0.113	-0.950	41.76°	47.10	-0.5	-0.5	60.0°	27.99	-0.5	-0.5	60.0°	71.49
	Fukunaga and Sekine (1995)	0.108	-0.977	41.90°	47.39	N.A.	N.A.	N.A.	N.A.	-0.503	-0.494	60.1°	69.17

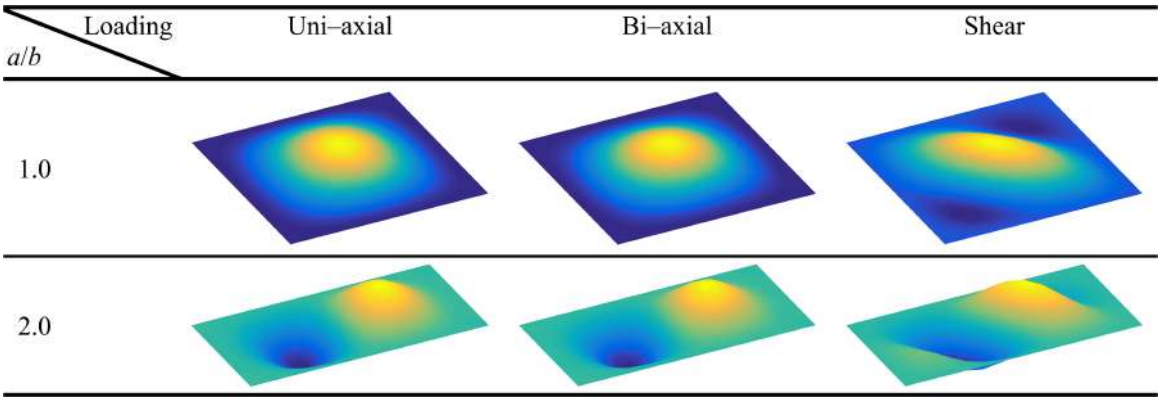

Figure 3.7: Critical buckling modes for the clamped panels with the maximum buckling load designs.

3.1.3 Effective Stiffness Maximization

Figure 3.8 shows the contours of effective stiffnesses: E_x, $\bar{E}$ and G_{xy} in lamination parameter plane. The optimal solutions are marked by magenta triangles, and their values are tabulated in Table 3.5. The optimum points for E_x and G_{xy} are ($V_1^{opt} = 1.0$, $V_3^{opt} = 1.0$) and ($V_1^{opt} = 0.0$, $V_3^{opt} = -1.0$) which correspond to 0° and ±45° laminates, respectively. For $\bar{E}$, the optimum is located at ($V_1^{opt} = 0.0$, $V_3^{opt} = 1.0$) which is only obtainable by [0° 90°] laminates.

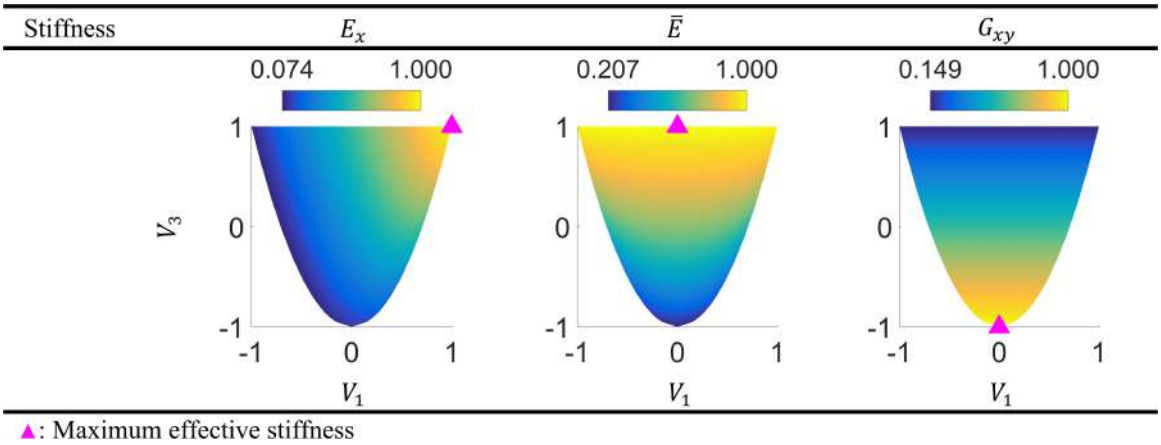

Figure 3.8: Contours of effective stiffnesses: E_x, $\bar{E}$ and G_{xy} in lamination parameter plane.

Table 3.5: Optimal design points yielding maximum effective stiffness values and corresponding layer angles

E_x				$\bar{E}$				G_{xy}			
V_1^{opt}	V_3^{opt}	θ^{opt}	E_x^{opt}	V_1^{opt}	V_3^{opt}	θ^{opt}	$\bar{E}^{opt}$	V_1^{opt}	V_3^{opt}	θ^{opt}	G_{xy}^{opt}
1.0	1.0	0.0	1.0	0.0	1.0	N.A.	1.0	0.0	-1.0	45°	1.0

3.2 Multi–objective Optimization Results

In multi-objective optimization studies, it is common that different objective functions require different optimal designs. In such cases, the set of best compromises among all the possible designs is called Pareto set which contains the non-dominated design points [Deb, 2001]. The best design points imply that the value of an objective in the set cannot be further improved without worsening at least one other objective value. Depending on the priorities, any point on the Pareto set can be regarded as the optimum.

In this section, multi-objective optimization results for combinations of maximum fundamental frequency, maximum critical buckling coefficient, and maximum effective stiffness are presented. Pareto-optimal solutions are determined, firstly for each binary combinations of objectives, and finally for all three objectives.

3.2.1 Fundamental Frequency and Buckling Load Maximization

Figure 3.9 shows Pareto-optimal points for maximum fundamental natural frequency and buckling coefficient considering simply-supported panels. The rows show the results for different panel aspect ratios where the columns represent different load cases. Maximum fundamental frequency and maximum critical buckling coefficient are indicated by black squares and red diamonds, respectively. Pareto-optimal points excluding the individual optimal points are designated by cyan circles. For the square panel, optimum point is ($V_1^{opt} = 0.0$, $V_3^{opt} = -1.0$) for both fundamental frequency and critical buckling coefficient for all load cases resulting in a single global optimum.

However, for $a/b = 2$, different requirements of individual performance metrics results in a Pareto set containing multiple points. By choosing a point from Pareto set, the designer makes a compromise between the values of individual performance metrics. In this particular problem, the Pareto-optimal points are located on the boundary of Miki's diagram. Hence, each point corresponds to a specific laminate angle which lie on the intervals: [±45°,90°], [±71.12°,90°], [±58.28°,90°] for uni-axial, bi-axial and shear loading, respectively.

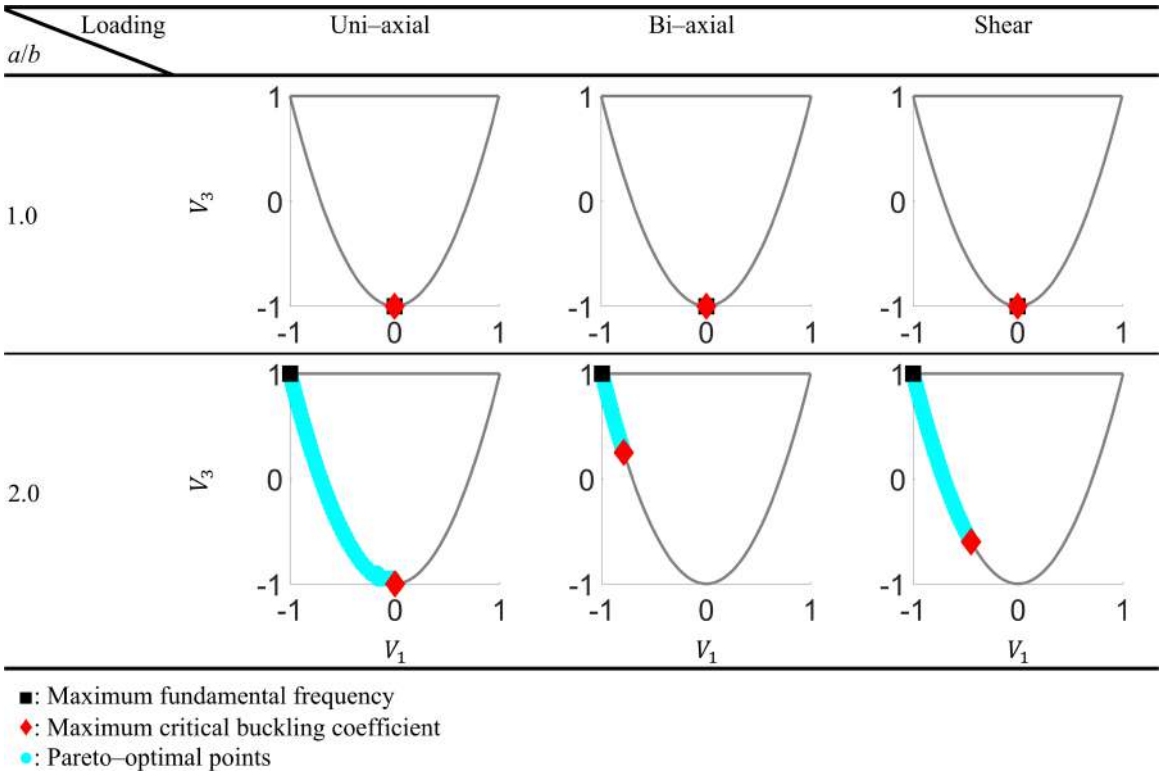

Figure 3.9: Pareto-optimal points for maximum fundamental natural frequency and critical buckling coefficient considering simply-supported panels subjected to different loadings.

Note that, optimum design for the maximum natural frequency may change due to pre-stressing effects caused by the loading used for the buckling and static analyses. However, under real operating conditions, the loading may fluctuate and even change sign. Therefore, it is reasonable to consider the unstressed panels for the fundamental frequency maximization.

Figure 3.10 shows Pareto-optimal points for maximum fundamental natural frequency and buckling coefficient considering clamped panels. For clamped boundary conditions, the conflict between the maximum fundamental frequency and maximum critical buckling coefficient points is greater. This fact can be seen by examining the newly formed Pareto-optimal points for the square panels under uni-axial and shear loading. In addition, the Pareto-optimal points do not always lie on the boundary of Miki's diagram in this case. This characteristic of the multi-objective optimization solutions is clearly different than that of single-objective solutions which ordinarily require single-angle laminates as shown in the previous section and also demonstrated by [Grenestedt, 1990]. Since the interior points in the diagram require at least two layer angles, a more elaborate stacking-sequence retrieval process is required for those points. One should also notice the deviation of the interior Pareto-optimal solutions

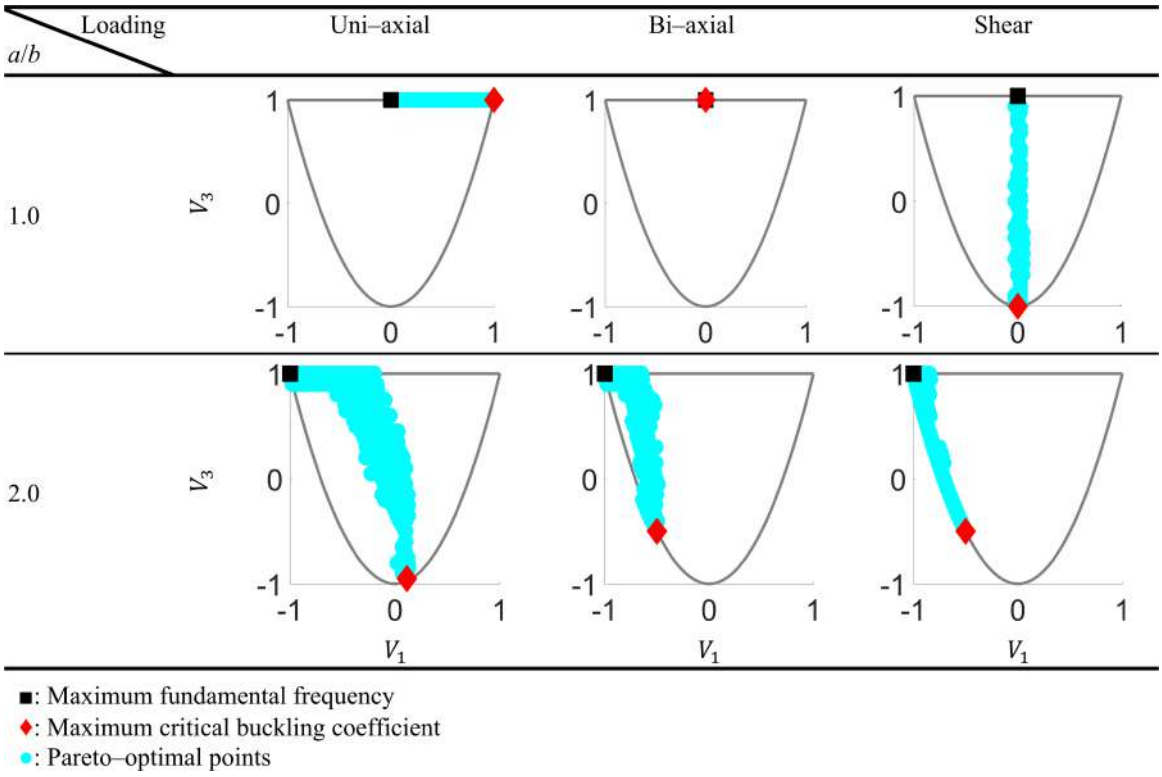

Figure 3.10: Pareto-optimal points for maximum fundamental natural frequency and critical buckling coefficient considering clamped panels subjected to different loadings.

from the line which interpolates lamination parameter values for individual optimum points, which is observed for uni-axial and bi-axial loading. In such cases, the optimal design candidates which are not exactly located in the vicinity of the line interpolating the individual optimal design parameters can be overlooked. Therefore, obtaining the Pareto sets with sufficient resolution of design variable increments is clearly important for the detection of the all optimal solutions.

3.2.2 Fundamental Frequency and Effective Stiffness Maximization

Figures 3.11 and 3.12 show Pareto-optimal points for maximum fundamental natural frequency and effective stiffnesses considering simply-supported and clamped panels, respectively. For this combination of performance metrics, the interior Pareto-optimal points are located around the line interpolating the individual optimum points.

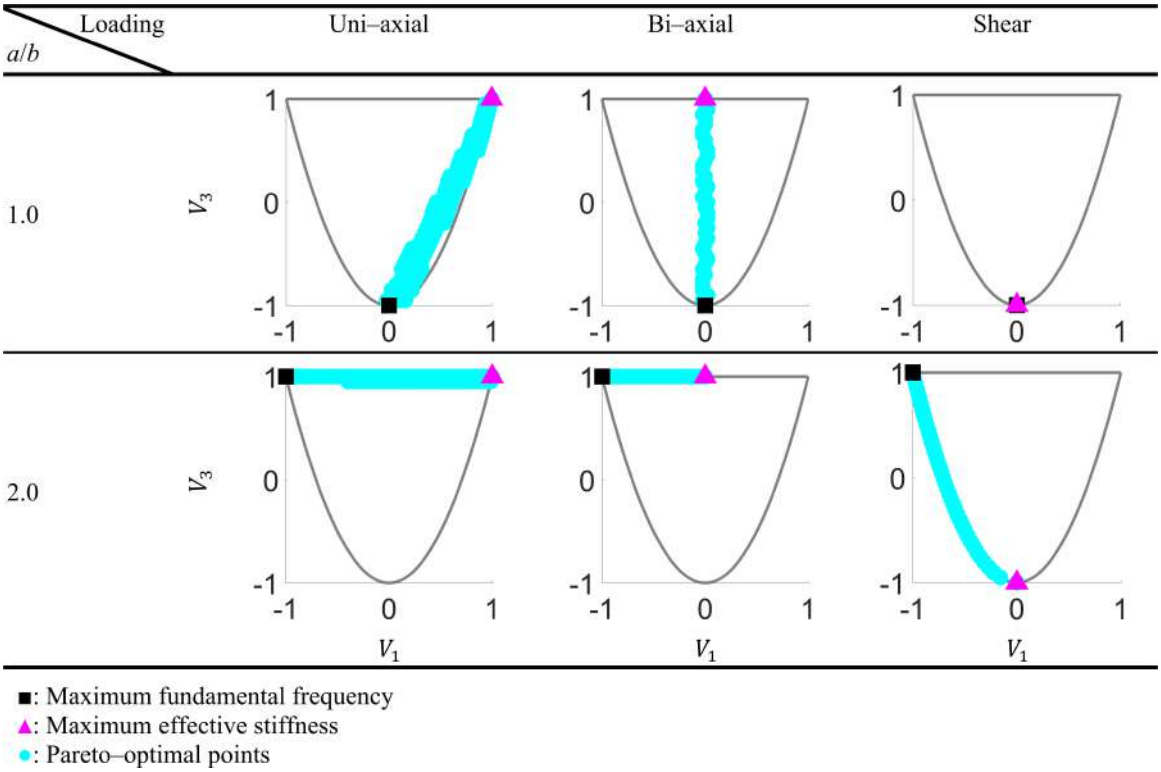

Figure 3.11: Pareto-optimal points for maximum fundamental natural frequency and effective stiffnesses considering simply-supported panels subjected to different loadings.

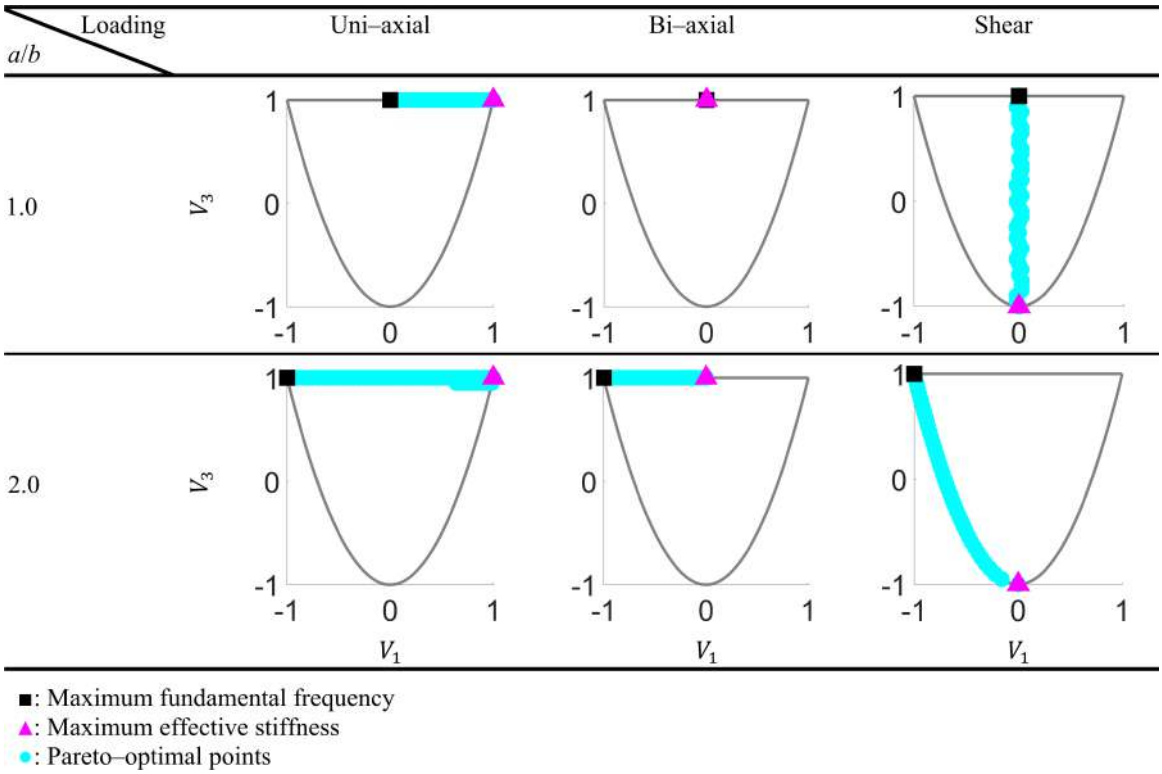

Figure 3.12: Pareto-optimal points for maximum fundamental natural frequency and effective stiffnesses considering clamped panels subjected to different loadings.

3.2.3 Buckling Load and Effective Stiffness Maximization

Pareto-optimal points for maximum buckling coefficient and effective stiffness considering simply-supported and clamped panels are presented in Figs. 3.13 and 3.14, respectively. For this combination of objectives, sharp changes in the optimal solution trends occur for the panels with $a/b = 2.0$ under uni-axial and bi-axial loading. This behavior is a result of the sharp bends on critical buckling coefficient response surface originating from the change of critical buckling mode indices (see Sect. 3.1.2). One should also note that, for the square clamped panels, optimal points for critical buckling coefficient and effective stiffness metrics are the same for all loading cases.

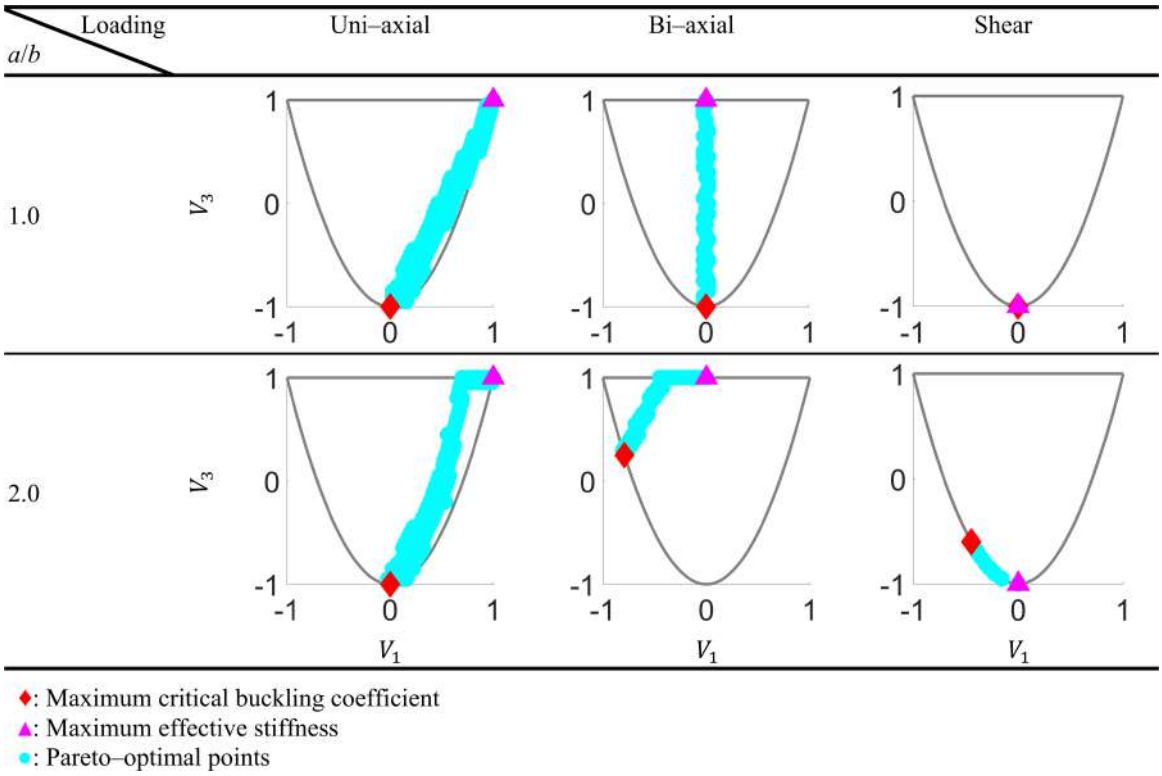

Figure 3.13: Pareto-optimal points for maximum critical buckling coefficient and effective stiffnesses for simply-supported panels subjected to different loadings.

3.2.4 Fundamental Frequency, Buckling Load and Effective Stiffness Maximization

As the ultimate optimization case, fundamental frequency (ω^*), buckling load (λ_{cr}) and effective stiffness (E) are aimed to be maximized, simultaneously. Figure 3.15 shows the Pareto-optimal solutions for this problem considering simply-supported panels. The results indicate that usage of 3 objectives may produce considerably enlarged Pareto sets, especially for higher aspect ratios. The Pareto sets for this problem appear to be a "filled" version of a frame consisting of 3 edges which are actually the Pareto sets belonging to each binary combinations of design objectives. Note that, binary Pareto sets can be considered as edges since the individual objectives are connected by the Pareto-optimal points which is a result of continuous response surfaces. When individual optimum points are located far away from each other, such as for panel with aspect ratio 2.0 under uni-axial loading, Pareto set gets too

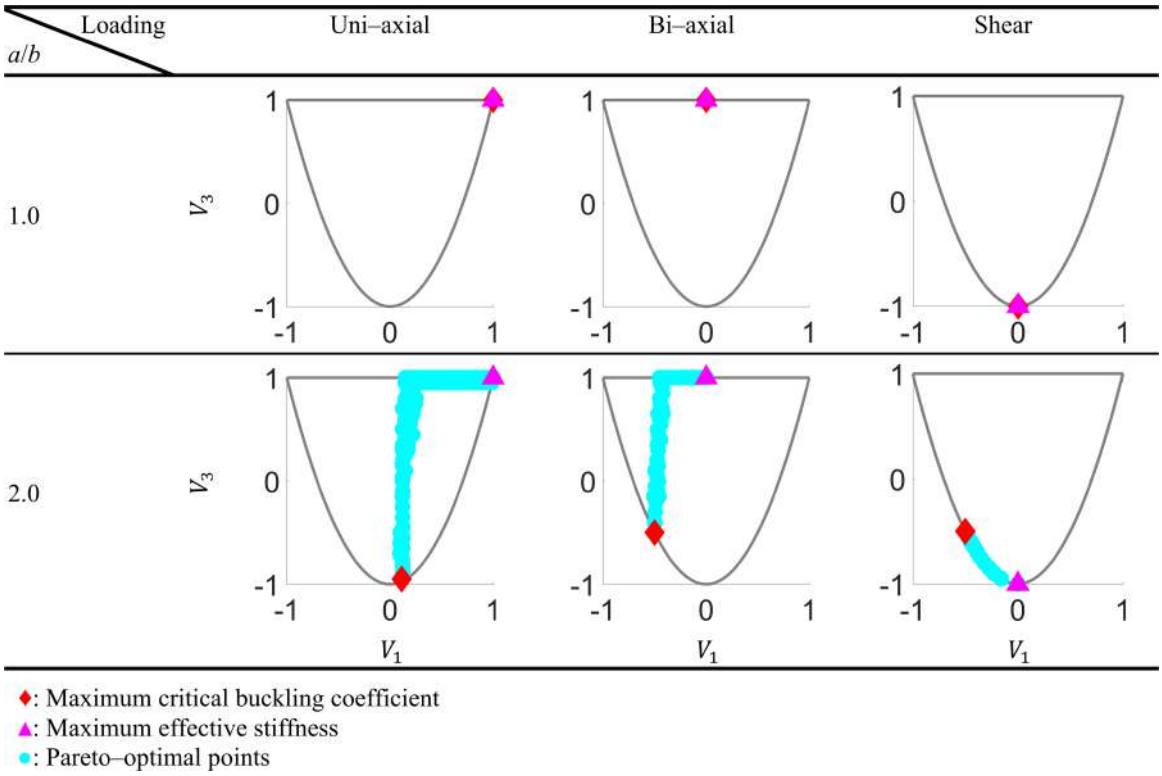

Figure 3.14: Pareto-optimal points for maximum critical buckling coefficient and effective stiffnesses for clamped panels subjected to different loadings.

crowded. In such cases, additional constraints on the objective function or design variable values can be applied to reduce the number of optimal design candidates.

In Table 3.6, the percentage changes in the fundamental frequency, critical buckling coefficient and effective stiffness metrics of the simply-supported panels are presented for the optimal point of each metric. The rows of the first column stand for the design point in consideration. The sub-rows contain the percentage changes for the specified performance metrics compared to the baseline values. The baseline laminate configuration is selected as quasi-isotropic laminate with ($V_1 = 0.0$, $V_3 = 0.0$) which is indicated by magenta asterisk in Fig. 2.3. The results show that the optimal solutions for different performance metrics can strongly conflict each other, as the increase in a certain metric can lead to a significant decrease in another one. Thus, finding Pareto sets for such multi-objective laminate optimization problems is important to detect

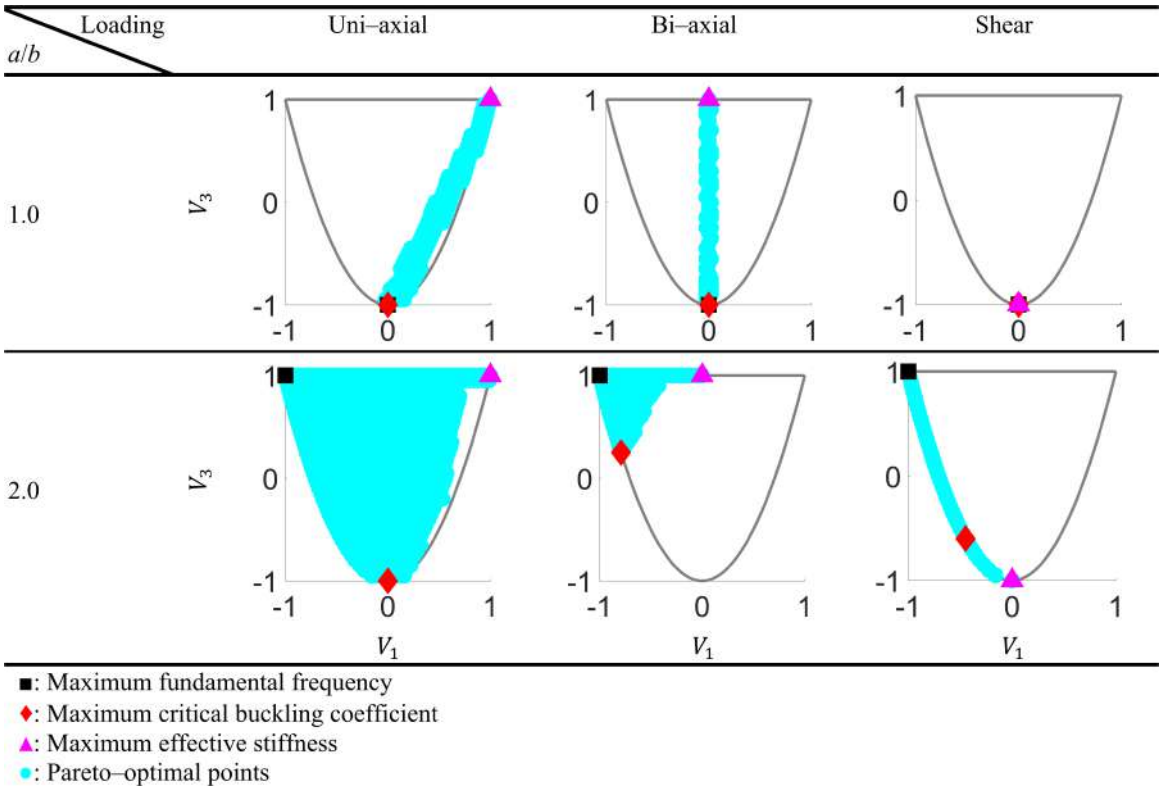

Figure 3.15: Pareto-optimal points for maximum fundamental frequency, critical buckling coefficient and effective stiffnesses considering simply-supported panels subjected to different loadings.

all the optimal solution candidates and find the best compromise among them. One should also remark that, for the square panels under shear loading, a single optimum point is detected considering all the objectives.

Figure 3.16 shows Pareto-optimal points for maximum fundamental frequency, critical buckling coefficient and effective stiffnesses considering clamped panels. Although their distribution is different, the large Pareto sets also appear for this case. Only for the square panels under bi-axial loading, a single optimum point is found. In Table 3.7, the percentage changes in the fundamental frequency, critical buckling coefficient and effective stiffness metrics of the clamped panels are presented for the optimal point of each metric.

Table 3.6: Relative to the baseline values, the percentage changes in the fundamental frequency (ω^*), critical buckling coefficient (λ_{cr}) and effective stiffness (E) at the optimal point of each metric considering simply-supported panels

		$a/b = 1.0$			$a/b = 2.0$		
Design point	Metric	Uni-axial	Bi-axial	Shear	Uni-axial	Bi-axial	Shear
ω^{*opt}	ω^*	12.21%	12.21%	12.21%	25.42%	25.42%	25.42%
	λ_{cr}	25.49%	25.44%	21.49%	-55.32%	5.64%	-18.11%
	E	-70.65%	-70.64%	73.91%	-80.26%	39.86%	-74.09%
λ_{cr}^{opt}	ω^*	12.21%	12.21%	12.21%	-55.52%	22.07%	15.38%
	λ_{cr}	25.49%	25.44%	21.49%	25.12%	49.51%	20.07%
	E	-70.65%	-70.64%	73.91%	-70.65%	-28.37%	44.35%
E^{opt}	ω^*	-13.68%	-13.68%	12.21%	-47.16%	-3.68%	3.34%
	λ_{cr}	-25.53%	-25.53%	21.49%	-55.76%	-6.91%	7.57%
	E	159.74%	41.84%	73.91%	159.74%	41.84%	73.91%

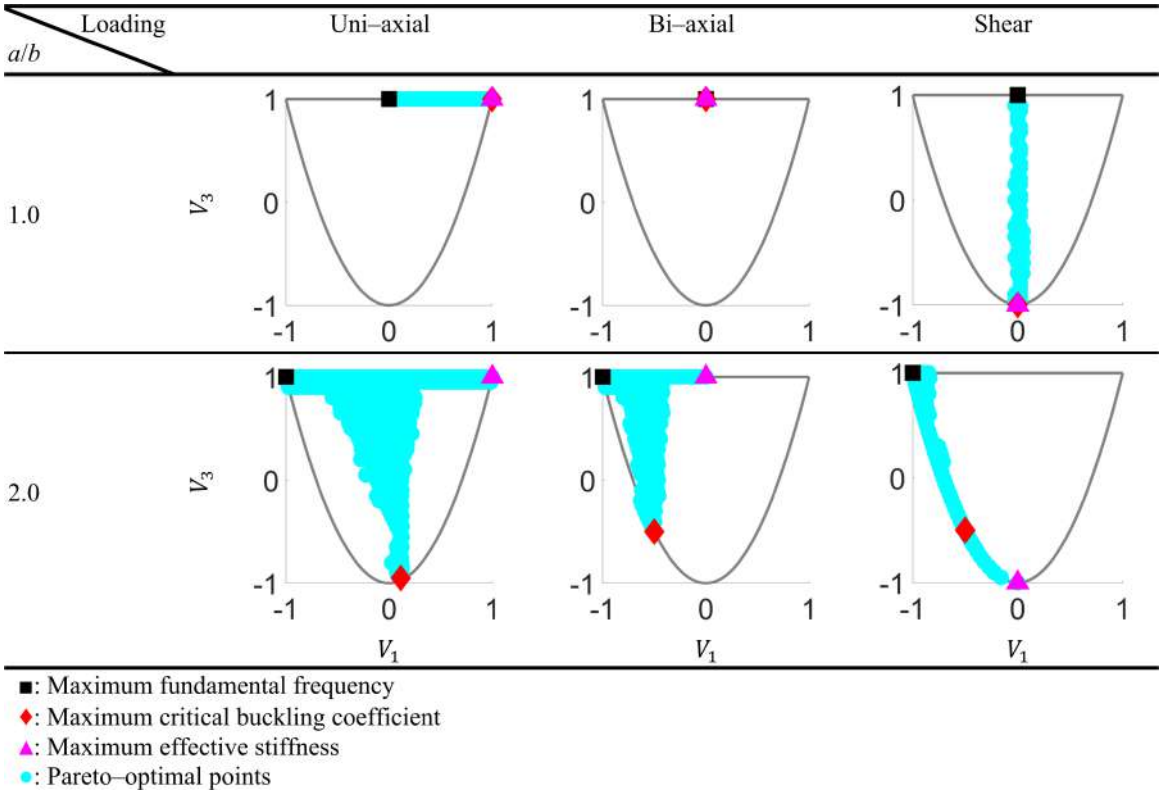

Figure 3.16: Pareto-optimal points for maximum fundamental frequency, critical buckling coefficient and effective stiffnesses considering clamped panels subjected to different loadings.

Table 3.7: Relative to the baseline values, the percentage changes in the fundamental frequency (ω^*), critical buckling coefficient (λ_{cr}) and effective stiffness (E) at the optimal point of each metric considering clamped panels

		$a/b = 1.0$			$a/b = 2.0$		
Design point	Metric	Uni-axial	Bi-axial	Shear	Uni-axial	Bi-axial	Shear
ω^{*opt}	ω^*	1.38%	1.38%	1.38%	39.50%	39.50%	39.50%
	λ_{cr}	1.36%	0.09%	-7.61%	-52.24%	-19.79%	-8.71%
	E	41.82%	41.84%	-74.09%	-80.26%	39.86%	-74.09%
λ_{cr}^{opt}	ω^*	1.20%	1.38%	-1.85%	12.33%	15.50%	15.50%
	λ_{cr}	25.49%	0.09%	21.49%	5.06%	22.28%	16.57%
	E	159.74%	41.84%	73.91%	-62.08%	-48.23%	36.87%
E^{opt}	ω^*	1.20%	1.38%	-1.85%	-45.50%	6.50%	-7.50%
	λ_{cr}	25.49%	0.09%	21.49%	-29.47%	4.67%	2.84%
	E	159.74%	41.84%	73.91%	159.74%	41.84%	73.91%

Chapter 4

DESIGN OF CURVED LAMINATED PANELS FOR OPTIMAL DYNAMIC RESPONSE

Design of composites panels for obtaining optimum dynamic response can be achieved by employing several approaches. Late–stage solutions involving the application of additional stiffening components and damping materials require a secondary engineering process and introduce extra structural weight. Hence, the design methods that rely on stiffness tailoring have certain advantages. One conventional method is the maximization of the frequency gap between adjacent natural frequencies of the structure neighboring excitation frequency range which is utilized in the studies: [Adali and Verijenko, 2001], [Farshi and Rabiei, 2007]. For relatively low excitation frequencies, typically, maximization of the fundamental frequency is used. For instance, [Bert, 1977] maximized the fundamental frequency of symmetric and balanced laminates by choosing fiber orientation angles as design variables. He used an analytical formula based on the classical lamination theory that he derived for simply–supported thin rectangular laminated plates. Many other studies rely on numerical solutions to handle various panel geometries, boundary conditions for which closed–form relations are not available. For example, [Narita, 2003] used Ritz method to calculate the natural frequencies of laminated composite plates. He conducted a layer–wise optimization to obtain the maximum fundamental frequency. [Hu and Peng, 2013] performed finite element analyses within an optimization framework based on golden section method to maximize the fundamental natural frequency of laminated cylindrical panels. In several recent studies, more advanced elements are utilized for the analysis of curved composite structures. For instance, [Fazzolari, 2014] carried out free vibration analysis of curved laminated shallow shells by using dynamic

stiffness elements based on higher–order shear deformation theory (HSDT). [Orefice et al., 2017] proposed a mechanical model composed of 2–node finite elements, which can capture the nonlinear shear stresses occurring within the composite cylinders.

Several researchers used lamination parameters technique to express laminate stiffness characteristics in a compact form independent of the number of layers and their respective thicknesses. For instance, [Fukunaga et al., 1994] expressed fundamental natural frequency ofsymmetrically laminated panels in terms of lamination parameters. Using Classical Laminated Plate Theory (CLPT) for formulating the stiffness properties and Rayleigh–Ritz method for solving the equations of motion, they determined optimal laminate configurations resulting in maximum fundamental frequencies. [Diaconu et al., 2002] conducted a similar study for thick panels by using First–order Shear Deformation Theory (FSDT) and compared the results with the ones obtained via CLPT. [Trias et al., 2016] used lamination parameters to obtain the optimal stacking–sequence providing maximum fundamental frequency. They used various plate aspect ratios, plate thicknesses, and layer numbers to investigate their effect on maximal fundamental frequency. [Honda et al., 2009] optimized lamination parameters to modify laminate natural frequencies according to three performance metrics. In addition to maximizing fundamental frequency, they also maximized the difference between two adjacent frequencies, and minimized the difference between the target and actual frequencies.

Even though maximizing frequency gaps works decently for specific problems, it does not provide exact quantification of the response magnitudes at different excitation frequencies. This problem is addressed by several studies through frequency–response analyses. For instance, [Bardell et al., 1997] conducted a vibration study of thin, laminated, cylindrically singly–curved shell panels using finite element method. They obtained receptance FRFs for balanced and symmetric laminates under the effect of point harmonic forces. Their work showed that variation of fiber angles significantly changes the dynamic response in terms of resonance frequencies and magnitudes. Similarly, [Assaee and Hasani, 2015] investigated forced vibration response of

curved composite cylindrical shells using spline finite strip method. They computed receptances for simply–supported and clamped panels subjected to point excitation. [Niu et al., 2010] conducted a discrete material optimization study to minimize the total sound power radiated out of vibrating laminated composite plates excited by harmonic dynamic pressure. They found optimal fiber orientations at discretized regions for different frequencies by calculating the responses of curved laminated panels using finite element analyses. Recently, [Sahoo et al., 2016] investigated the dynamic behavior of flat/curved laminated panel structures using finite elements based on HSDT and included experimental validations for free and forced vibration cases. They showed considerable effects of changing the panel curvature, aspect ratio and support conditions.

Existing design studies, which use lamination parameters formulation to optimize stiffness properties of the composite panels to improve dynamic response, are restricted to modifying natural frequencies. Performance of such panels under dynamic excitations has not been investigated in frequency domain using lamination parameters. Besides, fundamental frequency contours in lamination parameter plane for curved panels are not available. The present study addresses these gaps in the literature, and utilizes the lamination parameters technique to examine the dynamic response of flat and curved composite panels. Stiffness properties are modeled in terms of lamination parameters which are treated as design variables. Finite element analyses are performed to investigate the individual and combined effects of varying panel aspect ratios, curvatures and boundary conditions on the dynamic responses. Fundamental frequency contours in lamination parameters domain are obtained for different sets of model parameters. In addition, equivalent radiated power (ERP) contours for the panels excited by harmonic pressure are shown. Optimal laminate configurations providing the best dynamic performance are determined by initially maximizing the fundamental frequencies, then minimizing ERP at different frequencies. The relationship between the designs optimized for maximum fundamental frequency and minimum ERP responses is investigated to study the effectiveness of the

frequency maximization technique. The results demonstrated the potential of using lamination parameters technique in the design of flat/curved composite panels for the optimal dynamic response, and provided valuable insight into the effect of various design parameters.

4.1 Validations

Prior to the investigation of design parameter effects on the dynamic response of the composite panel, finite element model of the structure is validated. All analyses are conducted using carbon–epoxy composite layers as the laminate material whose properties are given in Table 4.1 [Narita, 2003], [Botelhoa et al., 2006]. Initially, a

Table 4.1: Material properties of uni–directional carbon–epoxy composite laminate.

E_1(GPa)	138.0
E_2(GPa)	8.96
G_{12}(GPa)	7.1
ν_{12}	0.3
ρ(kg/m^3)	1.6
η	0.01

study on the mesh size is conducted to achieve convergence for the modal analysis results. Afterwards, modal analyses are carried out for different boundary conditions, panel curvatures and laminate ply angles. Resulting 1$^{\text{st}}$ and 2$^{\text{nd}}$ natural frequencies are compared to the results from [Liew et al., 1997]. Table 4.2 shows the comparison of the non–dimensional frequency parameters obtained by $\lambda_n = \omega_n a_p b\sqrt{\rho h/D_\lambda}$, where a_p is planform panel length: $a_p = 2\sin(a/2r)$ and D_λ is the reference plate flexural rigidity: $D_\lambda = E_{11}h^3/12(1-\nu_{12}\nu_{21})$ The results agree very well with each other signifying the good accuracy of the developed finite element (FE) model. A further comparison is done for the maximum fundamental frequencies from [Abdalla et al., 2007] to validate

Table 4.2: Frequency parameters $\lambda_n = \omega_n a_p b\sqrt{\rho h/D_\lambda}$ for singly curved, 8–ply laminated graphite/epoxy cylindrical shells with $a_p/h = 100.0$, $a_p/b = 1.0$ and stacking sequence: $[-\theta, \theta, -\theta, \theta, \theta, -\theta, \theta, -\theta]$.

BC	a_p/r	θ	1st Mode		2nd Mode	
			[Liew et al., 1997]	FE	[Liew et al., 1997]	FE
SSSS	0.0	0°	11.290	11.311	17.132	17.235
		45°	14.089	14.108	30.901	31.091
	0.5	0°	30.220	30.618	31.125	31.552
		45°	63.235	64.088	64.373	65.133
		90°	50.807	51.116	73.522	74.435
CCCC	0.0	0°	23.853	23.913	29.720	29.916
		45°	22.887	22.901	43.954	44.302
	0.5	0°	37.669	38.059	40.228	40.643
		45°	67.634	68.465	73.414	74.156
		90°	68.339	68.819	85.251	86.263

the lamination parameter formulation. The frequencies are also calculated using the following analytical relation based on CLPT which gives the natural frequencies of a laminated plate (rad/s), in terms of its bending stiffness entities, dimensions, and mode numbers [Gürdal et al., 1999]:

$$\omega_n = \frac{\pi^2}{\sqrt{\rho h}}\sqrt{D_{11}\left(\frac{m}{a}\right)^4 + 2(D_{12}+2D_{66})\left(\frac{mn}{ab}\right)^2 + D_{22}\left(\frac{n}{b}\right)^4} \tag{4.1}$$

where m and n are the number of half–waves in x and y-directions, respectively. In the comparisons, normalized frequency parameter defined as $\Omega_n = \omega_n a^2\sqrt{\rho h/D_\Omega}$ is used, where $D_\Omega = E_{22}h^3/12(1-\nu_{12}\nu_{21})$. In Table 4.3, the results for the maximum fundamental frequency parameter Ω_1^{max} and corresponding optimal lamination parameters (V_1^{opt}, V_3^{opt}) are presented, which also show a very good agreement.

Table 4.3: Maximum fundamental frequency parameters $\Omega_1^{max} = \omega_1^{max} a^2 \sqrt{\rho h / D_\Omega}$ and corresponding optimal lamination parameters for simply–supported plates with different aspect ratios.

a/b		V_1^{opt}	V_3^{opt}	Ω_1^{max}
	[Abdalla et al., 2007]	0.0	-1.0	55.53
1.0	Eq. 4.1	0.0	-1.0	56.53
	FE	0.0	-1.0	56.60
	[Abdalla et al., 2007]	-1.0	1.0	159.89
2.0	Eq. 4.1	-1.0	1.0	159.89
	FE	-1.0	1.0	160.23

4.2 Fundamental Frequency Maximization

In this section, individual and combined effects of model parameters (panel aspect ratio, curvature, and boundary conditions) on the fundamental frequency responses are investigated. For all cases length–to–thickness ratio (a/h) is kept at 100.0.

4.2.1 Fundamental Frequency Contours

In the following, fundamental frequency contours together with points of minimum and maximum values are demonstrated on lamination parameter plane for different aspect ratios, panel curvatures, and boundary conditions. The frequency contours for simply–supported panels are presented in Fig. 4.1. Optimal design points providing maximum frequencies are indicated by black squares (■), whereas points of minima are marked by magenta diamonds (♦). The first column in Fig. 4.1 shows that frequency contours of flat panels rotate clockwise as a/b ratio is increased from 1.0 to 2.0 making laminate angles yielding maximum fundamental frequency move from $\pm 45°$ to $90°$. Further increase in a/b does not change the optimal point even though the frequency values vary. However, such convergence behavior is not observed for increasing panel curvature. Moreover, changing aspect ratio and curvature affect the

frequency contours in a dissimilar way. Therefore, obtaining responses for different sets of geometric parameters to determine combined effects is important. One can also observe that, for a/r ratios of 0.0 and 0.1, frequency contour lines in lamination parameter plane are rather straight where higher a/r values result in curved contour lines. The optimal results from Fig. 4.1 are tabulated in Table 4.4. Since all the optimal lamination parameters have been found to lie on the lower boundary of the feasible domain, corresponding ply angles (θ^{opt}) obtained by Eq. 2.6 are also provided.

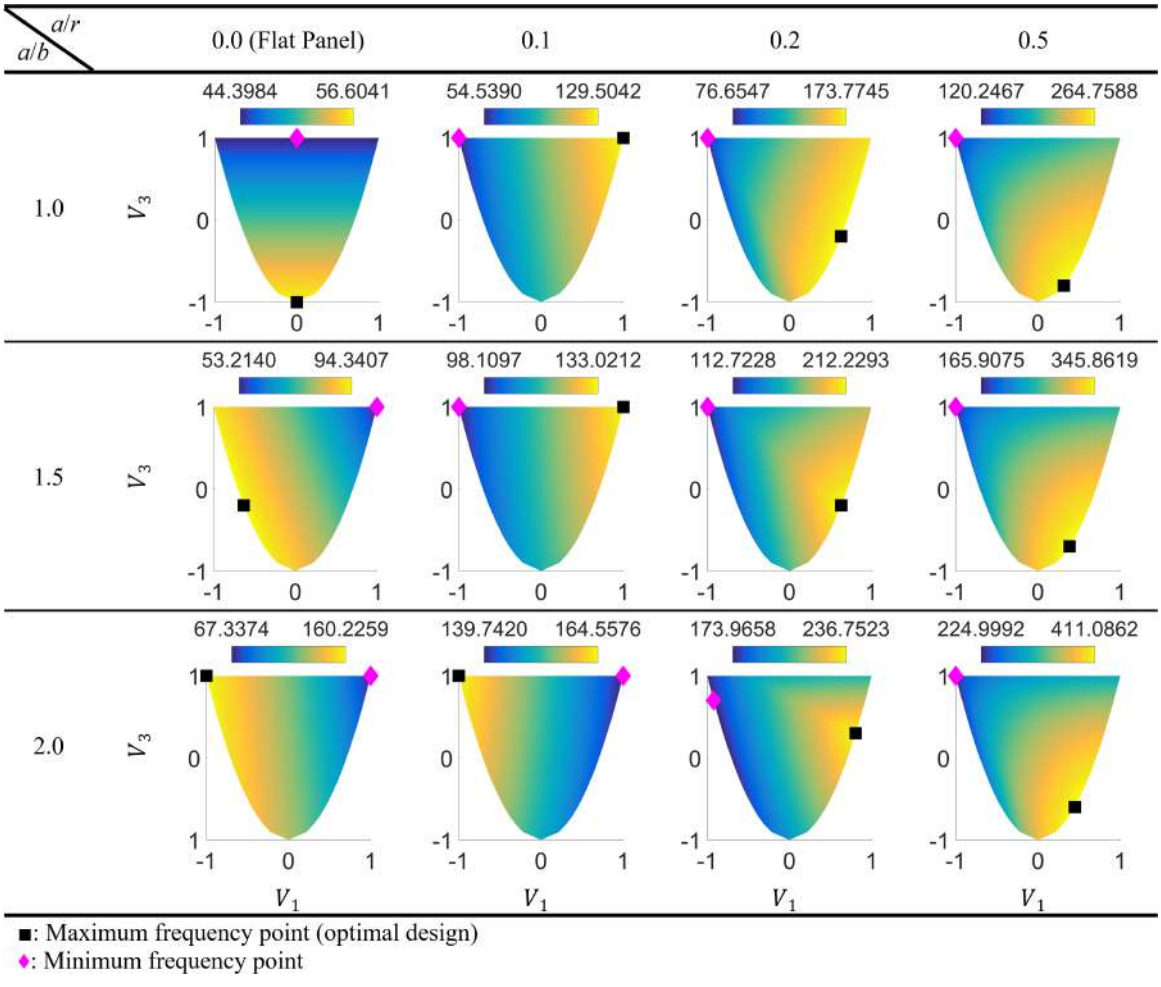

Figure 4.1: Fundamental frequency parameter $\Omega_1 = \omega_1 a^2 \sqrt{\rho h / D_\Omega}$ contours on lamination parameter plane for simply–supported panels with different aspect ratios and curvatures.

Table 4.4: Optimal design points yielding maximum fundamental frequency values and corresponding layer angles for simply–supported panels of different aspect ratios and curvatures.

	a/r											
a/b	0.0			0.1			0.2			0.5		
	V_1^{opt}	V_3^{opt}	$\pm\theta^{opt}$	V_1^{opt}	V_3^{opt}	$\pm\theta^{opt}$	V_1^{opt}	V_3^{opt}	$\pm\theta^{opt}$	V_1^{opt}	V_3^{opt}	$\pm\theta^{opt}$
1.0	0.0	-1.0	45°	1.0	1.0	0°	0.63	-0.2	25.4°	0.32	-0.8	35.8°
1.5	-0.63	-0.2	64.6°	1.0	1.0	0°	0.63	-0.2	25.4°	0.39	-0.7	33.6°
2.0	-1.0	1.0	90°	-1.0	1.0	90°	0.81	0.3	18.1°	0.45	-0.6	31.7°

Fig. 4.2 and Table 4.5 show the frequency contours and tabulated optimal design points for clamped panels, respectively. For clamped panels, all the design points except ($a/b = 1.0$, $a/r = 0.0$) are located on the lower boundary of Miki's diagram. In addition, the effect of aspect ratio is found to be more dominant over curvature compared to simply–supported panels. Another noteworthy finding is that optimal points for $a/r = 0.5$ are similar for all aspect ratios of both simply and clamped panels, located in the lower right quadrant of the feasible domain. This is because, the stiffening effect of high curvature dominates over the influence of aspect ratio and boundary conditions. Finally, the frequency contour lines of clamped panels look relatively straight until a/r is increased to 0.5 where they become significantly curved.

4.2.2 Mode Shapes for the Maximum Fundamental Frequency

Natural frequencies and mode shapes of structures are major factors affecting their responses to dynamic excitations. In this sub–section, mode shapes and non–dimensional natural frequencies of panels with lamination parameters yielding maximum fundamental frequency are demonstrated. The results, calculated for different aspect ratios and curvatures, are presented in Fig. 4.3 and Fig. 4.4 for simply–supported and clamped boundary conditions, respectively. Regarding simply–supported boundary

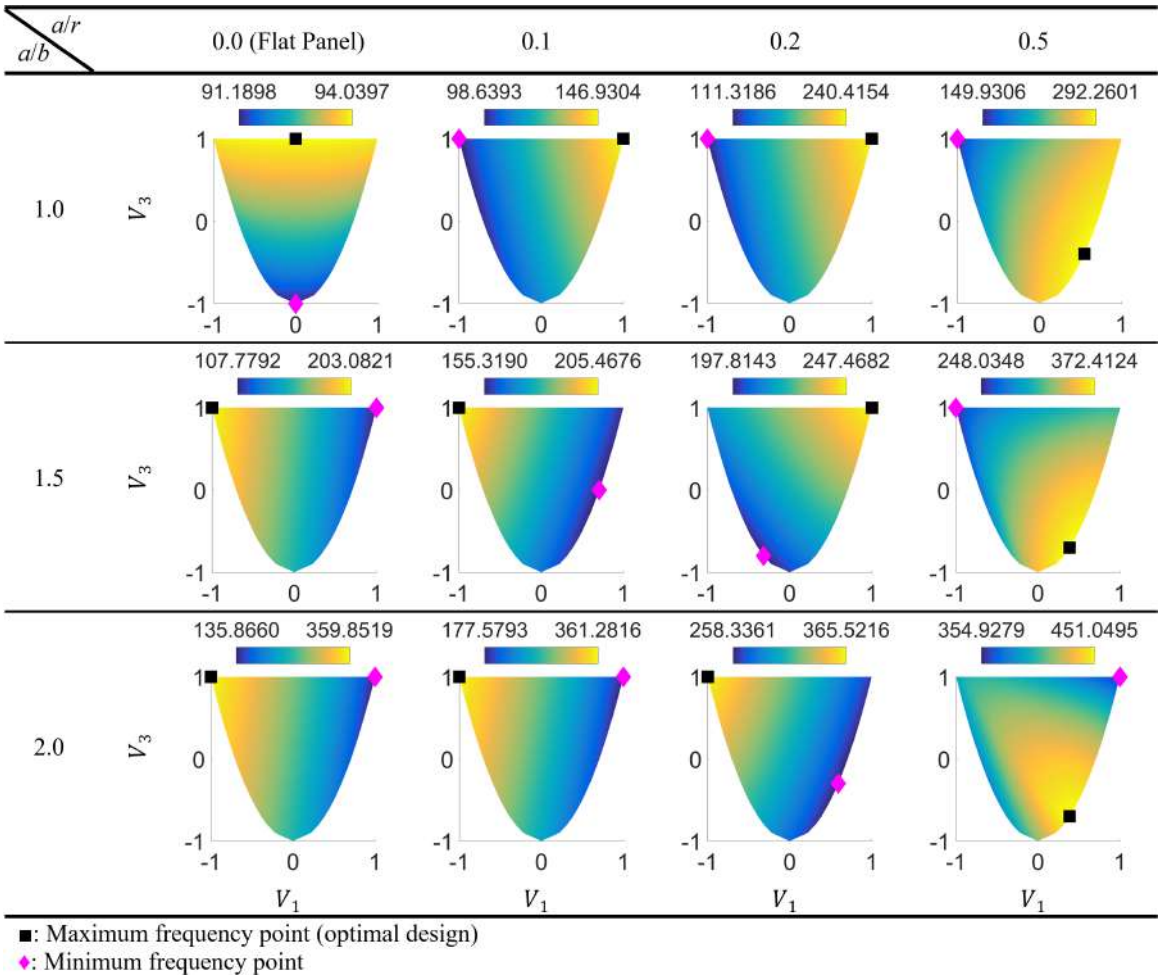

Figure 4.2: Fundamental frequency parameter $\Omega_1 = \omega_1 a^2 \sqrt{\rho h / D_\Omega}$ contours on lamination parameter plane for clamped panels with different aspect ratios and curvatures.

conditions, half–wave numbers of the fundamental frequency mode are ($m = 1$, $n = 1$) for flat panels and curved panels with $a/r = 0.1$. Higher a/r ratios change the fundamental vibration mode to ($m = 2$, $n = 1$). This transition is, in fact, the underlying reason for the form change in the fundamental frequency contours shown previously. It also significantly affects dynamic response of the panel to harmonic pressure excitation which is studied in the next section. Clamped panels show a similar behavior, where vibration mode transition from ($m = 1$, $n = 1$) to ($m = 2$, $n = 1$) occurs when a/r is increased to 0.5.

Table 4.5: Optimal design points yielding maximum fundamental frequency values and corresponding layer angles for clamped panels of different aspect ratios and curvatures.

	a/r											
a/b	0.0			0.1			0.2			0.5		
	V_1^{opt}	V_3^{opt}	$\pm\theta^{opt}$	V_1^{opt}	V_3^{opt}	$\pm\theta^{opt}$	V_1^{opt}	V_3^{opt}	$\pm\theta^{opt}$	V_1^{opt}	V_3^{opt}	$\pm\theta^{opt}$
1.0	0.0	1.0	N/A	1.0	1.0	0°	1.0	1.0	0°	0.55	-0.4	28.4°
1.5	-1.0	1.0	90.0°	-1.0	1.0	90°	1.0	1.0	0°	0.39	-0.7	33.6°
2.0	-1.0	1.0	90°	-1.0	1.0	90°	-1.0	1.0	90°	0.39	-0.7	33.6°

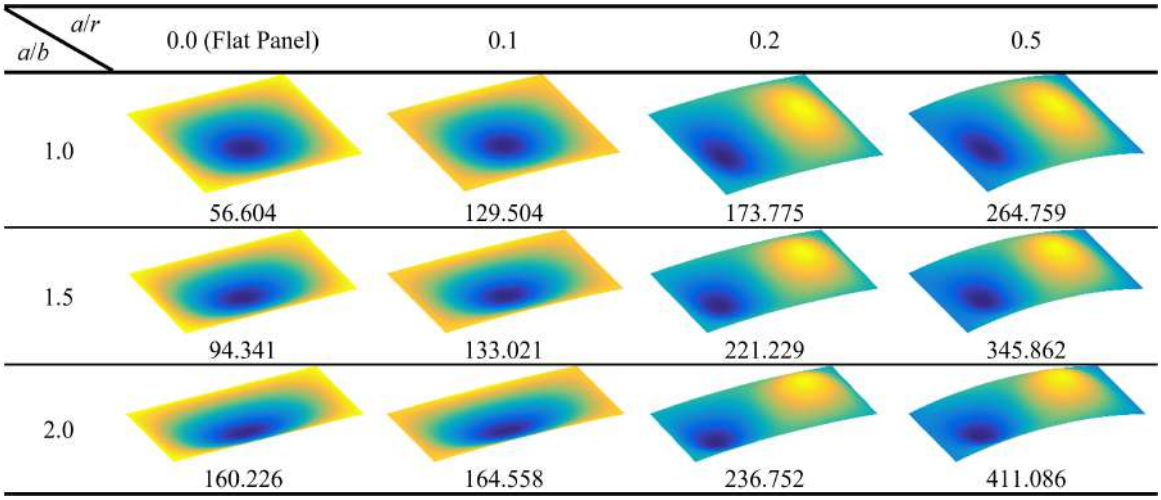

Figure 4.3: Optimal design points yielding maximum fundamental frequency values and corresponding layer angles for simply–supported panels of different aspect ratios and curvatures.

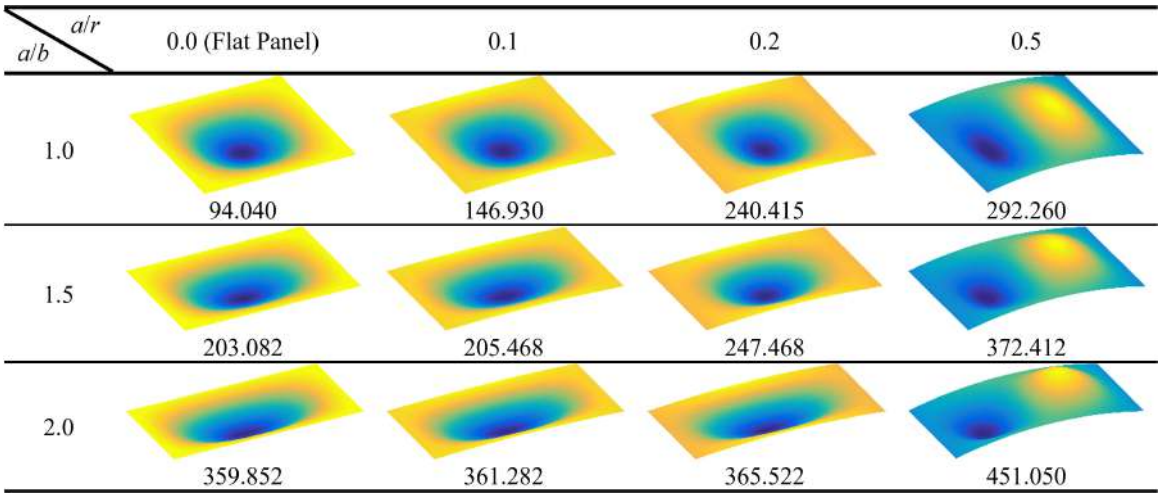

Figure 4.4: Optimal design points yielding maximum fundamental frequency values and corresponding layer angles for clamped panels of different aspect ratios and curvatures.

4.3 Equivalent Radiated Power Minimization

In this section, individual and combined effects of panel geometry and excitation frequency on the forced dynamic responses are investigated. Optimal lamination parameters providing the minimum ERP values for different excitation frequencies are calculated.

4.3.1 ERP Contours at the Fundamental Frequency

Equivalent radiated power contours and optimal design points for the panels of different aspect ratios and curvatures excited by harmonic pressure are presented in this sub–section. Fundamental frequencies are selected as the excitation frequencies to demonstrate the resonance effects where the results for the intermediate frequencies up to the fundamental frequencies are calculated in the next sub–section.

In Fig. 4.5, the contour plots for simply–supported boundary conditions are shown. The results are normalized (denoted by $\overline{ERP}$) for each case by dividing all response values by their maximum amplitudes. The optimal points are marked by red triangles (▲). When a/r is equal to 0.0 or 0.1, $\overline{ERP}$ contour graphs look similar

to the inverse of the fundamental frequency contours. This condition is a result of the fact that fundamental vibration mode shown in Fig. 4.3 has the number of half–waves of ($m = 1$, $n = 1$), which can be efficiently excited under harmonic pressure. If the curvature values are increased to $a/r = 0.2$ or 0.5, the mode changes to ($m = 2$, $n = 1$) and the response surfaces look significantly different as stripes of resonances appear in the middle regions of the feasible domain. These resonance bands get thicker and move towards the right side of the feasible domain as a/b increases. Increasing a/r ratio has a converse effect causing resonance bands to be thinner and move leftwards. In addition, for the panels with $a/r = 0.5$, considerably low relative response ampli-

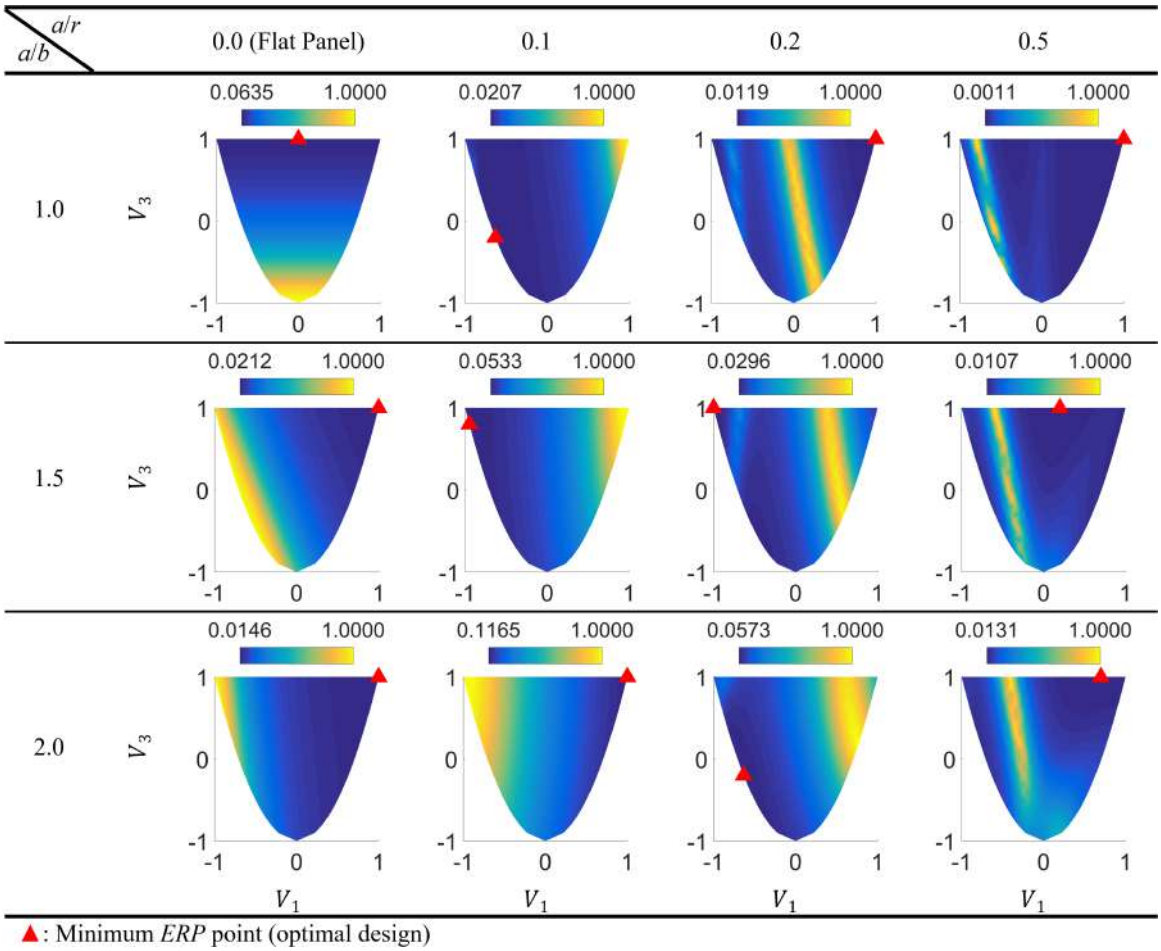

Figure 4.5: Optimal design points yielding maximum fundamental frequency values and corresponding layer angles for simply–supported panels of different aspect ratios and curvatures.

tudes are observed at the points where excitation and natural frequencies coincide, due to low modal excitation efficiency against harmonic pressure. This fact can be noticed by comparing last columns in Figs. 4.1 and 4.5. Furthermore, one should note that even though the individual increments in a/b or a/r values lead to the same optimum points, their combined effect may result in significantly different solutions. For instance, the cases with $(a/b = 1.5, a/r = 0.0)$ and $(a/b = 1.0, a/r = 0.2)$ both require $(V_1 = 1.0, V_3 = 1.0)$ as the optimal design point, very unlike the optimum for $(a/b = 1.5, a/r = 0.2)$ which is located at $(V_1 = 1.0, -V_3 = 1.0)$. In Table 4.6, the optimal design points from Fig. 4.5 are tabulated.

Table 4.6: Optimal design points yielding minimum ERP and corresponding layer angles for simply–supported panels of different aspect ratios and curvatures excited by harmonic pressure with frequency ω_1^{max}.

	a/r											
a/b	0.0			0.1			0.2			0.5		
	V_1^{opt}	V_3^{opt}	$\pm\theta^{opt}$	V_1^{opt}	V_3^{opt}	$\pm\theta^{opt}$	V_1^{opt}	V_3^{opt}	$\pm\theta^{opt}$	V_1^{opt}	V_3^{opt}	$\pm\theta^{opt}$
1.0	0.0	1.0	N/A	-0.63	-0.2	64.6°	1.0	1.0	0°	1.0	1.0	0°
1.5	1.0	1.0	0°	-0.95	0.8	80.8°	-1.0	1.0	90°	0.2	1.0	N/A
2.0	1.0	1.0	0°	1.0	1.0	0°	-0.63	-0.2	64.6°	0.7	1.0	N/A

As an additional remark, one can observe the non–convex behavior of frequency–response quantities in lamination parameters space. This is somewhat unusual since problem formulations using lamination parameters generally lead to convex responses, which is previously shown by [Grenestedt and Gudmundson, 1993]. However, this is not the case in frequency–response quantities due to resonance effects. For this reason, using gradient–based optimization algorithms to reduce forced dynamic response of composite panels using lamination parameters might result in locally optimal solutions.

Fig. 4.6 and Table 4.7 show $\overline{ERP}$ contours for clamped panels excited by harmonic pressure with fundamental panel frequency and tabulated optimal design points, re-

spectively. Again, the transition of vibration mode from ($m = 1$, $n = 1$) to ($m = 2$, $n = 1$) changes the nature of the response surfaces, which occurs when a/r becomes 0.5. In this case, however, the resonance bands look rather blurry and discontinuous contrary to simply–supported boundary conditions. Also, the square flat panel shows an unusual response where a large region of resonance occurs and the difference between the maximum and the minimum amplitudes is significantly smaller than the other cases.

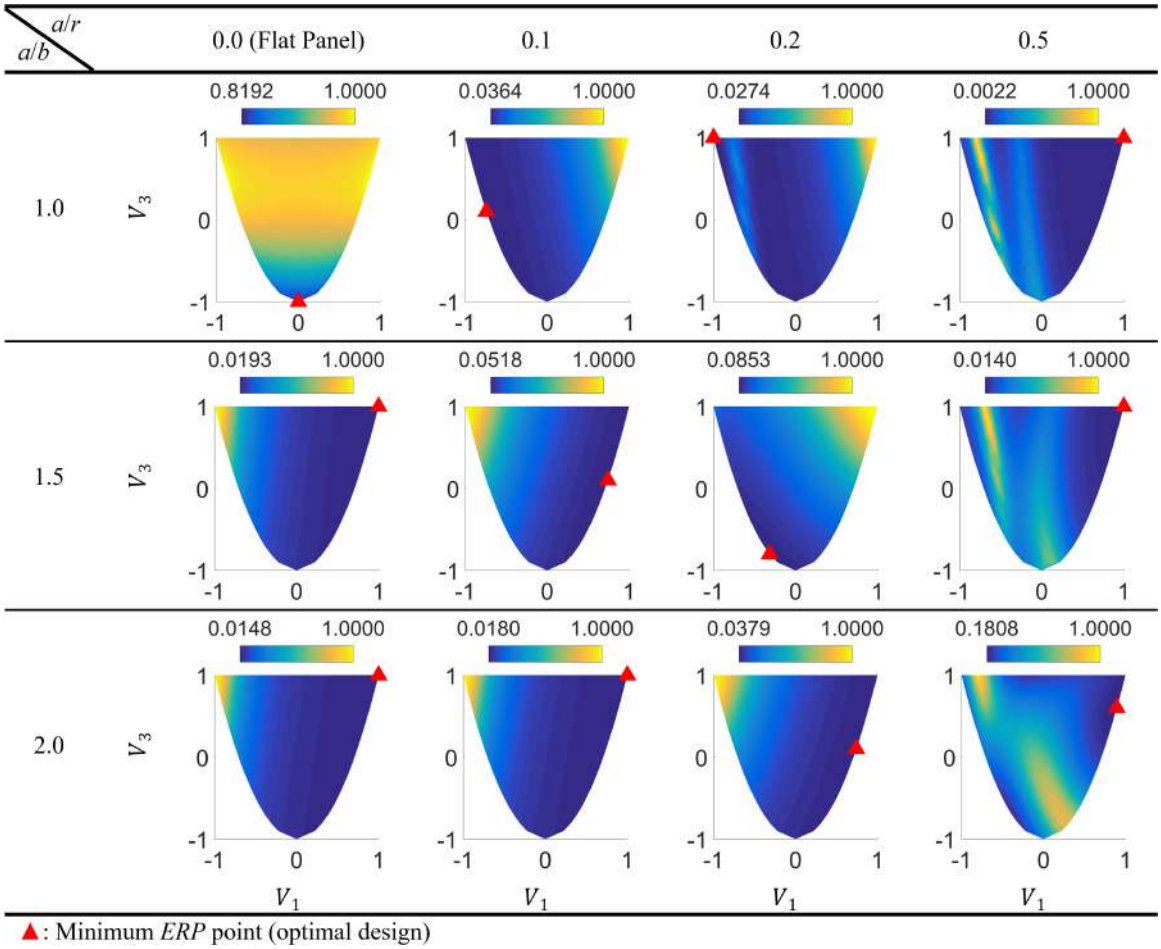

Figure 4.6: Optimal design points yielding maximum fundamental frequency values and corresponding layer angles for clamped panels of different aspect ratios and curvatures.

Table 4.7: Optimal design points yielding minimum ERP and corresponding layer angles for clamped panels of different aspect ratios and curvatures excited by harmonic pressure with frequency ω_1^{max}.

	a/r											
a/b	0.0			0.1			0.2			0.5		
	V_1^{opt}	V_3^{opt}	$\pm\theta^{opt}$	V_1^{opt}	V_3^{opt}	$\pm\theta^{opt}$	V_1^{opt}	V_3^{opt}	$\pm\theta^{opt}$	V_1^{opt}	V_3^{opt}	$\pm\theta^{opt}$
1.0	0.0	-1.0	45°	-0.74	0.1	68.9°	-1.0	1.0	90°	1.0	1.0	0°
1.5	1.0	1.0	0°	0.74	0.1	21.1°	-0.32	-0.8	54.2°	1.0	1.0	0°
2.0	1.0	1.0	0°	1.0	1.0	0°	0.74	0.1	21.1°	0.89	0.6	13.3°

4.3.2 Minimum ERP Points for Different Excitation Frequencies

In the following, optimal lamination parameters providing minimum ERP values are calculated for different frequencies of harmonic pressure excitation considering various panel geometries and boundary conditions. The results are calculated by sweeping the excitation frequency from 0 up to the maximum fundamental frequency, which corresponds to the range: $\overline{\omega}$ =0–1.0, where $\overline{\omega} = \omega/\omega_1^{max}$ is the frequency ratio. At each frequency, the lamination parameter pair that gives the minimum ERP is determined. For each panel configuration, FRF curves are shown for three laminate designs:

1. Optimal design that provides the minimum ERP starting from $\overline{\omega} = 0$, which will be referred as "●",

2. Optimal design that provides the minimum ERP around $\overline{\omega} = 1$, which is shown by "▲" in Figs. 4.5 and 4.6,

3. Maximum fundamental frequency design, which is shown by "■" in Figs. 4.1 and 4.2.

Conformity and difference between these responses are analyzed. In addition, the effective frequency ranges for "●" and "▲" are demonstrated. Moreover, the sensitivity

of FRFs with respect to the model parameters is investigated.

Figs. 4.7 and 4.8 show normalized $\widetilde{ERP}$ vs. $\overline{\omega}$ curves for various panels having simply–supported and clamped boundary conditions, respectively. In these graphs, the normalization is performed by dividing all response values by the minimum ERP amplitude at $\overline{\omega} = 1.0$ for each case. The FRFs referring to "●", "▲", and "■" are represented by green dashed line, red dotted line, and black solid line, respectively. The effective frequency ranges for "●" and "▲", in which they are the optimum designs, are indicated by green and red transparent background shadings, respectively. If the optimum design is the same for entire frequency range, green–red hatched shading is used meaning that "●" and "▲" coalesce. If a frequency interval exists where neither "●" nor "▲" is the true optimum, it is demonstrated by yellow shading. The FRF curves of these additional optimal solutions are not plotted for the sake of clarity since there can be more than one solution. For both simply–supported and clamped panels, "●" and "■" are the same for the cases where fundamental vibration mode is: $(m = 1,\ n = 1)$. This can be observed by inspecting the overlap of the green and black lines on the first two columns in Fig. 4.7 and the first three columns in Fig. 4.8. For other cases with $(m = 2,\ n = 1)$, "●" and "■" differ. This observation shows that frequency maximization technique is effective in minimizing forced dynamic response under certain conditions.

In most cases, the optimal designs change drastically due to the resonance effects when the excitation frequency is increased from 0 to a critical value. This transition frequency can be very different depending on the case; whose smallest value is around $\overline{\omega} = 0.67$ observed for simply–supported panel with $a/b = 2.0$ & $a/r = 0.5$, and highest value is $\overline{\omega} = 0.99$ occurring for the clamped square flat panel. Only for simply–supported panels with $a/b = 1.0$ & $a/r = (0.2, 0.5)$ and clamped panels with $a/b = (1.0, 1.5)$ & $a/r = 0.5$, the optimum point remains unchanged for entire frequency range. In these cases, fundamental frequency maximization is observed to be ineffective for reducing forced dynamic response amplitudes, since the FRFs for "■" lie above the optimal ones in the entire frequency range.

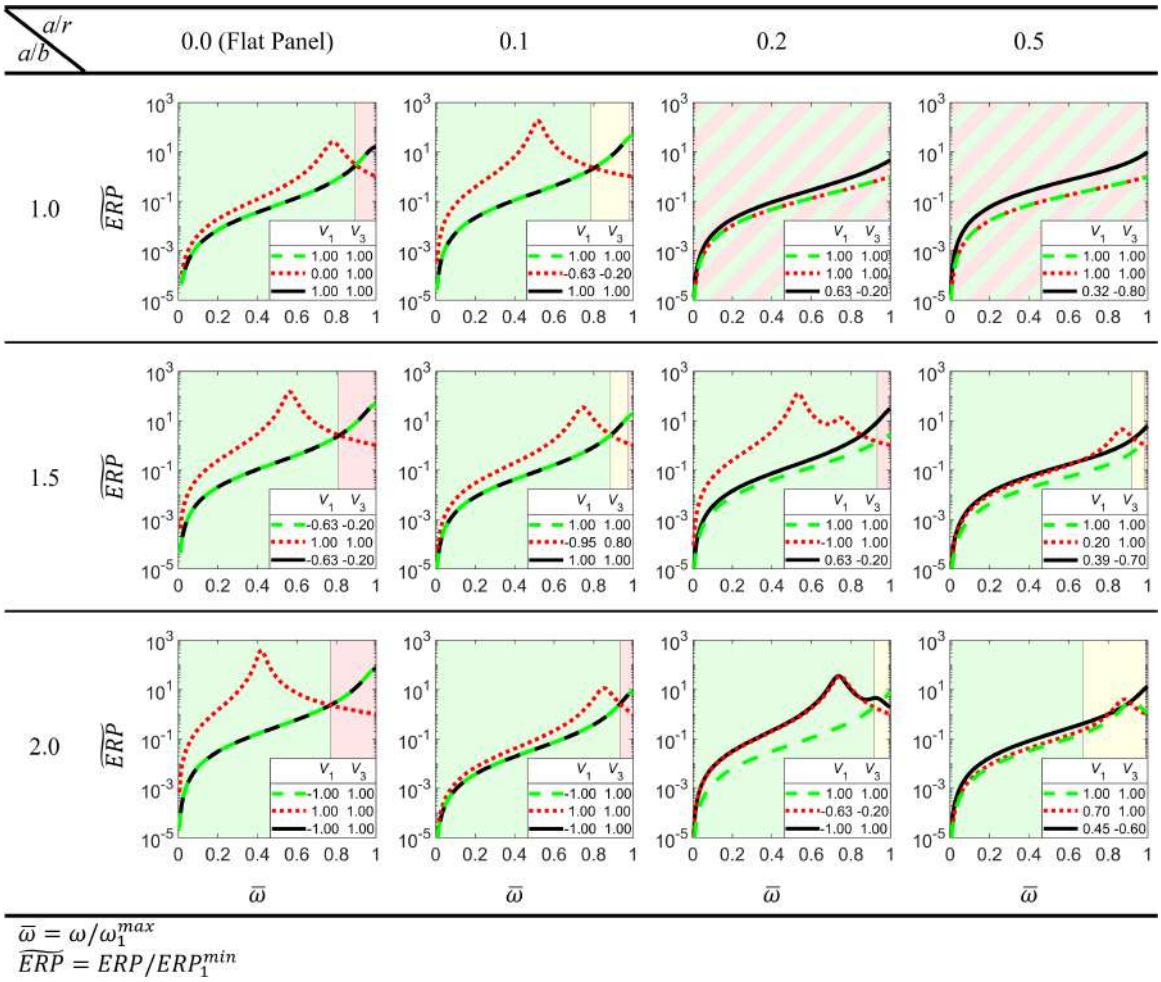

Figure 4.7: $\widetilde{ERP}$ vs. $\bar{\omega}$ plots of "●" (green dashed line), "▲" (red dotted line), and "■" (black straight line) for simply–supported panels of various geometries excited by harmonic pressure.

Additionally, no yellow regions (additional optimal solutions) exist for flat panels, highlighting the importance of the optimal solutions for relatively lower frequencies (●), and around maximum fundamental frequency (▲). For a/r values of 0.0 and 0.1, the effective interval of optimal design around maximum fundamental frequency is enlarged as a/b ratio is increased. For curved panels, intermediate optimal solutions might appear, which can cover a significant portion of the frequency range of interest. The widest region of intermediate optima is around one–third of the entire analysis frequency range, occurring for simply–supported panel with $a/b = 2.0$ & $a/r = 0.5$.

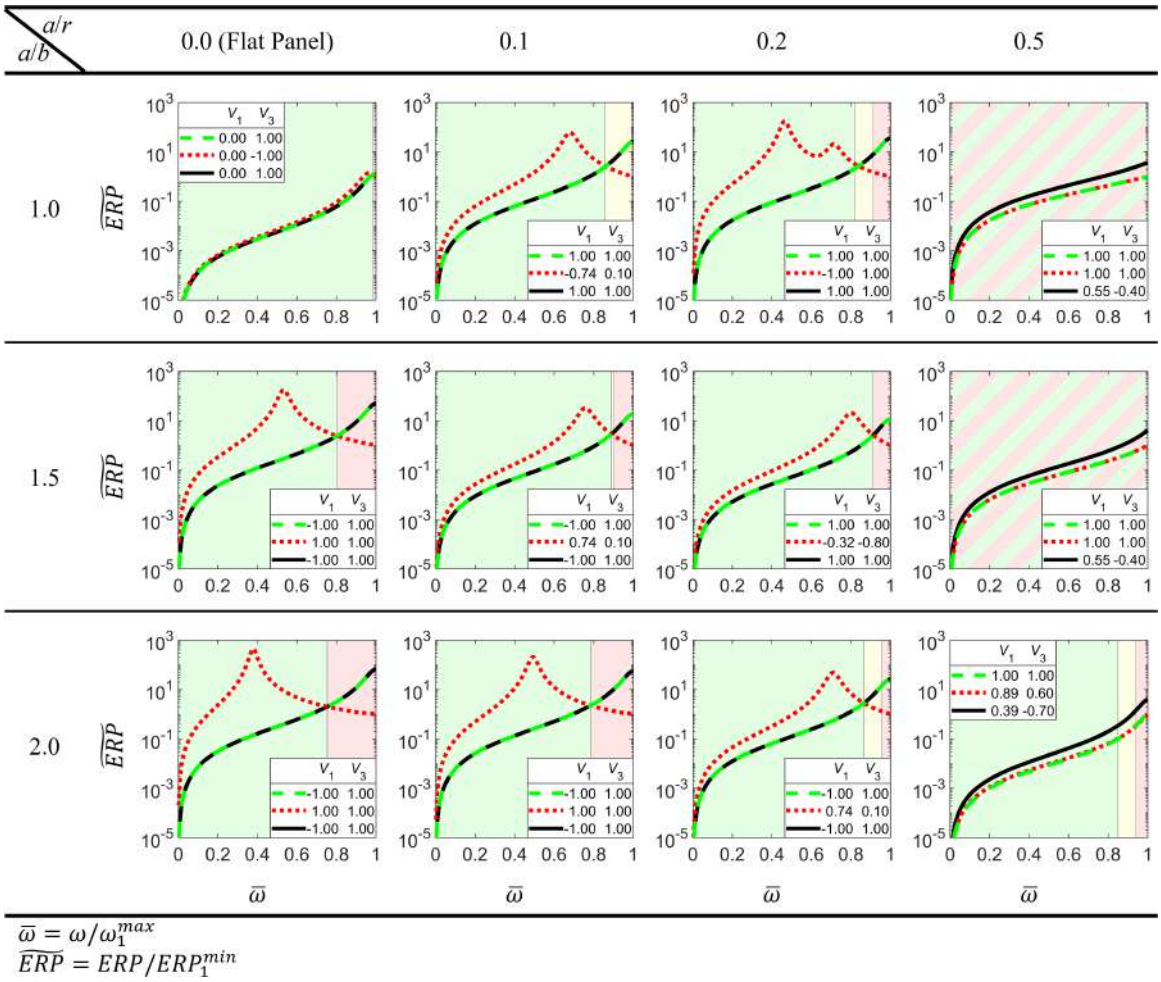

$\bar{\omega} = \omega/\omega_1^{max}$
$\widetilde{ERP} = ERP/ERP_1^{min}$

Figure 4.8: $\widetilde{ERP}$ vs. $\bar{\omega}$ plots of "●" (green dashed line), "▲" (red dotted line), and "■" (black straight line) for clamped panels of various geometries excited by harmonic pressure.

The effective interval of intermediate optima shrinks with the increasing a/b ratio for lightly curved panels with $a/r = 0.1$.

Chapter 5

MODELING AND OPTIMIZATION OF VARIABLE–STIFFNESS LAMINATES

Prior to the development of variable–stiffness laminates, many optimization studies have been conducted considering constant–stiffness laminates. Modification of the natural frequencies has been extensively used for achieving satisfactory dynamic properties concerning the specific application. In this context, the problem of fundamental frequency maximization has been frequently studied. For instance, [Apalak et al., 2008] determined optimal configurations of the laminated composites yielding the maximum fundamental frequency. They used finite element analysis (FEA) to compute the responses and used genetic algorithm for the optimization process. Similar studies have also been conducted for curved panels. For example, [Narita and Robinson, 2006] used Ritz method for layerwise optimization of thin cylindrical laminates for maximization of the fundamental frequency. Likewise, [Ameri et al., 2012] conducted an optimization study to find optimal laminate configurations that provide maximum fundamental natural frequencies for cylindrical panels. They used finite element analysis to calculate solutions for different geometric parameters and boundary conditions. In the literature, studies with the aim of maximizing the difference between adjacent natural frequencies are also prevalent. For instance, [Adali, 1984] optimized shear–deformable antisymmetric angle–ply laminates for maximizing both fundamental frequency and separation of two neighboring frequencies. He considered simply–supported plates and calculated the responses using analytical relations. [Farshi and Rabiei, 2007] performed a layerwise laminate optimization study by using Rayleigh–Ritz method to obtain solutions for various boundary conditions. They determined the stacking–sequences that give maximum values for the first natural

frequency and the difference between the first and the second frequencies. [Kayikci and Sonmez, 2012] also maximized the separation between adjacent frequencies of laminated plates. They utilized an analytical method based on Fourier series which accounts for bending–twisting coupling.

The potential of constant–stiffness laminates reach its limits for the enhancement of operational performance. The existing values of the optimal responses can be further improved by using variable–stiffness laminates [Gürdal and Olmedo, 1993]. One design technique to achieve variable–stiffness properties is dividing the plate into discrete elements and optimizing the fiber angle of each element. For example, [Honda and Narita, 2008] optimized the short fiber angles of laminated composite plates for achieving maximum fundamental frequency. They used finite element method to model the non–uniform structure and genetic algorithm as the optimization method. Their results indicate that higher fundamental frequency values can be achieved by varying elemental fiber angles instead of using parallel fiber laminates. However, when the fiber angles are optimized without imposing any relation between neighboring elements, abrupt differences between the adjacent fiber orientations might occur hindering the manufacturability [Peeters et al., 2015]. To overcome this problem, several approaches utilizing curved continuous fibers within the laminate layers were proposed. For instance, [Honda and Narita, 2011] maximized the fundamental frequency of composites having curvilinear fibers in addition to the ones with short straight fibers. They used cubic polynomial functions to represent curvilinear fiber paths and computed natural frequencies using FEA. Their results show that the fiber shapes significantly influence the fundamental frequency values as well as corresponding vibration mode shapes. For curved panels there are relatively fewer number of studies when variable–stiffness laminates are considered. For instance, [Ribeiro, 2016] investigated free vibration of cylindrical laminates consisting of layers with curvilinear fiber paths. He determined that with the increasing panel curvature, usage of curvilinear fibers instead of straight ones affects the natural frequencies and mode shapes more significantly.

One shortcoming of the optimization approaches using number of layers, layer thicknesses and angles is that, the solution depends on the initial assumptions on the laminate configuration. As a remedy, lamination parameters formulation has been utilized in various studies to describe laminate stiffness properties in a compact form. For constant–stiffness laminates, there are many studies based on lamination parameters. For example, [Fukunaga et al., 1994] calculated the optimal lamination parameters for maximizing the fundamental frequency of symmetrically laminated plates with different aspect ratios. They used Rayleigh–Ritz and Galerkin methods for the analysis of simply–supported and clamped plates, respectively. [Diaconu et al., 2002] adopted lamination parameters as the design variables to obtain the optimal laminate configurations for maximizing the fundamental frequencies of symmetrically laminated thick plates. They investigated the effects of using CLPT or FSDT for the kinematic relations and found that two theories may produce different optimal results in some cases. However, all optimal laminate configurations showed the characteristics of specially orthotropic laminates which exhibit no shear–extension or bending–twisting coupling. [Honda et al., 2009] used lamination parameters to maximize the difference of two adjacent natural frequencies in addition to the fundamental frequency. They used Ritz method to solve for the modal frequencies and displacements together with layerwise optimization approach. Serhat and Basdogan maximized the fundamental frequency of laminated plates [Serhat and Basdogan, 2016a] and curved panels [Serhat and Basdogan, 2018] in lamination parameter domain using an optimization framework based on finite analysis.

For variable–stiffness laminates, there are a few available design studies relying on lamination parameters. [Setoodeh et al., 2006] introduced the concept of using lamination parameters for the design of variable–stiffness laminates and showed that the structural performance can be improved significantly by using such methodology. However, the fiber paths corresponding to the optimal lamination parameter distribution were not obtained in that study. The authors outlined the difficulty of finding fiber paths satisfying spatially changing lamination parameters while keeping

the ply thickness constant and respecting the minimum radius of curvature. Later, [Abdalla et al., 2007] maximized the fundamental frequency of variable–stiffness composite plates using lamination parameters. In their study, they searched an optimum distribution of lamination parameters for a simply–supported plate. Since they only investigated theoretical limits for the maximum value of the fundamental frequency, manufacturing constraints were disregarded and the laminate configurations satisfying optimal lamination parameters distributions were not found. Their results showed that, in the absence of manufacturing constraints, resulting lamination parameter distribution can be very irregular complicating the retrieval of an actual laminate configuration. Utilization of lamination parameters in an optimization framework which properly considers manufacturing constraints is an active research topic, and only a few studies addressing the problem are available in the literature. In two recent studies, a three–step approach was followed where optimal lamination parameters and corresponding stacking–sequence for variable–stiffness laminates was presented [Peeters et al., 2015], [Peeters et al., 2018]. They found the optimal stiffness distribution in terms of the lamination parameters in the first step, calculated the optimal manufacturable fiber angle distribution in the second step, and retrieved the fiber paths in the third step.

In this chapter, a novel variable–stiffness laminate optimization technique that considers the manufacturability of the composite panels is proposed. It constrains the design space which controls the direction of change for the lamination parameters and subsequently leads a smooth change in the layer angles. The method differs from the existing methods by its simplicity and provides an efficient mean to estimate the required stiffness distributions within variable–stiffness composite panels. Finite element analyses are used to calculate solutions for various panel geometries and boundary conditions. After finding optimal lamination parameter distributions, corresponding fiber orientations of the layers are also calculated. In addition to the novelty of the proposed method, the eigenfrequency separation problem for curved variable–stiffness panels is studied for the first time using lamination parameters.

The developed method is utilized to maximize the fundamental frequencies of panels having different aspect ratios, curvatures and boundary conditions as example cases. The results demonstrated that variable–stiffness designs with smooth manufacturable fiber paths can be obtained and better performances can be achieved compared to the constant–stiffness designs by utilizing the proposed method.

5.1 Design Procedure

In this section, the proposed interpolation method for the design of variable–stiffness laminates is presented. It is developed to utilize the lamination parameter formulation while considering manufacturability of the optimal design. The method follows a 3–step approach:

1. Obtaining optimal lamination parameter distribution
2. Computation of fiber angle distribution
3. Retrieval of fiber paths

5.1.1 Obtaining Optimal Lamination Parameter Distribution

At the first step, the optimal lamination parameter distribution is sought. The method relies on constraining the change of lamination parameters within the feasible domain in a controlled manner. Each discrete panel element is assigned a lamination parameter pair lying on the prescribed curves that are functions of the volumetric ratio. These prescribed curves are defined by the following relation:

$$V_1 = (2R_r - 1)\sqrt{(V_3 + 1)/2} \tag{5.1}$$

assuming that there are maximum of two different layer angle distributions. R_r is the volumetric ratio of the layer angles located at the right boundary of the Miki's diagram (45°–0°). The volumetric ratio of the layer angles located at the left boundary (45°–90°) can inherently be found as $R_l = 1.0 - R_r$, where R_l and R_r take values between

0.0 and 1.0. In Fig. 5.1, several prescribed curves of design points for different volumetric ratios are illustrated on Miki's diagram. During the optimization process,

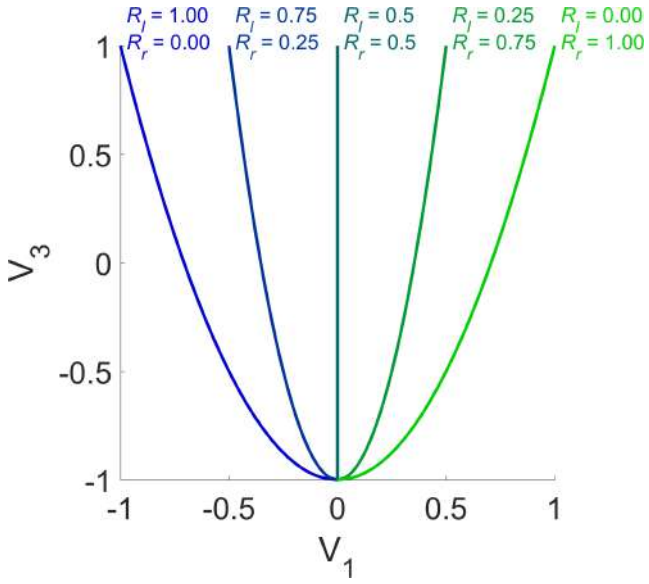

Figure 5.1: Several curves of design points for different volumetric ratios.

the lamination parameters pertaining to the adjacent elements are enforced to have close values to ensure a smooth distribution over the panel. This is ensured by using master nodes and applying a distancebased interpolation for the elemental values. For instance, let the coordinates of the first and the second master nodes be: (x_1,y_1) and (x_2,y_2). For each element of the discretized plate, let (x_e,y_e) be the central coordinates of the elements. The distances between the element centers and the master nodes can be found as: $d_1 = \sqrt{(x_e - x_1)^2 + (y_e - y_1)^2}$ and $d_2 = \sqrt{(x_e - x_2)^2 + (y_e - y_2)^2}$ for the first and the second nodes, respectively. The elemental lamination parameters can then be calculated by finding the point P_e on the arc $\widehat{P_1P_2}$ satisfying the relation:

$$\widehat{P_eP_1}/\widehat{P_eP_2} = d_1/d_2 \tag{5.2}$$

This search can be performed numerically by discretizing the arc and going over all the points. Note that, the influence of the master nodes on the elemental lamination parameters decreases as the distance between the nodes and the elements increases.

In Fig. 5.2, an example design with ($R_l = 0.75$, $R_r = 0.25$), $P_1(V_1, V_3) = (-0.1768, -0.75)$, $P_2(V_1, V_3) = (-0.4677, 0.75)$ is used with the proposed method and it is illustrated on Miki's diagram. Note that, for any V_3 value, the proportion of the horizontal distances between the prescribed curve and the diagram boundaries remain the same. Next, lamination parameter distribution is obtained using the described

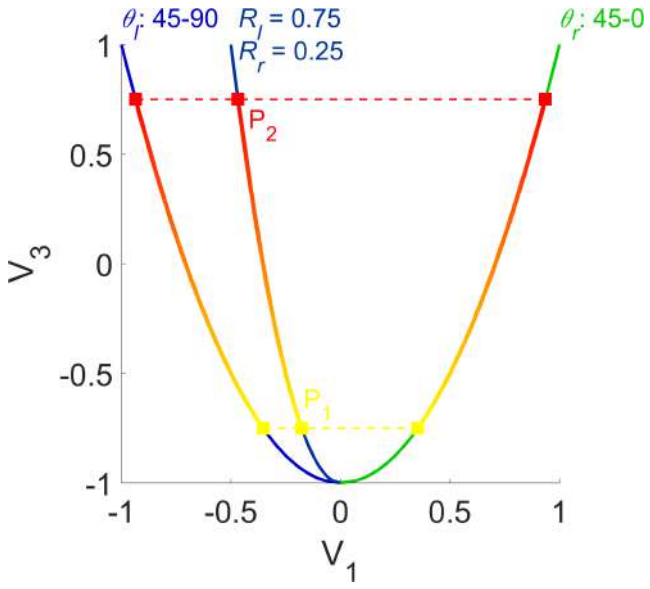

Figure 5.2: Exemplary design with ($R_l = 0.75$, $R_r = 0.25$), $P_1(V_1, V_3) = (-0.1768, -0.75)$, $P_2(V_1, V_3) = (-0.4677, 0.75)$.

interpolation approach. For this example, the master node locations are chosen as one corner and the center of the panel. Symmetricity is applied in the horizontal and the vertical planes. Figure 5.3 shows the lamination parameter distribution corresponding to the exemplary points illustrated in Fig. 5.2. One may notice the smooth change in the lamination parameter variables as the outcome of the interpolation approach. In this study, a design approach with two master nodes is employed for simplicity. However, more points can be easily used by following the same principles.

5.1.2 Computation of Fiber Angle Distribution

The second step of the optimization procedure is the computation of the fiber angle distribution. This is a straight–forward operation which firstly requires computing

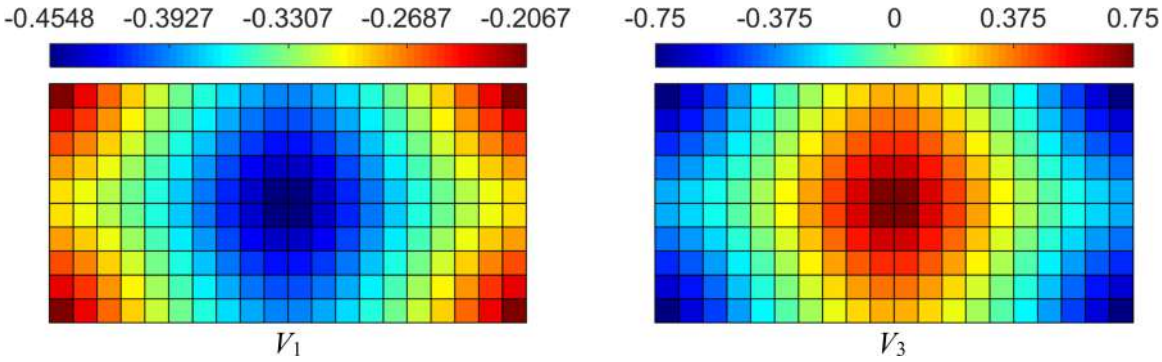

Figure 5.3: The elemental angles corresponding to the lamination parameter distribution for the exemplary design with ($R_l = 0.75$, $R_r = 0.25$), $P_1(V_1, V_3) = (-0.1768, -0.75)$, $P_2(V_1, V_3) = (-0.4677, 0.75)$.

$V_1 = \pm(V_3 + 1)/2$ for each element using V_3's as the input. After that, the positive and the negative values of V_1 can be inserted into Eq. (6) to obtain elemental fiber angles θ_l and θ_r, respectively. Figure 5.4 shows the distribution of elemental angles corresponding to the lamination parameter distribution presented in Fig. 5.3. The adjacent fiber angles reflect the smooth transition feature of the input V_3 distribution. This is because, the laminate angles are calculated at the two boundary points of the Miki's diagram, both having the elemental V_3 values (see Fig. 5.2).

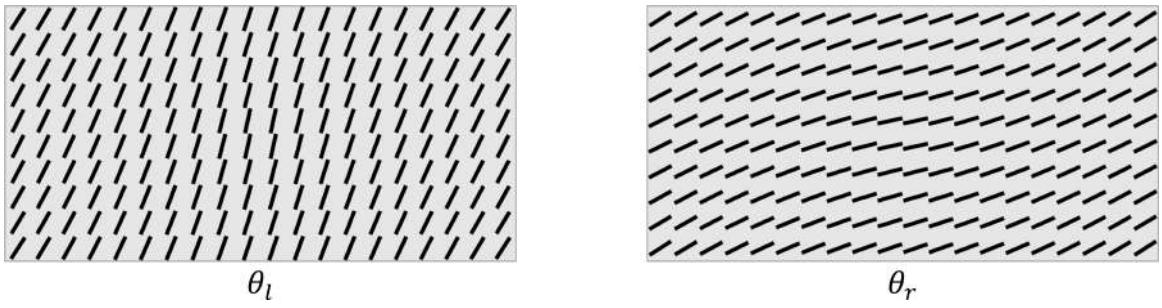

Figure 5.4: The elemental angles corresponding to the lamination parameter distribution for the exemplary design with ($R_l = 0.75$, $R_r = 0.25$), $P_1(V_1, V_3) = (-0.1768, -0.75)$, $P_2(V_1, V_3) = (-0.4677, 0.75)$.

5.1.3 Retrieval of Fiber Paths

The last step in the optimization procedure is the retrieval of the continuous fiber paths suitable for manufacturing out of the optimal discrete fiber distribution. This problem has been previously studied by [Blom et al., 2010] who used stream functions to represent the fiber paths. They defined the stream functions: $\Psi(x, y) = C$ by using the following relation:

$$\frac{\mathrm{d}\Psi}{\mathrm{d}s} = \frac{\mathrm{d}\Psi}{\mathrm{d}x}\frac{\mathrm{d}x}{\mathrm{d}s} + \frac{\mathrm{d}\Psi}{\mathrm{d}y}\frac{\mathrm{d}y}{\mathrm{d}s} = \frac{\mathrm{d}\Psi}{\mathrm{d}x}\sin\theta + \frac{\mathrm{d}\Psi}{\mathrm{d}y}\cos\theta = 0 \tag{5.3}$$

for a given fiber angle distribution $\theta(x, y)$. This methodology is utilized to obtain fiber paths from the available fiber angle distribution. In Fig. 5.5, the laminate fiber paths corresponding to the elemental fiber angle distribution shown in Fig. 5.4 is presented. Due to the controlled pattern of the input fiber angle distribution, smooth fiber paths appropriate for tow–steering could be obtained. The thickness build–up due to the overlap of fiber tows during the steering process is disregarded in this study, which is also a topic of investigation in the literature [Blom et al., 2010].

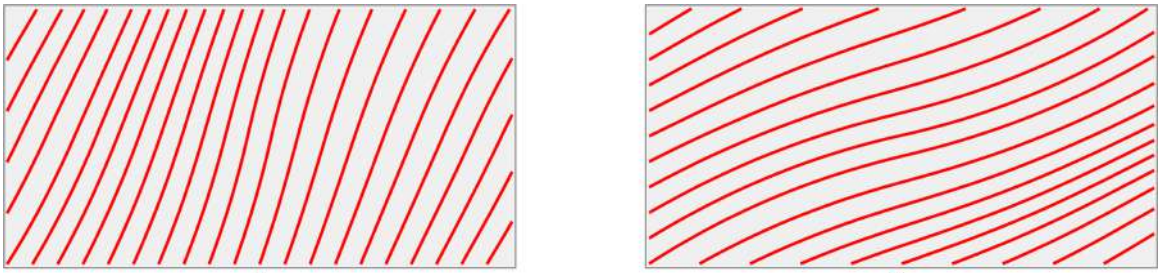

Figure 5.5: The laminate fiber paths corresponding to the fiber angle distribution for the exemplary design with ($R_l = 0.75$, $R_r = 0.25$), $P_1(V_1, V_3) = (-0.1768, -0.75)$, $P_2(V_1, V_3) = (-0.4677, 0.75)$.

5.1.4 Design Procedure Summary

The design procedure is summarized as a flow–chart which is given in Fig. 5.6. In this study, entire lamination parameter design space is scanned by using a full–factorial

search for finding optimal design variables. However, gradient–based optimization methods can also be used to improve the computational efficiency. Moreover, the locations of the master nodes which were held constant to simplify the problem can also be optimized in the future studies.

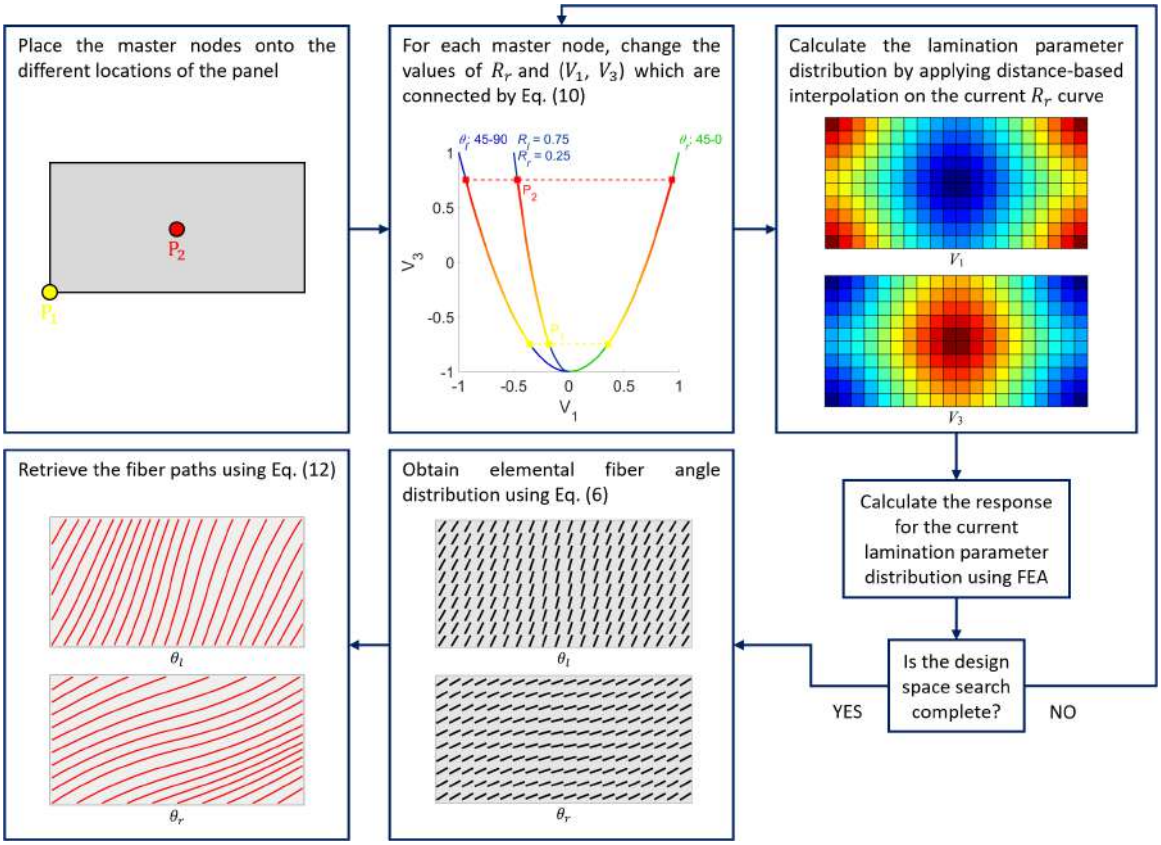

Figure 5.6: The laminate fiber paths corresponding to the fiber angle distribution for the exemplary design with ($R_l = 0.75$, $R_r = 0.25$), $P_1(V_1, V_3) = (-0.1768, -0.75)$, $P_2(V_1, V_3) = (-0.4677, 0.75)$.

5.2 Variable–stiffness Designs for Eigenfrequency Separation

In this section, the results obtained using the proposed methodology are presented. Fundamental frequency and the difference between the first and the second natural frequencies are chosen as the performance metrics to be maximized. The frequency

values are nondimensionalized using the relation [Abdalla et al., 2007]:

$$\overline{\omega}_n = \omega_n (b^2/h)\sqrt{\rho/E_2} \tag{5.4}$$

Various cases with different panel aspect ratios, curvatures and boundary conditions are considered. In all analyses, horizontal and vertical symmetricity is applied for the lamination parameter distributions. The panel material is chosen as graphite/epoxy laminae with the properties given in Table 5.1.

Table 5.1: Material properties of graphite/epoxy laminae [Diaconu et al., 2002]

E_1	$25E_2$
$G_{12} = G_{13}$	$0.5E_2$
G_{23}	$0.2E_2$
ν_{12}	0.25
$\rho(\mathrm{kg/m^3})$	1.6

5.2.1 Maximization of the 1st Natural Frequency

The results for the maximization of fundamental frequency $\overline{\omega}_1$ are presented in this sub–section. Initially, the results are obtained for simply–supported flat panels and compared with the ones from [Abdalla et al., 2007]. Table 5.2 shows the maximum fundamental frequency parameters for the constant–stiffness and variable–stiffness laminates ($\overline{\omega}_1^{cs}$ and $\overline{\omega}_1^{vs}$) for different panel aspect ratios. The results show that the constant–stiffness frequency values agree well with each other which can be regarded as a validation. For square panels, no improvement is observed using variable–stiffness approach. For the a/b ratio of 1.5, variable–stiffness frequencies significantly surpass the constant–stiffness values. When a/b is further increased to 2.0, the effectiveness of variable–stiffness designs decreases. This trend highlights the significant influence of aspect ratio on the potency of variable–stiffness concept. The present variable–stiffness approach provides lesser improvement percentages compared to the one used

in [Abdalla et al., 2007], since the manufacturability is disregarded in the latter study which aimed to investigate the theoretical limits.

Table 5.2: Maximum fundamental frequency parameters: $\overline{\omega}_1 = \omega_1(b^2/h)\sqrt{\rho/E_2}$ for simply–supported flat panels.

a/b	$\overline{\omega}_1^{cs}$	$\overline{\omega}_1^{vs}$	% imp.	$\overline{\omega}_1^{cs}$	$\overline{\omega}_1^{vs}$	% imp.
	[Abdalla et al., 2007]			Present FEM		
1.0	20.57	20.57	0.00	20.55	20.55	0.00
1.5	14.83	16.50	11.24	15.08	15.91	5.50
2.0	14.46	15.37	6.29	14.49	14.70	1.45

In Table 5.3, the optimal results yielding the maximum fundamental frequency are tabulated for simply–supported flat panels with different aspect ratios. Note that the optimal lamination parameter pairs at the master nodes are the same for the square panels ($a/b = 1.0$) leading to constant–stiffness design. For the variable–stiffness designs, R_l is 1.0 and R_r is 0.0, implying that the optimal laminates consist of only θ_l–layers. Figure 5.7 shows the optimal variable–stiffness lamination parameter distributions and corresponding discrete fiber angles/fiber paths for simply–supported flat panels with different aspect ratios. The optimal results are not visualized when they lead to constant–stiffness laminates, since the lamination parameters and the fiber angles do not change across the panels in those cases.

Table 5.3: Optimal results yielding maximum $\overline{\omega}_1$ for simply–supported panels with $a/r = 0.0$ (flat panels).

a/b	$\overline{\omega}_1^{cs}$	$\overline{\omega}_1^{vs}$	% imp.	R_l	R_r	$(V_1, V_3)^1$	$(V_1, V_3)^2$	$(\theta_l, \theta_r)^1$	$(\theta_l, \theta_r)^2$
1.0	20.55	20.55	0.0	N.A.	N.A.	(0.0, -1.0)	(0.0, -1.0)	(45°, 45°)	(45°, 45°)
1.5	15.08	15.91	5.50	1.0	0.0	(0.0, -1.0)	(-1.0, 1.0)	(45°, 45°)	(90°, 0°)
2.0	14.49	14.70	1.45	1.0	0.0	(0.0, -1.0)	(-1.0, 1.0)	(45°, 45°)	(90°, 0°)

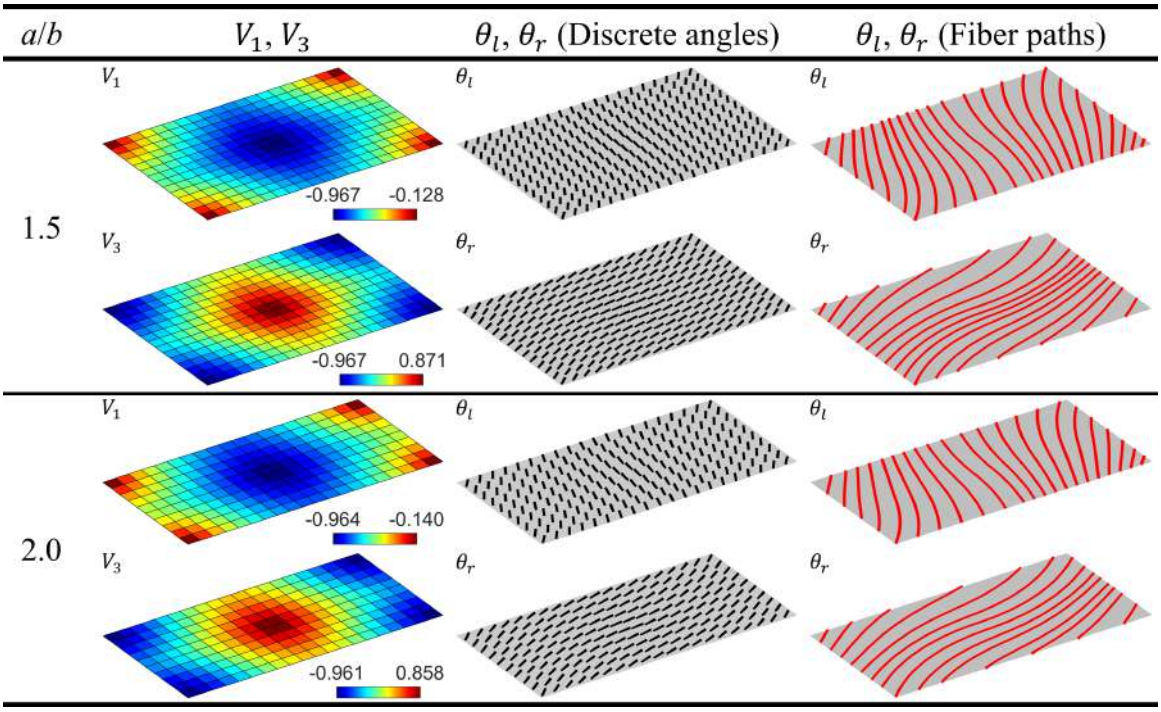

Figure 5.7: Optimal lamination parameter distributions and corresponding discrete fiber angles/fiber paths yielding maximum $\overline{\omega}_1$ for simply–supported panels with $a/r = 0.0$.

Table 5.4 and Figure 5.8 show the optimal results yielding maximum $\overline{\omega}_1$ for simply–supported panels with $a/r = 0.2$ and the optimal lamination parameter distributions with the corresponding discrete fiber angles/fiber paths, respectively. When a/r ratio is 0.2, the effectiveness trend of variable–stiffness methodology notably changes as it provides the highest performance increment for $a/b = 1.0$ and the lowest one for $a/b =$

Table 5.4: Optimal results yielding maximum $\overline{\omega}_1$ for simply–supported panels with $a/r = 0.2$.

a/b	$\overline{\omega}_1^{cs}$	$\overline{\omega}_1^{vs}$	% imp.	R_l	R_r	$(V_1, V_3)^1$	$(V_1, V_3)^2$	$(\theta_l, \theta_r)^1$	$(\theta_l, \theta_r)^2$
1.0	62.15	64.45	3.70	0.0	1.0	(0.0, -1.0)	(1.0, 1.0)	(45°, 45°)	(90°, 0°)
1.5	33.64	34.04	1.19	0.0	1.0	(0.0, -1.0)	(0.87, 0.5)	(45°, 45°)	(75°, 15°)
2.0	21.06	21.40	1.61	0.0	1.0	(0.55, -0.4)	(1.0, 1.0)	(62°, 28°)	(90°, 0°)

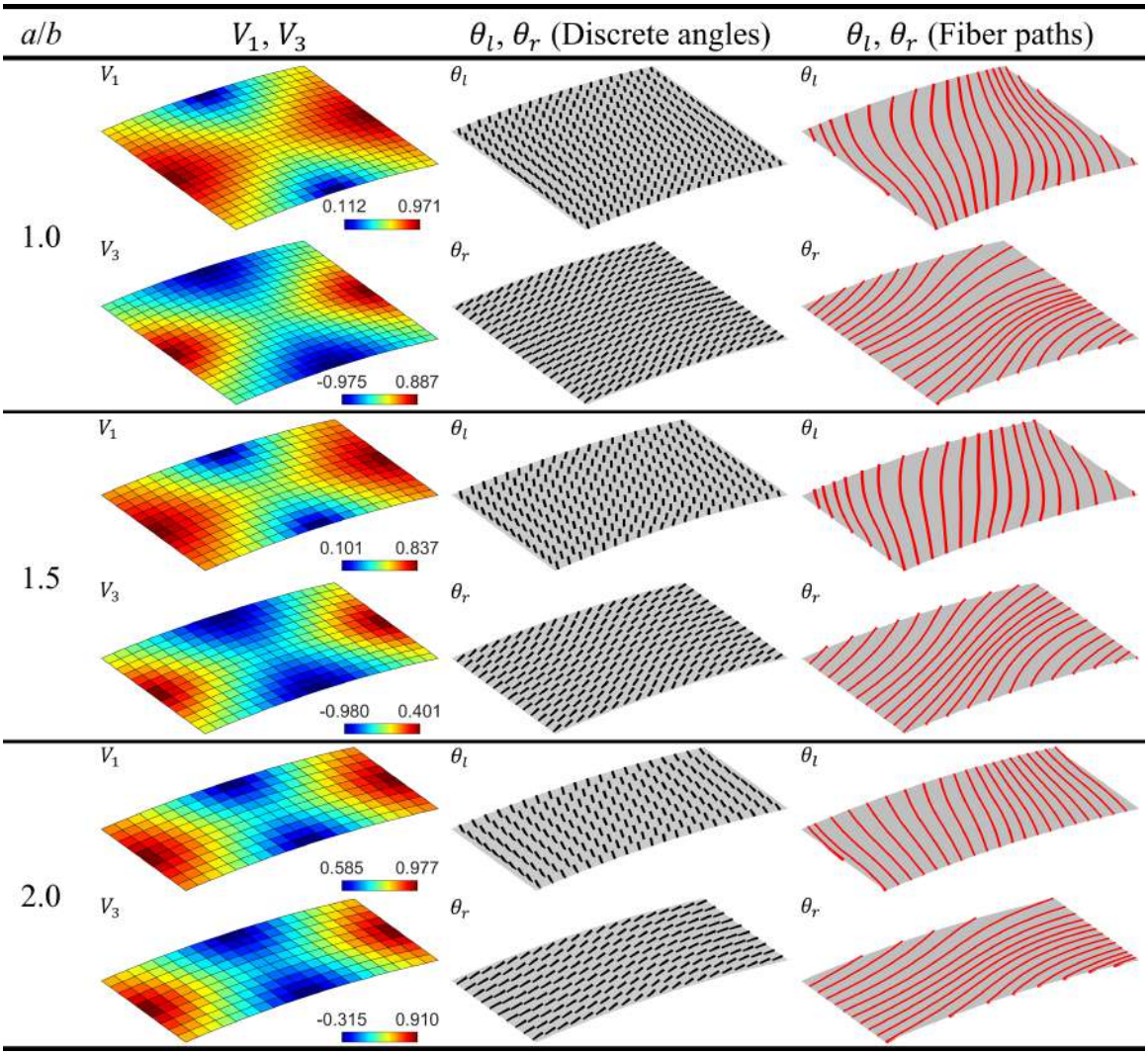

Figure 5.8: Optimal lamination parameter distributions and corresponding discrete fiber angles/fiber paths yielding maximum $\overline{\omega}_1$ for simply–supported panels with $a/r = 0.2$.

1.5. When the panel curvature is further increased to $a/r = 0.5$, variable–stiffness frequencies do not significantly exceed constant–stiffness values (the difference is below 1%), therefore the results are not presented for those cases.

For clamped panels of lower a/r ratios (0.0, 0.2), the proposed formulation with 2 master nodes did not provide any significant improvements except the flat square panel where almost 5% improvement is achieved. Table 5.5 and Figure 5.9 show the optimal results yielding maximum $\overline{\omega}_1$ for clamped flat panels and the optimal

lamination parameter distributions with the corresponding discrete fiber angles/fiber paths, respectively.

Table 5.5: Optimal results yielding maximum $\overline{\omega}_1$ for clamped panels with $a/r = 0.0$ (flat panels).

a/b	$\overline{\omega}_1^{cs}$	$\overline{\omega}_1^{vs}$	% imp.	R_l	R_r	$(V_1, V_3)^1$	$(V_1, V_3)^2$	$(\theta_l, \theta_r)^1$	$(\theta_l, \theta_r)^2$
1.0	33.37	35.01	4.91	1.0	0.0	(-1.0, 1.0)	(0.0, -1.0)	(90°, 0°)	(45°, 45°)
1.5	32.27	32.27	0.00	1.0	0.0	(-1.0, 1.0)	(-1.0, 1.0)	(90°, 0°)	(90°, 0°)
2.0	31.87	31.87	0.00	1.0	0.0	(-1.0, 1.0)	(-1.0, 1.0)	(90°, 0°)	(90°, 0°)

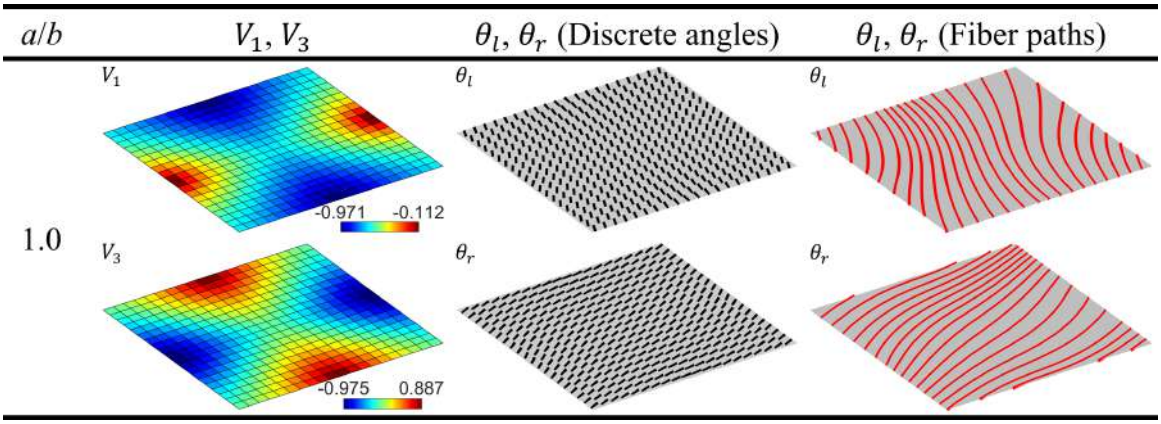

Figure 5.9: Optimal lamination parameter distributions and corresponding discrete fiber angles/fiber paths yielding maximum $\overline{\omega}_1$ for clamped panels with $a/r = 0.0$.

When the a/r ratio of the clamped panels is increased to 0.5, variable–stiffness designs yield substantial improvements in the maximum $\overline{\omega}_1$ values which can be seen in Table 5.6 showing the optimal results. In Fig. 5.10, the optimal lamination parameter distributions with the corresponding discrete fiber angles/fiber paths for clamped panels with $a/r = 0.5$ are presented. The results indicate that, the a/r values at which variable–stiffness formulation is effective in fundamental frequency maximization differ according to the boundary conditions. This result is in accordance with the trend of fundamental vibration mode switching, which occurs at smaller curvatures

for simply–supported panels and at higher curvatures for clamped panels [Serhat and Basdogan, 2018]. Therefore, the effectiveness of the proposed optimization method may change depending on the boundary conditions and the corresponding vibration mode shapes.

Table 5.6: Optimal results yielding maximum $\overline{\omega}_1$ for clamped panels with $a/r = 0.5$.

a/b	$\overline{\omega}_1^{cs}$	$\overline{\omega}_1^{vs}$	% imp.	R_l	R_r	$(V_1, V_3)^1$	$(V_1, V_3)^2$	$(\theta_l, \theta_r)^1$	$(\theta_l, \theta_r)^2$
1.0	103.6	108.5	4.73	0.0	1.0	(0.0, -1.0)	(0.98, 0.9)	(45°, 45°)	(84°, 6°)
1.5	58.79	61.39	4.42	0.0	1.0	(0.0, -1.0)	(0.81, 0.3)	(45°, 45°)	(72°, 18°)
2.0	39.67	41.67	5.09	0.0	1.0	(0.0, -1.0)	(0.92, 0.7)	(45°, 45°)	(79°, 11°)

5.2.2 Maximization of the Difference between the 1st and 2nd Natural Frequencies

In this sub–section, the results for the maximization of frequency difference between the first and second natural frequencies ($\overline{\omega}_{21} = \overline{\omega}_2 - \overline{\omega}_1$) are presented. Table 5.7 and Figure 5.11 show the optimal results yielding maximum $\overline{\omega}_{21}$ for simply–supported flat panels and the optimal lamination parameter distributions with the corresponding discrete fiber angles/fiber paths, respectively. In this case, the influence of aspect ratio on the effectiveness variable–stiffness methodology is similar to the fundamental frequency maximization of simply–supported flat panels. When a/b is increased to 1.5, the variable–stiffness design outperforms the constant stiffness one, providing over 3% increase in the maximum frequency difference. For $a/b = 2.0$, the variable–stiffness frequency difference still exceeds the constant–stiffness value, but the performance increment reduces to below 3%.

In Table 5.8 and Fig. 5.12 the optimal results yielding maximum $\overline{\omega}_{21}$ for simply–supported panels with $a/r = 0.2$ and the optimal lamination parameter distributions with the corresponding discrete fiber angles/fiber paths are presented, respectively. The results for this case show that, variable–stiffness frequencies exceed constant–stiffness ones for $a/b = 1.0$ and $a/b = 2.0$, but no improvement occurs for $a/b = 1.5$.

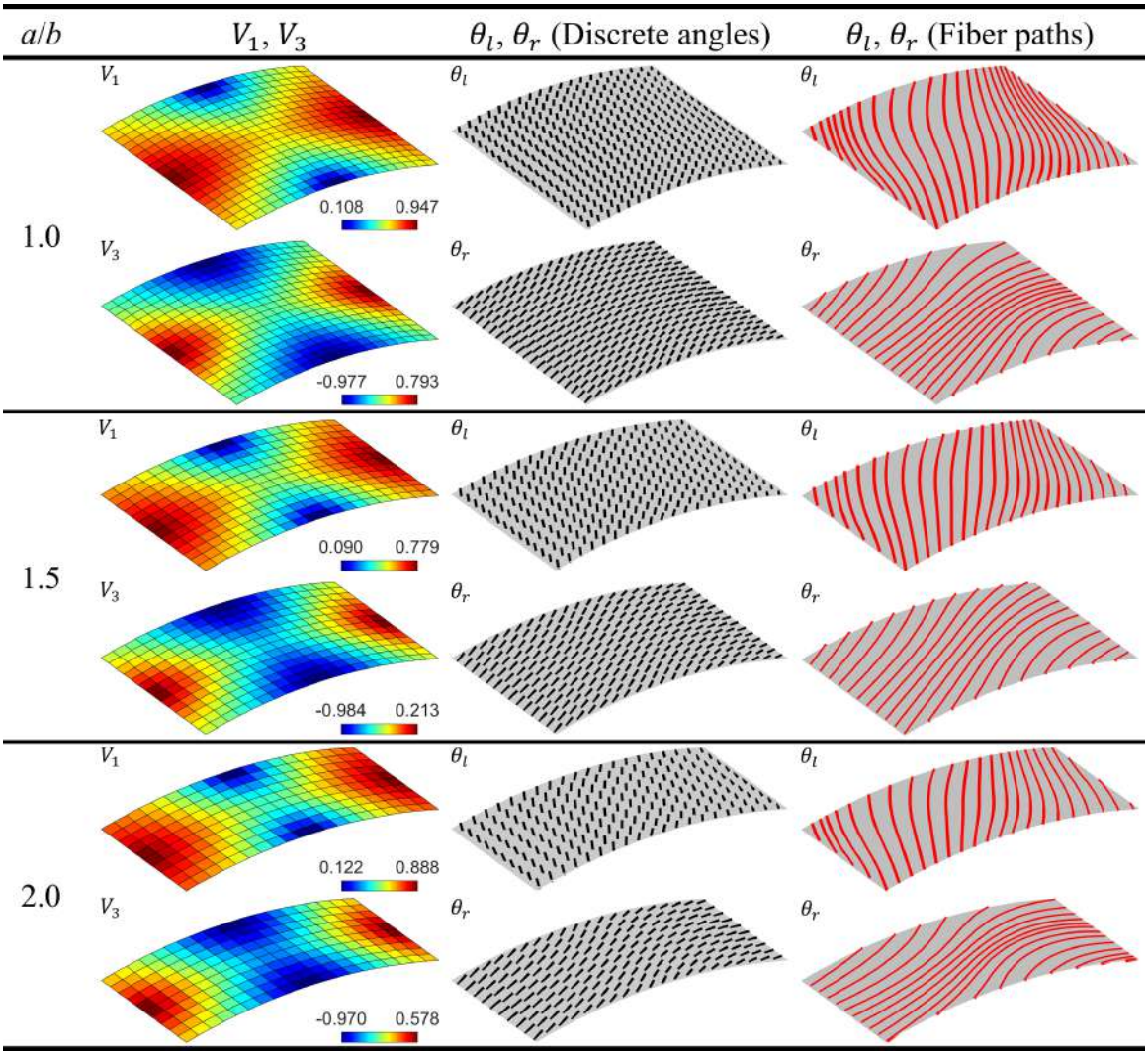

Figure 5.10: Optimal lamination parameter distributions and corresponding discrete fiber angles/fiber paths yielding maximum $\overline{\omega}_1$ for clamped panels with $a/r = 0.5$.

Table 5.7: Optimal results yielding maximum $\overline{\omega}_{21}$ for simply–supported panels with $a/r = 0.0$ (flat panels).

a/b	$\overline{\omega}_{21}^{cs}$	$\overline{\omega}_{21}^{vs}$	% imp.	R_l	R_r	$(V_1, V_3)^1$	$(V_1, V_3)^2$	$(\theta_l, \theta_r)^1$	$(\theta_l, \theta_r)^2$
1.0	28.29	28.29	0.00	N.A.	N.A.	(0.0, -1.0)	(0.0, -1.0)	(45°, 45°)	(45°, 45°)
1.5	16.18	16.69	3.15	0.0	1.0	(0.0, -1.0)	(0.78, 0.2)	(45°, 45°)	(70°, 20°)
2.0	10.13	10.41	2.76	0.0	1.0	(0.45, -0.6)	(1.0, 1.0)	(58°, 32°)	(90°, 0°)

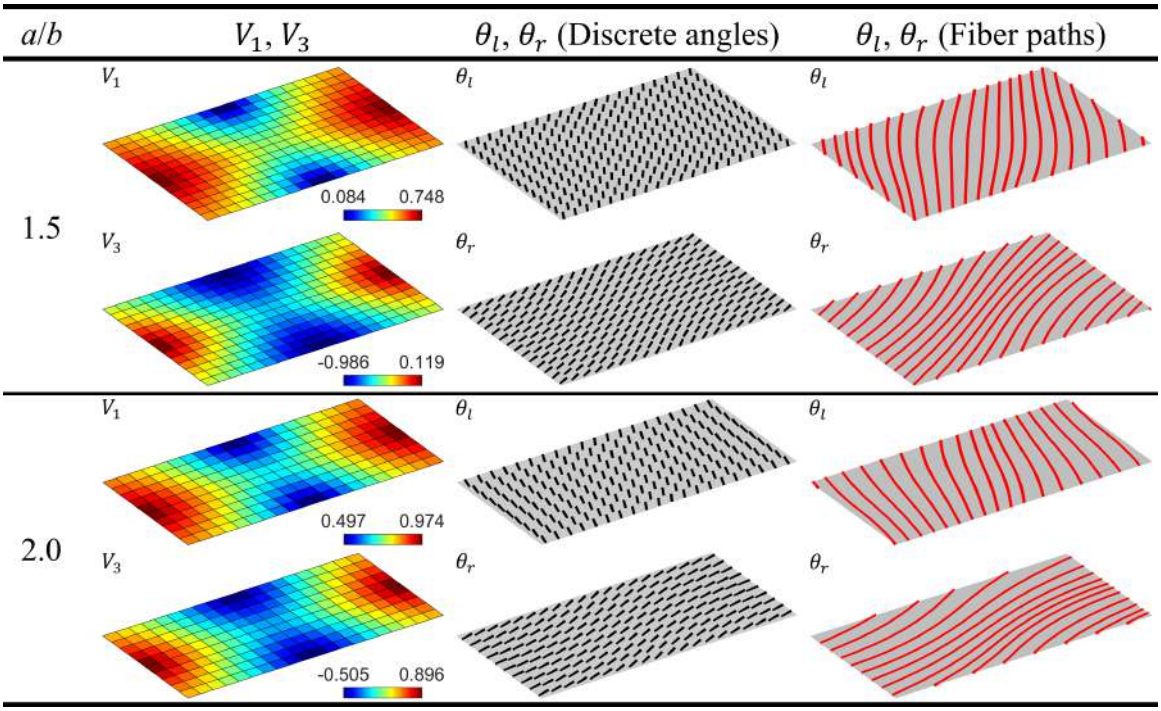

Figure 5.11: Optimal lamination parameter distributions and corresponding discrete fiber angles/fiber paths yielding maximum $\overline{\omega}_{21}$ for simply–supported panels with $a/r = 0.0$.

Table 5.8: Optimal results yielding maximum $\overline{\omega}_{21}$ for simply–supported panels with $a/r = 0.2$.

a/b	$\overline{\omega}_{21}^{cs}$	$\overline{\omega}_{21}^{vs}$	% imp.	R_l	R_r	$(V_1, V_3)^1$	$(V_1, V_3)^2$	$(\theta_l, \theta_r)^1$	$(\theta_l, \theta_r)^2$
1.0	19.49	19.91	2.15	0.1	0.9	(0.8, 1.0)	(0.54, -0.1)	(90°, 0°)	(66°, 24°)
1.5	10.79	10.79	0.00	0.1	0.9	(0.8, 1.0)	(0.8, 1.0)	(90°, 0°)	(90°, 0°)
2.0	6.26	6.37	1.76	1.0	0.0	(0.0, -1.0)	(-0.22, -0.9)	(45°, 45°)	(51°, 39°)

For simply–supported panels with $a/r = 0.5$ optimal results yielding maximum $\overline{\omega}_{21}$ are presented in Table 5.9. For this curvature value, variable–stiffness design outperformed the constant–stiffness one only for square panels. Figure 5.13 shows the optimal lamination parameter distributions with the corresponding discrete fiber angles/fiber paths for this case.

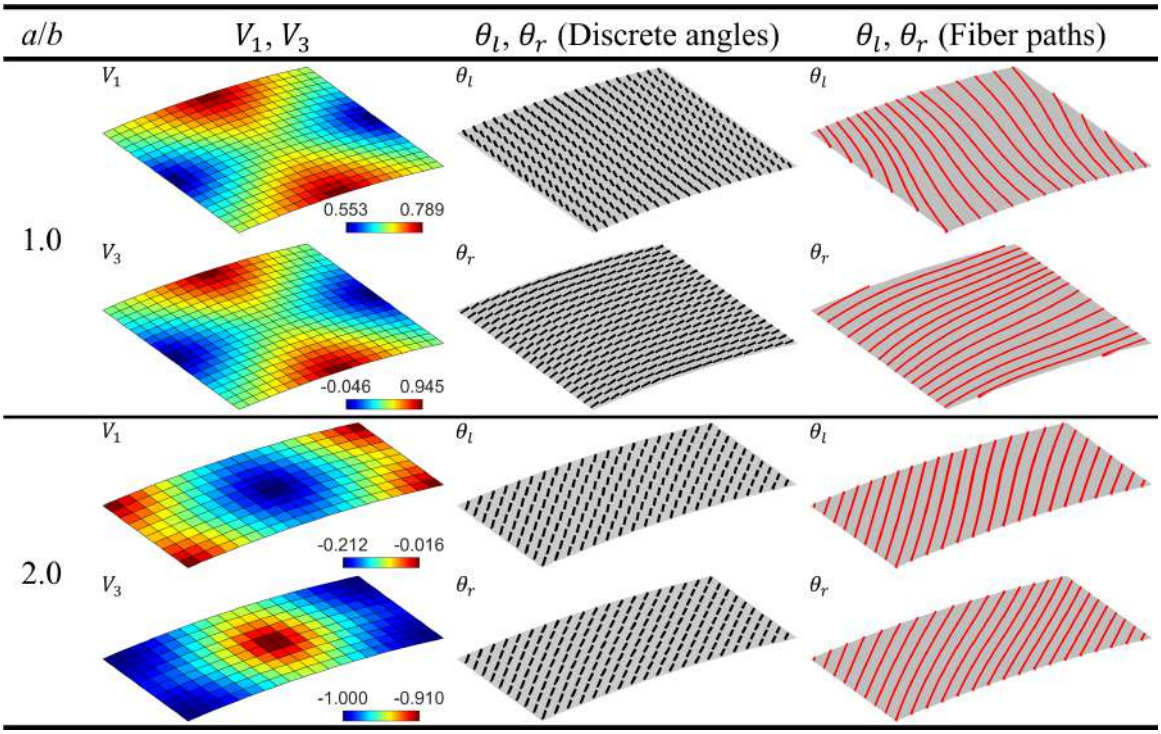

Figure 5.12: Optimal lamination parameter distributions and corresponding discrete fiber angles/fiber paths yielding maximum $\overline{\omega}_{21}$ for simply–supported panels with $a/r = 0.2$.

Table 5.9: Optimal results yielding maximum $\overline{\omega}_{21}$ for simply–supported panels with $a/r = 0.5$.

a/b	$\overline{\omega}_{21}^{cs}$	$\overline{\omega}_{21}^{vs}$	% imp.	R_l	R_r	$(V_1, V_3)^1$	$(V_1, V_3)^2$	$(\theta_l, \theta_r)^1$	$(\theta_l, \theta_r)^2$
1.0	41.38	42.36	2.37	0.0	1.0	(0.95, 0.8)	(0.81, 0.3)	(81°, 9°)	(72°, 18°)
1.5	19.80	19.80	0.00	0.15	0.85	(0.7, 1.0)	(0.7, 1.0)	(90°, 0°)	(90°, 0°)
2.0	10.93	10.93	0.00	0.0	1.0	(1.0, 1.0)	(1.0, 1.0)	(90°, 0°)	(90°, 0°)

For clamped flat panels, the optimal results providing maximum $\overline{\omega}_{21}$ and the optimal lamination parameter distributions with the corresponding discrete fiber angles/fiber paths are presented in Table 5.10 and Fig. 5.14, respectively. In this case, variable–stiffness frequencies slightly exceed the constant–stiffness ones for $a/b = 1.5$ and $a/b = 2.0$. However, no improvement is achieved for square panels.

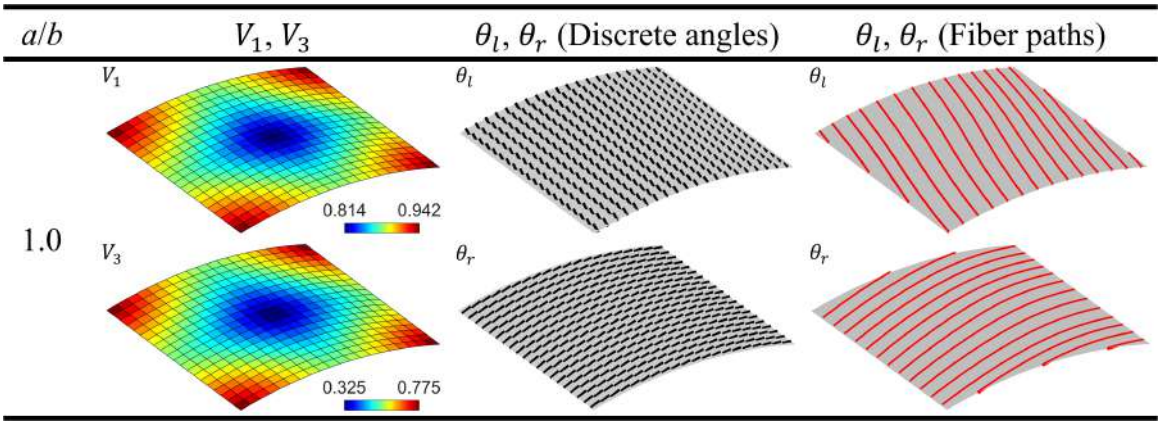

Figure 5.13: Optimal lamination parameter distributions and corresponding discrete fiber angles/fiber paths yielding maximum $\overline{\omega}_{21}$ for simply–supported panels with $a/r = 0.5$.

Table 5.10: Optimal results yielding maximum $\overline{\omega}_{21}$ for clamped panels with $a/r = 0.0$ (flat panels).

a/b	$\overline{\omega}_{21}^{cs}$	$\overline{\omega}_{21}^{vs}$	% imp.	R_l	R_r	$(V_1, V_3)^1$	$(V_1, V_3)^2$	$(\theta_l, \theta_r)^1$	$(\theta_l, \theta_r)^2$
1.0	16.87	17.32	2.67	1.0	0.0	(0.0, -1.0)	(-0.22, -0.9)	(45°, 45°)	(52°, 38°)
1.5	10.74	11.38	5.96	0.0	1.0	(0.55, -0.4)	(0.0, -1.0)	(62°, 28°)	(45°, 45°)
2.0	12.62	12.83	1.66	0.0	1.0	(0.74, 0.0)	(1.0, 1.0)	(68°, 22°)	(45°, 45°)

Table 5.11 shows the optimal results yielding maximum $\overline{\omega}_{21}$ for clamped panels with $a/r = 0.2$. In this case, the variable–stiffness methodology performs effectively for all the aspect ratios. When a/b is 1.5, variable–stiffness frequency difference is almost 6% higher than the constant–stiffness one. The optimal lamination parameter distributions with the corresponding discrete fiber angles/fiber for clamped panels with $a/r = 0.2$ are presented in Fig. 5.15.

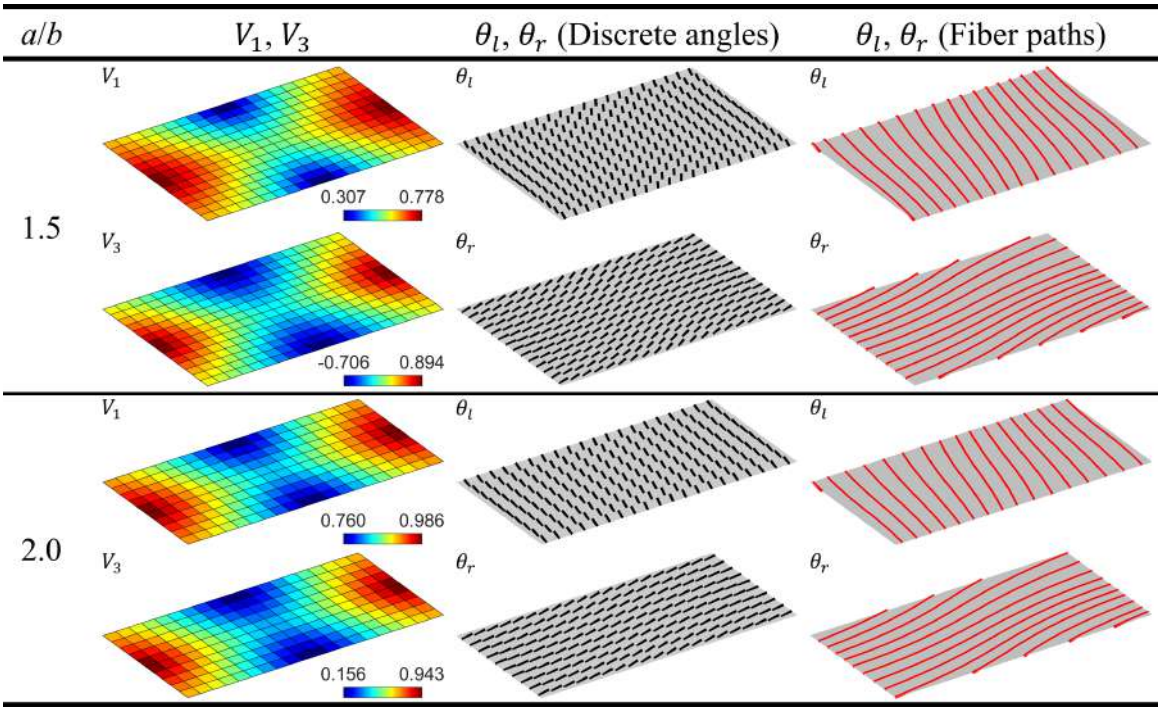

Figure 5.14: Optimal lamination parameter distributions and corresponding discrete fiber angles/fiber paths yielding maximum $\overline{\omega}_{21}$ for clamped panels with $a/r = 0.0$.

Table 5.11: Optimal results yielding maximum $\overline{\omega}_{21}$ for clamped panels with $a/r = 0.2$.

a/b	$\overline{\omega}_{21}^{cs}$	$\overline{\omega}_{21}^{vs}$	% imp.	R_l	R_r	$(V_1, V_3)^1$	$(V_1, V_3)^2$	$(\theta_l, \theta_r)^1$	$(\theta_l, \theta_r)^2$
1.0	41.38	42.36	2.37	0.0	1.0	(0.95, 0.8)	(0.81, 0.3)	(45°, 45°)	(52°, 39°)
1.5	19.80	19.80	0.00	0.15	0.85	(0.71, 0.0)	(0.0, -1.0)	(62°, 28°)	(45°, 45°)
2.0	10.93	10.93	0.00	0.0	1.0	(1.0, 1.0)	(0.0, -1.0)	(78°, 22°)	(45°, 45°)

Table 5.12 shows the optimal results yielding maximum $\overline{\omega}_{21}$ for clamped panels with $a/r = 0.5$. In this case, the variable–stiffness design method found to be effective only for $a/b = 1.0$ similar to simply–supported boundary conditions. Figure 5.16 shows the optimal lamination parameter distributions with the corresponding discrete fiber angles/fiber paths for clamped square panels with $a/r = 0.5$.

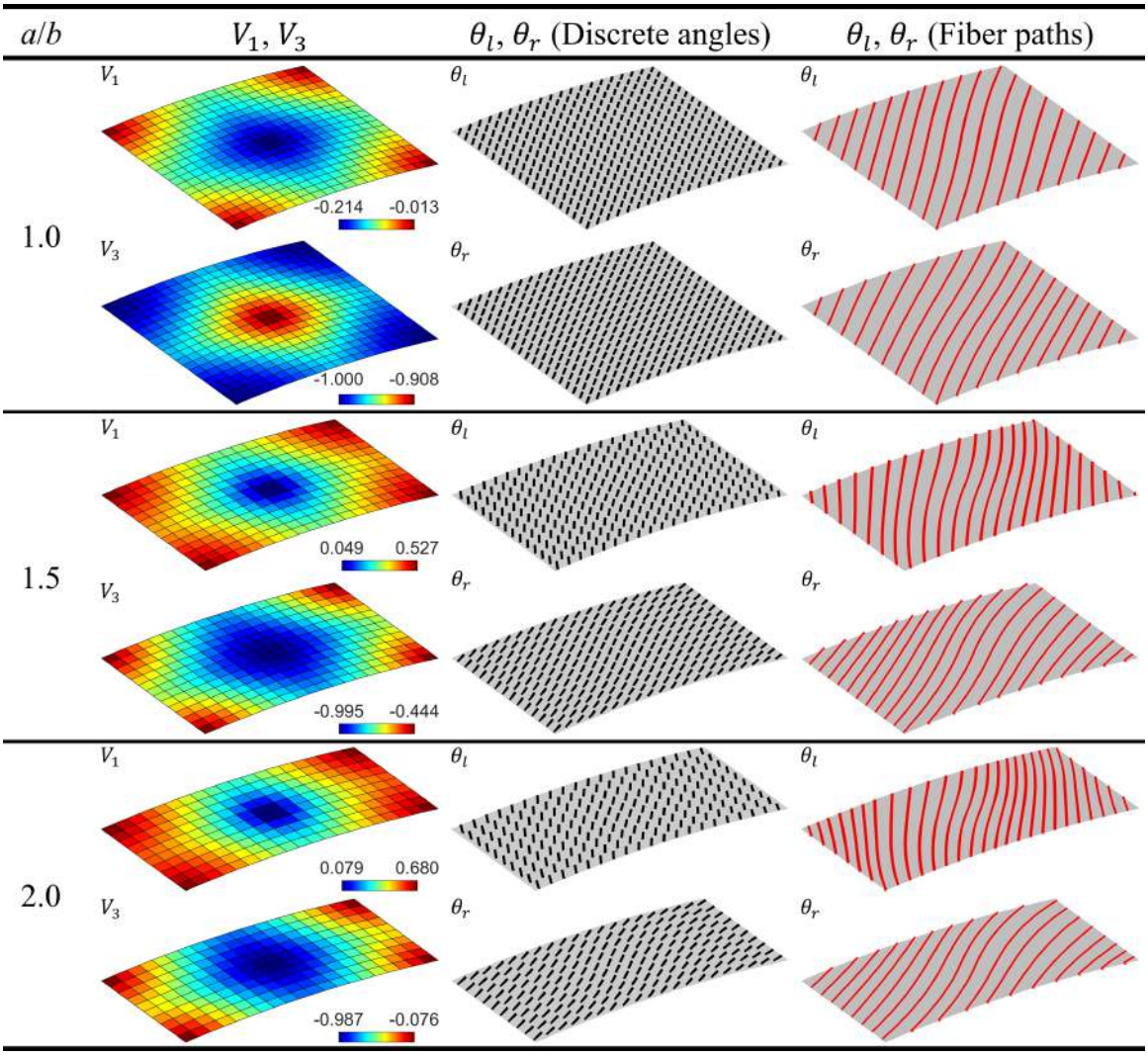

Figure 5.15: Optimal lamination parameter distributions and corresponding discrete fiber angles/fiber paths yielding maximum $\overline{\omega}_{21}$ for clamped panels with $a/r = 0.2$.

Table 5.12: Optimal results yielding maximum $\overline{\omega}_{21}$ for clamped panels with $a/r = 0.5$.

a/b	$\overline{\omega}_{21}^{cs}$	$\overline{\omega}_{21}^{vs}$	% imp.	R_l	R_r	$(V_1, V_3)^1$	$(V_1, V_3)^2$	$(\theta_l, \theta_r)^1$	$(\theta_l, \theta_r)^2$
1.0	39.44	40.69	3.17	0.0	1.0	(0.98, 0.9)	(0.63, -0.2)	(84°, 6°)	(65°, 25°)
1.5	20.44	20.44	0.00	0.15	0.85	(0.7, 1.0)	(0.7, 1.0)	(90°, 0°)	(90°, 0°)
2.0	11.73	11.73	0.00	0.0	1.0	(1.0, 1.0)	(1.0, 1.0)	(90°, 0°)	(90°, 0°)

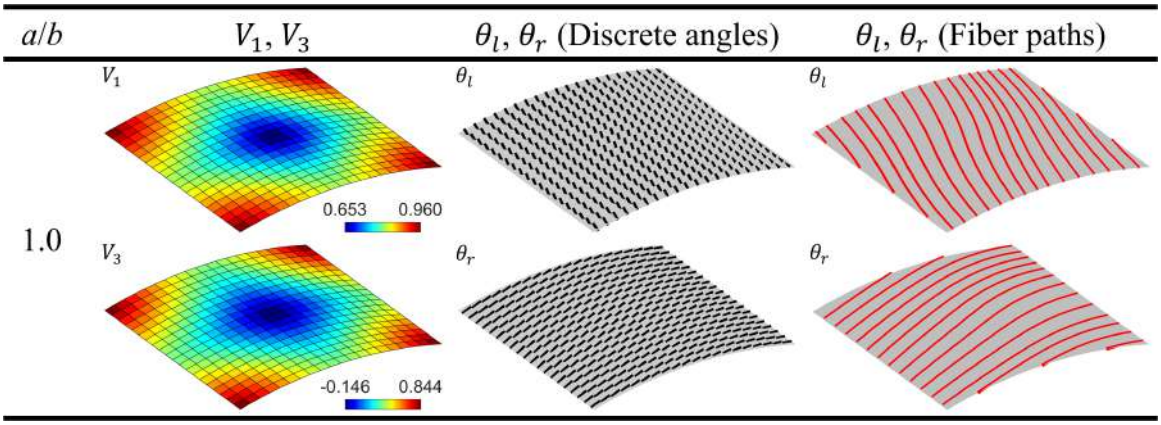

Figure 5.16: Optimal lamination parameter distributions and corresponding discrete fiber angles/fiber paths yielding maximum $\overline{\omega}_{21}$ for clamped panels with $a/r = 0.5$.

Chapter 6

CONCLUSIONS

In this thesis, novel techniques for the design and optimization of nonconventional laminated composite panels were developed. Lamination parameters method is used to characterize laminate stiffness matrices in a compact form. An optimization framework based on finite element analysis was developed to calculate the solutions for different panel geometries, boundary conditions and load cases. The contributions of the study can be summarized in three main parts.

Firstly, a multi-objective design methodology was presented for maximizing the fundamental frequency, buckling load and effective stiffness of laminated composite plates. Multi-objective optimization solutions were computed in lamination parameter domain for different combinations of design objectives. Initially, the responses for individual performance metrics were obtained as a function of lamination parameters and single-objective optimal designs were determined. Then, multi-objective optimization studies were performed where the trends of the objective functions with respect to design variables were observed to be conflicting for several problem types. For these cases, Pareto-optimal solutions were calculated to obtain sets of non-dominated designs. The distributions of Pareto sets on lamination parameter space were presented which are notably informative for multi-objective optimization studies. The results showed that, even though individual optimum solutions lie on the boundary of Miki's diagram, Pareto-optimal solutions do not necessarily follow this trend. Therefore, searching the interior region of the feasible domain is particularly important in multi-objective optimization problems. The values of the fundamental frequency, buckling load and effective stiffness metrics at the optimal point of each metric were also investigated. The analyses revealed that the optimal solutions for different per-

formance metrics could strongly conflict with each other, as the increase in a certain metric could lead to a significant decrease in another one. This result demonstrated the importance of finding Pareto sets for multi-objective laminate optimization problems to detect all the optimal solution candidates and find the best compromise among them.

Secondly, the design of curved laminated composite panels for optimal dynamic response was studied in detail. Various aspect ratios, panel curvatures and boundary conditions were considered to investigate the individual and combined effects of model parameters on dynamic responses. Initially, fundamental frequency contours were obtained in lamination parameter domain. For curved panels, such results were acquired for the first time in the literature. The maximum frequency points were regarded as the optimal designs. The stiffening effect of high curvature dominated over the influence of aspect ratio and boundary conditions. In addition, vibration mode shapes were observed to strongly influence the fundamental frequency contours. Following fundamental frequency maximization, optimal lamination parameters that minimize equivalent radiated power (ERP) of the panels subject to harmonic pressure excitation were investigated. In several cases, resonance bands formed in the ERP contours. This demonstrated that, the surfaces of frequency–response quantities in lamination parameters space can be non–convex, unlike natural frequency. For relatively low excitation frequencies, optimum design points providing minimum ERP were found to be the same as maximum fundamental frequency points, if the fundamental vibration mode half–waves numbers in the x and y–directions are both one. Therefore, frequency maximization technique is effective in minimizing forced dynamic response under certain conditions. When the excitation frequency was increased, the optimum points changed drastically for certain panel models.

In the last part, a new variable–stiffness laminate design approach that considers the manufacturability was presented. The proposed method is based on using master nodes and constrained interpolation of lamination parameter variables. The values at the master nodes are optimized to obtain the best lamination parameter

distributions maximizing the chosen performance metric. The interpolation approach ensures the optimal lamination parameter distributions to change smoothly through the panel. In the next step, the discrete fiber angles are retrieved using the elemental lamination parameters. The fiber angle distributions inherit the smoothness property of the optimal lamination parameter distributions. The fiber paths required for the manufacturing process are obtained from the discrete fiber angle distributions using stream functions. These fiber paths also change smoothly through the panel conforming to the fiber angle distributions. The proposed method was utilized for the maximization of two different panel responses: fundamental natural frequency and the difference between the first and the second frequencies. Various cases with different model parameters including panel aspect ratios, curvatures and boundary conditions were investigated. For all the considered cases, the presented method could generate smooth fiber paths corresponding to the optimal lamination parameter distributions.

The focus of this work was on building an efficient optimization framework and providing the necessary methodologies for the design of nonconventional composite plates. The proposed methods were shown to be effective and they provided significantly informative results. In the future studies, these techniques can be utilized to investigate laminate design problems involving various panel geometries, boundary conditions, load cases and performance metrics.

BIBLIOGRAPHY

[Abdalla et al., 2007] Abdalla, M. M., Setoodeh, S., & Gürdal, Z. (2007). Design of variable stiffness composite panels for maximum fundamental frequency using lamination parameters. *Composite Structures*, 81(2):283–291. DOI: 10.1016/j.compstruct.2006.08.018

[Abouhamze and Shakeri, 2007] Abouhamze, M., & Shakeri, M. (2007). Multi-objective stacking sequence optimization of laminated cylindrical panels using a genetic algorithm and neural networks. *Composite Structures*, 81:253–263. DOI: 10.1016/j.compstruct.2006.08.015

[Adali, 1984] Adali, S. (1984). Design of shear-deformable antisymmetric angle-ply laminates to maximize the fundamental frequency and frequency separation. *Composite Structures*, 2:349–369. DOI: 10.1016/0263-8223(84)90005-9

[Adali and Verijenko, 2001] Adali, S., & Verijenko, V. E. (2001). Optimum stacking sequence design of symmetric hybrid laminates undergoing free vibrations. *Composite Structures*, 54:131–138. DOI: 10.1016/S0263-8223(01)00080-0

[Ameri et al., 2012] Ameri, E., Aghdam, M. M., & Shakeri, M. (2012). Global optimization of laminated cylindrical panels based on fundamental natural frequency. *Composite Structures*, 94(9):2697–2705. DOI: 10.1016/j.compstruct.2012.04.005

[Anderson et al., 1968] Anderson, R. G., Irons, B. M., & Zienkiewicz, O. C. (1968). Global Vibration and stability of plates using finite elements. *Composite Structures*, 4(10):1031–1055. DOI: 10.1016/0020-7683(68)90021-8

[Apalak et al., 2008] Apalak, M. K., Yildirim, M., & Ekici, R. (2008). Layer optimisation for maximum fundamental frequency of laminated composite plates for

different edge conditions. *Composites Science and Technology*, 68(2):537–550. DOI: 10.1016/j.compscitech.2007.06.031

[Assaee and Hasani, 2015] Assaee, H., & Hasani, H. (2015). Forced vibration analysis of composite cylindrical shells using spline finite strip method. *Thin-Walled Structures*, 97:207–214. DOI: 10.1016/j.tws.2015.09.014

[Bardell et al., 1997] Bardell, N. S., Dunsdon, J. M., & Langley, R. S. (1997). Free and forced vibration analysis of thin, laminated, cylindrically curved panels. *Composite Structures*, 38(14):453–462. DOI: 10.1016/S0263-8223(97)00080-9

[Bert, 1977] Bert, C. W. (1977). Optimal design of composite material plates to maximize its fundamental frequency. *Journal of Sound and Vibration*, 50:229–237. DOI: 10.1016/0022-460X(77)90357-1

[Botelhoa et al., 2006] Botelhoa, E. C., Campos, A. N., de Barros, E., Pardinia, L. C., & Rezende, M. C. (2006). Damping behavior of continuous fiber/metal composite materials by the free vibration method. *Composites Part B: Engineering*, 37:255–263. DOI: 10.1016/j.compositesb.2005.04.003

[Blom et al., 2010] Blom, A. W., Abdalla, M. M., & Gürdal, Z. (2010). Optimization of course locations in fiber-placed panels for general fiber angle distributions. *Composites Science and Technology*, 7(4):564–570. DOI: 10.1016/j.compscitech.2009.12.003

[Deb, 2001] Deb, K. (2001). Multi-Objective Optimization using Evolutionary Algorithms. Chichester: John Wiley & Sons.

[Diaconu et al., 2002] Diaconu, C. G., Sato, M., & Sekine, H. (2002). Layup optimization of symmetrically laminated thick plates for fundamental frequencies using lamination parameters. *Structural and Multidisciplinary Optimization*, 24(4):302–311. DOI: 10.1007/s00158-002-0241-z

[Erdal and Sonmez, 2005] Erdal, O., & Sonmez, F. O. (2005). Optimum design of composite laminates for maximum buckling load capacity using simulated annealing. *Composite Structures*, 71(1):45–52. DOI: 10.1016/j.compstruct.2004.09.008

[Farshi and Rabiei, 2007] Farshi, B., & Rabiei, R. (2007). Optimum design of composite laminates for frequency constraints. *Composite Structures*, 81:587–597. DOI: 10.1016/j.compstruct.2006.10.009

[Fazzolari, 2014] Fazzolari, F. A. (2014). A refined dynamic stiffness element for free vibration analysis of crossply laminated composite cylindrical and spherical shallow shells. *Composites Part B: Engineering*, 62:143–158. DOI: 10.1016/j.compositesb.2014.02.021

[Fritze et al., 2009] Fritze, D., Marburg, S., & Hardtke, H. J. (2009). Estimation of radiated sound power: a case study on common approximation methods. *Acta Acoustica united with Acoustica*, 95:833–842. DOI: 10.3813/AAA.918214

[Fukunaga and Vanderplaats, 1991] Fukunaga, H., & Vanderplaats, G. N. (1991). Stiffness optimization of orthotropic laminated composites using lamination parameters. *AIAA Journal*, 29(4):641–646. DOI: 10.2514/3.59931

[Fukunaga and Sekine, 1992] Fukunaga, H., & Sekine, H. (1992). Stiffness design method of symmetric laminates using lamination parameters. *Journal of Sound and Vibration*, 30(11):2791–2793. DOI: 10.2514/3.11304

[Fukunaga et al., 1994] Fukunaga, H., Sekine, H., & Sato, M. (1994). Optimal design of symmetric laminated plates for fundamental frequency. *Journal of Sound and Vibration*, 171(2):219–229. DOI: 10.1006/jsvi.1994.1115

[Fukunaga et al., 1995] Fukunaga, H., Sekine, H., Sato, M., & Iino, A. (1995). Buckling design of symmetrically laminated plates using lamination parameters. *Computers and Structures*, 57(4):643–649. DOI: 10.1016/0045-7949(95)00050-Q

[Grenestedt, 1990] Grenestedt, J. L. (1990). Composite plate optimization only requires one parameter. *Structural Optimization*, 2(1):29–37. DOI: 10.1007/BF01743518

[Grenestedt, 1991] Grenestedt, J. L. (1991). Layup optimization against buckling of shear panels. *Structural Optimization*, 3(2):115–120. DOI: 10.1007/BF01743281

[Grenestedt and Gudmundson, 1993] Grenestedt, G. L., & Gudmundson, P. (1993). Layup optimization of composite material structures. In *Proc. of IUTAM symposium on optimal design with advanced materials*, pages 311–336, Amsterdam.

[Gürdal and Olmedo, 1993] Gürdal, Z., & Olmedo, R. (1993). In-Plane Response of Laminates with Spatially Varying Fiber Orientations: Variable Stiffness Concept. *AIAA Journal*, 31(4):751–758. DOI: 10.2514/3.11613

[Gürdal et al., 1999] Gürdal, Z., Haftka, R., & Hajela, P. (1999). *Design and Optimization of Laminated Composite Materials*. New York: John Wiley & Sons.

[Gürdal et al., 2008] Gürdal, Z., Tatting, B. F., & Wu, C. K. (2008). Variable stiffness composite panels: effects of stiffness variation on the in-plane and buckling response. *Composites Part A: Applied Science and Manufacturing*, 39(5):911–922. DOI: 10.1016/j.compositesa.2007.11.015

[Hirano, 1979] Hirano, Y. (1979). Optimum design of laminated plates under axial compression. *AIAA Journal*, 17(9):1017-1079. DOI: 10.2514/3.61269

[Honda and Narita, 2008] Honda, S., & Narita, Y. (2008). Design for the maximum natural frequency of laminated composite plates by optimally distributed short fibers. *Journal of System Design and Dynamics*, 6(2):1195–1205. DOI: 10.1299/jsdd.2.1195

[Honda et al., 2009] Honda, S., Narita, Y., & Sasaki, K. (2009). Discrete Optimization for Vibration Design of Composite Plates by Using Lamination Parameters. *Advanced Composite Materials*, 18(2):297–314. DOI: 10.1163/156855109X434739

[Honda and Narita, 2011] Honda, S., & Narita, Y. (2011). Vibration design of laminated fibrous composite plates with local anisotropy induced by short fibers and curvilinear fibers. *Composite Structures*, 93(2):902–910. DOI: 10.1016/j.compstruct.2010.07.003

[Hu and Lin, 1995] Hu H. T., & Lin B. H. (1995). Buckling optimization of symmetrically laminated plates with various geometries and end condition. *Composites Science and Technology*, 55(3):277–285. DOI: 10.1016/0266-3538(95)00105-0

[Hu and Peng, 2013] Hu H. T., & Peng H. W. (2013). Maximization of fundamental frequency of axially compressed laminated curved panels with cutouts. *Composites Part B: Engineering*, 47:8–25. DOI: 10.1016/j.compositesb.2012.10.047

[Ijsselmuiden et al., 2010] Ijsselmuiden, S. T., Abdalla, M. M., Gürdal, Z. (2010). Optimization of variable-stiffness panels for maximum buckling load using lamination parameters. *Composite Structures*, 48(1):134–143. DOI: 10.2514/1.42490

[Kam and Chang, 1993] Kam, T. Y., & Chang, R. R. (1993). Design of laminated composite plates for maximum buckling load and vibration frequency. *Computer Methods in Applied Mechanics and Engineering*, 106(12):65–81. DOI: 10.1016/0045-7825(93)90185-Z

[Kam and Lai, 1995] Kam, T. Y., & Lai, F. M. (1995). Maximum stiffness design of laminated composite plates via a constrained global optimization approach. *Composite Structures*, 32(14):391–398. DOI: 10.1016/0263-8223(95)00070-4

[Kayikci and Sonmez, 2012] Kayikci, R., & Sonmez, F. O. (2012). Design of compos-

ite laminates for optimum frequency response. *Journal of Sound and Vibration*, 331(8):1759–1776. DOI: 10.1016/j.jsv.2011.12.020

[Liew et al., 1997] Liew, K. M., Lim, C. W., & Kitipornchai, S. (1997). Effects of general laminations and boundary constrains on vibration of composite shallow shells. *Composites Part B: Engineering*, 27:155–171. DOI: 10.1016/1359-8368(95)00038-0

[Liu and Quek, 2003] Liu, G. R., & Quek, S. S. (2003). *The Finite Element Method: A Practical Course*. Oxford, UK: Butterworth-Heinemann.

[Marsh, 2014] Marsh, G. (2014). Composites and metals a marriage of convenience? *Reinforced Plastics*, 58:38–42. DOI: 10.1016/S0034-3617(14)70108-0

[Miki, 1984] Miki, M. (1984). Laminated Fibrous Composites Plates with Required Flexural Stiffness. In J. Carlsson & N. G. Ohlson (Eds.), *Mechanical Behaviour of Materials – IV* (pp. 465–471). Oxford: Pergamon Press.

[Miki and Sugiyama, 1993] Miki, Y., & Sugiyama, Y. (1993). Optimum design of laminated composite plates using lamination parameters. *AIAA Journal*, 31(5):921–922. DOI: 10.2514/3.49033

[Narita, 2003] Narita, Y. (2003). Layerwise optimization for the maximum fundamental frequency of laminated composite plates. *Journal of Sound and Vibration*, 263(5):1005–1016. DOI: 10.1016/S0022-460X(03)00270-0

[Narita and Robinson, 2006] Narita, Y., & Robinson, P. (2006). Maximizing the fundamental frequency of laminated cylindrical panels using layerwise optimization. *International Journal of Mechanical Sciences*, 48(12):1516–1524. DOI: 10.1016/j.ijmecsci.2006.06.008

[Nik et al., 2012] Nik M. A., Fayazbakhsh, K., Pasini, D., & Lessard, L. (2012). Surrogate-based multi-objective optimization of a composite lam-

inate with curvilinear fibers. *Composite Structures*, 94:2306–2313. DOI: 10.1016/j.compstruct.2012.03.021

[Niu et al., 2010] Niu, B., Olhoff, N., Lund, E., & Cheng, G. (2010). Discrete material optimization of vibrating laminated composite plates for minimum sound radiation. *International Journal of Solids and Structures*, 47:2097–2114. DOI: 10.1016/j.ijsolstr.2010.04.008

[Orefice et al., 2017] Orefice, A., Mancusi, G., Feo, L., & Fraternali, F. (2017). Cohesive interface behaviour and local shear strains in axially loaded composite annular tubes. *Composite Structures*, 160:1126–1135. DOI: 10.1016/j.compstruct.2016.10.117

[Peeters et al., 2015] Peeters, D. M. J., Hesse, S., & Abdalla, M. M. (2015). Stacking sequence optimisation of variable stiffness laminates with manufacturing constraints. *Composite Structures*, 125:596–604. DOI: 10.1016/j.compstruct.2015.02.044

[Peeters et al., 2018] Peeters, D., Hong, Z., & Abdalla, M. (2018). A compliance approximation method applied to variable stiffness composite optimization. *Structural and Multidisciplinary Optimization*. DOI: 10.1007/s00158-018-2007-2

[Ribeiro, 2016] Ribeiro, P. (2016). Linear modes of vibration of cylindrical shells in composite laminates reinforced by curvilinear fibres. *Journal of Vibration and Control*, 22(20):4141–4158. DOI: 10.1177/1077546315571661

[Sahoo et al., 2016] Sahoo, S. S., Panda, S. K., Mahapatra, & T. R. (2016). Static, free vibration and transient response of laminated composite curved shallow panel an experimental approach. *European Journal of Mechanics - A/Solids*, 59:95–113. DOI: 10.1016/j.euromechsol.2016.03.014

[Setoodeh et al., 2006] Setoodeh. S., Abdalla, M. M., & Grdal, Z. (2006). Design of variable–stiffness laminates using lamination parameters. *Composites Part B: Engineering*, 37(45):301–309. DOI: 10.1016/j.compositesb.2005.12.001

[Serhat and Basdogan, 2018] Serhat, G., & Basdogan, I. (2018). Design of curved composite panels for optimal dynamic response using lamination parameters. *Composites Part B: Engineering*, 147:135–146. DOI: 10.1016/j.compositesb.2018.04.033

[Serhat et al., 2016] Serhat, G., Faria, T. G., & Basdogan, I. (2016). Multi-Objective Optimization of Stiffened, Fiber-Reinforced Composite Fuselages for Mechanical and Vibro-Acoustic Requirements. In *Proceedings of 17th AIAA/ISSMO Multidisciplinary Analysis and Optimization Conference*. DOI: 10.2514/6.2016-3509

[Serhat and Basdogan, 2016a] Serhat, G., & Basdogan, I. (2016). Effect of Aspect Ratio and Boundary Conditions on the Eigenfrequency Optimization of Composite Panels using Lamination Parameters. In *Proceedings of 11th ASMO-UK/ISSMO/NOED2016 International Conference on Numerical Optimisation Methods for Engineering Design*.

[Serhat and Basdogan, 2016b] Serhat, G., & Basdogan, I. (2016). Comparison of Vibro–acoustic Performance Metrics in the Design and Optimization of Stiffened Composite Fuselages. In *Proceedings of 45th International Congress and Exposition on Noise Control Engineering, INTER–NOISE 2016*.

[Trias et al., 2016] Trias, D., Maimi, P., & Blanco, N. (2016). Maximization of the fundamental frequency of plates and cylinders. *Composite Structures*, 156:375–384. DOI: 10.1016/j.compstruct.2015.08.034

[Tsai and Hahn, 1980] Tsai, S. W., & Hahn, H. T. (1980). *Introduction of composite materials*. Lancaster, CA: Technomic.